A DYNAMIC WIRELESS ELECTRIC VEHICLE CHARGING SYSTEM WITH UNIFORM COUPLING FACTOR AND NEGLIGIBLE POWER TRANSFER FLUCTUATION

MD MORSHED ALAM

FACULTY OF ENGINEERING
UNIVERSITY OF MALAYA
KUALA LUMPUR

2018

A DYNAMIC WIRELESS ELECTRIC VEHICLE CHARGING SYSTEM WITH UNIFORM COUPLING FACTOR AND NEGLIGIBLE POWER TRANSFER FLUCTUATION

MD MORSHED ALAM

DISSERTATION SUBMITTED IN FULFILMENT OF THE REQUIREMENTS FOR THE DEGREE OF MASTER OF ENGINEERING SCIENCE

FACULTY OF ENGINEERING
UNIVERSITY OF MALAYA
KUALA LUMPUR

2018

UNIVERSITY OF MALAYA

ORIGINAL LITERARY WORK DECLARATION

Name of Candidate: **Md Morshed Alam**

Matric No: **KGA150008**

Name of Degree: **Master of Engineering Science**

Title of Dissertation: **A Dynamic Wireless EV Charging System with Uniform Coupling Factor and Negligible Power Transfer Fluctuation**

Field of Study: **Power Electronics**

I do solemnly and sincerely declare that:

(1) I am the sole author/writer of this work;
(2) This work is original;
(3) Any use of any work in which copyright exists was done by way of fair dealing and for permitted purposes and any excerpt or extract from, or reference to or reproduction of any copyright work has been disclosed expressly and sufficiently and the title of the work and its authorship have been acknowledged in this work;
(4) I do not have any actual knowledge nor do I ought reasonably to know that the making of this work constitutes an infringement of any copyright work;
(5) I hereby assign all and every rights in the copyright to this work to the University of Malaya (UM), who henceforth shall be owner of the copyright in this work and that any reproduction or use in any form or by any means whatsoever is prohibited without the written consent of UM having been first had and obtained;
(6) I am fully aware that if in the course of making this work I have infringed any copyright whether intentionally or otherwise, I may be subject to legal action or any other action as may be determined by UM.

Candidate's Signature   Date:

Subscribed and solemnly declared before,

Witness's Signature   Date:

Name:

Designation:

ABSTRACT

To minimize the dependency on the petroleum products, electric vehicles (EV) have been selected as a feasible solution for transportation purpose. EV was introduced with the appearance of the hybrid electric vehicle (HEV), which causes to bring the development of plug-in hybrid electric vehicles (PHEVs). On the other hand, PHEV is responsible for various drawbacks such as the necessity of connecting cables and plug in charger, galvanic isolation of on-board electronics, the weight and size of the charger, and more important safety issues associated with the operation in the rainy and snowing condition. For user friendly and any prevention from the risk by electricity, inductive power transfer (IPT) method has emerged to charge the EV inductively over the large air gap. There are two types of IPT based EV charging system: stationary and dynamic. High efficiency inductive power transfer (IPT) with low misalignment effect is one of the key issues for the dynamic charging electric vehicle (EV) system. This research presents an advanced concept of analysis and design of transmitter and receiver pads with a special arrangement of pad assembly for dynamic charging of EV. In each transmitter pad, the large rectangular section is series connected with two zigzag- shaped small rectangular sections. These small sections are back-to-back series connected and located inside the large rectangular section. An adjacent pair of proposed transmitter pad with back-to-back series connection, named as extended DD transmitter is used throughout this work. One of the contributions of this work is uniform surface magnetic flux distribution, obtained by the zigzag-shaped rectangular sections. Designing of the proposed transmitter and receiver with the simulation results are done by the 2-D finite element analysis (FEA). In the case of extended DD transmitter, negligible power transfer fluctuation is the major contribution regardless of the horizontal (x-direction) misalignment of the receiver pad. Justification of the pad design is

performed with the load independent voltage gain and power transfer fluctuation characteristics. A compensation technique named LC-LC^2 is used in order to obtain the load independent operation and the better tolerance of the air gap variation. Experimental results prove that power transfer fluctuation with load independent unique voltage gain is within ±6% and efficiency is about 93% under any horizontal (x-direction) misalignment condition of the receiver pad with an air gap of 140mm.

Keywords: extended DD, surface flux density, power transfer fluctuation, load independent voltage gain

ABSTRAK

Untuk mengurangkan kebergantungan produk petroleum, kenderaan elektrik (EV) telah dipilih sebagai penyelesaian yang boleh dilaksanakan untuk tujuan pengangkutan. EV telah diperkenalkan selaras dengan kemunculan kenderaan hibrid elektrik (HEV), yang menyebabkan pembangunan kemudahan kenderaan plug-in elektrik hibrid (PHEVs). Sebaliknya, PHEV bertanggungjawab untuk pelbagai kelemahan seperti keperluan untuk penyambungan kabel dan palam pengecas, pengasingan galvani elektronik mudah alih, berat dan saiz pengecas, dan yang lebih penting isu-isu keselamatan berkaitan dengan operasi dalam keadaan hujan dan salji. Untuk membuatkan ia mesra pengguna dan sebarang pencegahan daripada risiko berkaitan elektrik, kaedah pemindahan kuasa induktif (IPT) telah diperkenalkan untuk pengecasan EV secara induktif dengan ruang udara yang lebih besar. Terdapat dua jenis IPT dalam sistem pengecasan EV: bergerak dan dinamik. Kecekapan pemindahan kuasa induktif (IPT) yang tinggi berkuasa salah jajaran rendah adalah salah satu isu utama untuk menggunakan sistem kenderaan elektrik dinamik (EV). Kajian ini membentangkan konsep analisis yang unggul dan reka bentuk pemancar dan penerima pad dengan susunan khas gabungan pad untuk pengecasan EV secara dinamik. Dalam setiap pad pemancar, bahagian segi empat tepat yang besar adalah disambungkan secara siri dengan dua zig-zag berbentuk bahagian segi empat tepat kecil. Bahagian-bahagian kecil ini disambungkan siri-selari dan terletak di dalam bahagian segi empat tepat yang besar. Sepasang pad juga dicadangkan untuk bahagian pemancar dengan sambungan siri-selari yang sama, ia dinamakan sebagai pemancar DD digunakan dalam penyelidikan ini. Salah satu daripada sumbangan kerja ini adalah taburan fluks magnet permukaan seragam, yang diperolehi oleh zigzag berbentuk bahagian segi empat tepat. Rakaan pemancar yang dicadangkan dan penerima dengan keputusan simulasi yang dilakukan oleh

analisis unsur sehingga 2-D (FEA). Sekiranya pemancar DD digunakan, pengabaian pemindahan kuasa turun-naik adalah sumbangan utama tanpa mengira salah jajaran mendatar pad penerima. Justifikasi reka bentuk pad dilakukan dengan beban gandaan voltan bebas dan pemindahan kuasa ciri-ciri turun naik. Satu teknik pampasan bernama LC-LC^2 digunakan untuk mendapatkan beban operasi bebas dan toleransi yang lebih baik daripada perubahan ruang udara. Keputusan eksperimen membuktikan bahawa, perubahan kuasa yang turun-naik dengan beban bebas gandaan voltan yang unik terletak $\pm$ 6% dan kecekapan adalah kira-kira 93% di bawah semua syarat salah jajaran mendatar pad penerima dengan jurang udara 140mm.

Kata kunci: lanjutan DD, kepadatan permukaan flux, ketidakseimbangan pemindahan kuasa, beban gandaan voltan bebas

ACKNOWLEDGEMENTS

TABLE OF CONTENTS

LIST OF FIGURES

LIST OF TABLES

LIST OF ABBREVIATIONS

EV   : Electric Vehicle

PHEV   : Plug-in Hybrid Electric Vehicle

IPT   : Inductive Power Transfer

PFC   : Power Factor Correction

OLEV   : Online Electric Vehicle

OFEV   : Offline Electric Vehicle

FEA   : Finite Element Analysis

SFD   : Surface Flux Density

ZPA   : Zero Phase Angle

ICE   : Internal Combustion Engine

ZVS   : Zero Voltage Switching

CVTR   : Constant Voltage Transfer Ratio

CPT   : Capacitive Power Transfer

BEVs   : Battery Electric Vehicles

EMF   : Electromagnetic Field

ICNIRP   : International Commission on Non-Ionizing Radiation Protection

ICES   : International Committee on Electromagnetic Safety

SAE   : Society of Automotive Engineers

AWG   : American Wire Gauge

LIST OF SYMBOLS

μ_r	: Relative permeability of the ferrite plate
$\tan\Theta$	: Magnetic loss tangent of the ferrite plate
δ	: Skin depth of the aluminum shield
σ	: Conductivity of the aluminum shield
L_{path1}	: Inductance of the path1
L_{path2}	: Inductance of the path2
$M_{(path1-path2)}$	: Mutual inductance between path1 and path2
$I_{(path1)}$	: Current of path1
$N_{(path2)}$	: Number of turns of path2
$\emptyset_{(path1-path2)}$	: Magnetic flux generated by path1 that links with path2
$\mathbf{B}_{(path1)}$	: Magnetic flux density generated by $I_{(path1)}$
$S_{(path2)}$	: Surface of path2
N	: Turns ratio of the IPT transformer
$\mathbf{n}$	: Normal vector to the $S_{(path2)}$
k	: Coupling coefficient
$N_{large}=N_1=N_{1'}$	: Number of turns for large rectangular section
$N_{small}= N_2= N_3= N_{2'} = N_{3'}$	: Number of turns for small rectangular section
L_{M1}	: Mutual inductance between one parts of extended DD transmitter and receiver
L_{M2}	: Mutual inductance between another part of extended DD transmitter and receiver
L_M	: Mutual inductance between extended DD transmitter and receiver

VA	: Uncompensated load power
L_{l1}	: Leakage inductance of the extended DD transmitter pad
L_{l2}	: Leakage inductance of the receiver pad
L_T	: Inductance of the extended DD transmitter pad
L_R	: Inductance of the receiver pad
L_{f2}	: Compensating inductor
L_{Mf}	: Equivalent inductance of L_M and L_{f2}
C_1	: Compensation capacitance for L_{l1}
C_2	: Compensation capacitance for L_{l2}
C_{f2}	: Compensation capacitance for L_{Mf}
V_i	: Input dc supply for high frequency inverter
V_0	: Voltage across the battery
R_L	: Load resistance of the battery
L_f	: Inductance of the filter
C_f	: Capacitance of the filter
I_1	: Pad current of the transmitter
I_2	: Pad current of the receiver
N_{AB}	: Number of turns generated by the AB segment
N_{EF}	: Number of turns generated by the EF segment
$\mathbf{A}_{AB}$	: Magnetic vector potential of segment AB
$\mathbf{A}_{EF}$	: Magnetic vector potential of segment EF
$\varnothing_{AB, EF}$	: Magnetic flux generated by N_{AB} turns of AB segment that links with segment EF

$\emptyset_{EF, AB}$: Magnetic flux generated by N_{EF} turns of EF segment that links

                 with segment AB

$M_{AB, EF}$: Mutual inductance between AB & EF segments

f : Frequency

ω_r : Resonant frequency

R_E : Equivalent ac load resistance looking into the high frequency

                 rectifier

V_{LM} : Voltage across L_M

V_{AB} : Output voltage of the high frequency inverter

V_{ab} : Voltage across the high frequency rectifier

Z_i : Input impedance of the proposed IPT system

G_V : Voltage gain

R_L : Load resistance

P_L : Load power

H : Air gap

Θ_i : Input phase angle

CHAPTER 1: INTRODUCTION

1.1 Research background

Globally, the second highest energy utilizing sector after the industrial sector is the transportation sector which represents almost 27% of the world's total supplied energy. Nowadays, a large amount of energy from petroleum products has been used for transportation that increases the oil prices and global warming issues (Madawala & Thrimawithana, 2011).
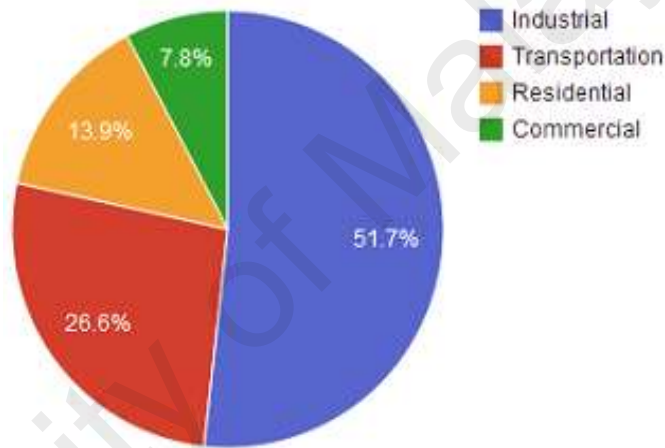
Figure 1.1: Percentage of energy utilization for different sectors (EIA, 2012).

Conventional vehicles run by petroleum products are powered by an internal combustion engine (ICE). These vehicles are restricted in efficiency because of thermodynamics and can obtain maximum efficiencies around 26%. Electric vehicles (EVs) have been selected as a feasible solution (Boys, Elliott, & Covic, 2007) to create the world less dependency on the petroleum products (Chau, Wong, & Chan, 1999; Tie & Tan, 2013). If the vehicles are operated by electricity, it will generate negligible emissions of carbon dioxide compared to vehicles operated by the petroleum products (Covic & Boys, 2013).

1

The idea of EV was introduced with the appearance of the hybrid electric vehicle (HEV), which brings the development of plug-in hybrid electric vehicles (PHEVs). PHEV has various drawbacks such as the necessity of connecting cables and plug in charger, galvanic isolation of on-board electronics, the weight and size of the charger, and more important safety issues associated with the operation in the rainy and snowing condition (Su, Eichi, Zeng, & Chow, 2012). In order to overcome the above drawbacks in PHEV, simple EV has been established (Zhang et al., 2016). Plug-in and wireless are the two methods for the charging of EV. The wireless method is sub-divided into three methods: IPT (Inductive Power Transfer), CPT (Capacitive Power Transfer) and MPT (Microwave Power Transfer). Among them, IPT method has been emerged to charge the EV inductively over the large air gap (Bosshard & Kolar, 2016) because it is user-friendly and provides prevention from the risk by electricity. On the other hand, CPT is not well-established method for EV charging as it is only applicable for low power and short distance applications (Zhang, Lu, Hofmann, Liu, & Mi, 2016). Also, MPT is not suitable for EV charging because it needs frequency in MHz range which is dangerous for human safety (Kim et al., 2016). This charging method can operate reliably even in the most adverse weather conditions of snow and rain. The idea of inductive power transfer comes from the concept of electromagnetic waves by the German physicist Heinrich Hertz who made a spark gap transmitter and receiver and noticed a small spark through a microscope, which was energized by the generation of spark from the transmitter. Inspired by the work of Hertz, Nicola Tesla experimented and established IPT in the 1890s (Tesla, 1914). As power is delivered across an air gap in IPT, it is also referred to as loosely coupled IPT system which is compared with a traditional transformer. Unfortunately, IPT did not become a well established growing research topic or reliable for the industry until the beginning of 21st century, appear with the availability

of high-frequency switching devices, the popularity of mobile network and digital devices, and electric transportation (Siqi & Mi, 2015). Inductive power transfer may seem as an alternative method to power future's transportation system. Depending on the position of the vehicle with respect to the transmitter, IPT based EV charging system can be classified as: stationary and dynamic. Most of the current IPT systems concentrate on stationary charging applications. In this case, the users simply need to park the EV over the plug- less charging pad and the receiver mounted on EV should be well-aligned with the transmitter buried under the road. Otherwise, large misalignment between the receiver and transmitter causes the significant drop in output power and efficiency (Deng, Fei, Li, Ruiqing, & Mi, 2015).

On the other hand, dynamic charging is a promising technology which enables the charging of moving vehicles on the roadway. When the vehicle is running on the roadway, it can be continuously powered. So that, driving range of the electric vehicle can be extended, and a smaller battery pack can be used in order to reduce the vehicle weight and improve the power transfer efficiency (Gilchrist, Wu, & Sealy, 2012; Jeong, Jang, & Kum, 2015). Even though the IPT based EV charging method yields a solution to large consumption of petroleum products for the traditional vehicles, global warming issues associated with some other benefits but this technology still needs huge research and not industrialized perfectly for dynamic charging due to some practical challenges. In spite of research over decades for dynamic charging technology, the technical challenges of less efficiency, load independent operation, fluctuation of power transfer and limitation of misalignment tolerance are still unsolved yet (Aldhaher, Luk, & Whidborne, 2014; Budhia, Boys, Covic, & Chang-Yu, 2013; Kurschner, Rathge, & Jumar, 2013; Zhu, Guo, Wang, Liao, & Li, 2015). The loss in efficiency of IPT based dynamic charging of EV system is mainly

occurred by the problems of two main parts: charging pad and the compensation network. The charging pad design as well as compensation network design has a great contribution for IPT based dynamic charging of EV.

1.2 Problem statement

To obtain the high efficiency, designing of the charging pad plays an important role in the EV charging system. By increasing the dimensions and materials of the charging pad, higher efficiency can be obtained. But, from an engineering point of view, it is not a good approach. The flux path height of a circular pad is about one-fourth of the pad's diameter so that it provides poor coupling between the transmitter and receiver pads. Therefore, to obtain high power transfer efficiency needs a larger dimension of the circular pad which makes the EV charging system impractical. Also, circular pads are not effective for dynamic charging of EV as there is a null zone of power transfer when receiving pad is horizontally misaligned by 38% of the transmitter pad diameter (Budhia, Covic, & Boys, 2011). For a homogeneous size of the circular pad, DD pad has a notable improvement in the coupling. The charging zone for a DD pad is almost two times larger than a circular pad with similar material cost. Generally, DD pad has a potential tolerant in the y-direction. This makes the DD pad effective for the dynamic charging when the driving direction is along with the y-direction. However, there is a null zone of power transfer for DD pad in case of x-direction at about 34% misalignment (Budhia et al., 2013). To improve the misalignment tolerant in x-direction, an extra quadrature coil named Q coil is suggested to work together with the DD pad, which is named as DDQ pad (Budhia et al., 2013; Budhia, Covic, Boys, & Chang-Yu, 2011; Covic, Kissin, Kacprzak, Clausen, & Hao, 2011). Working with a DDQ receiving pad on a DD transmitting pad, the charge zone is about five times larger than the circular pad. Since Q coil is on the receiver side, the DDQ over DD

configuration requires almost two times copper compared to the circular (Budhia et al., 2013). By increasing the size of each D pad and having some overlap between the two D coils, the new bipolar pad could have a similar performance of a DDQ pad with 25% less copper. But it's misalignment tolerance is almost similar to the DD pad. Therefore, a better charging pad design may lead to a 50%−100% improvement compared with the conventional designs.

Another key factor that affects the efficiency and output power controllability of IPT system is the compensation network. P-S and P-P compensated IPT systems are safe for the supply in the absence of receiver pad. But these compensation techniques are not suitable to transfer the rated power in case of misalignment condition, as resonant capacitor value strongly depends on the magnetic coupling coefficient and the output load (Chwei-Sen, Covic, & Stielau, 2004). The efficiency of the S-S compensated IPT system is high when self inductances of the transmitter and receiver are tuned which is very sensitive to the output load changes (Wei, Siu-Chung, Tse, & Qianhong, 2014b). In order to improve the sensitivity of the output voltage under wide load variation, S-S compensated IPT system is designed to operate around the frequency of load independent voltage gain (Q. Chen, Wong, Tse, & Ruan, 2009; Xiaoyong et al., 2012). In this case, efficiency may be lower because of circulating current as ZPA of the input impedance is not maintained. In (Wei et al., 2014b), a tradeoff between output voltage controllability and efficiency of the S-S topology is presented. Moreover, the problem still exists as tuning of compensating capacitors is not easy to obtain. S-P compensation is not effective for a wide variation of coupling coefficient and misalignment as load independent voltage gain is inversely related to the coupling coefficient (Hou et al., 2013). To maintain a unique output power under the changes of coupling, SP-S compensation network was presented in (Villa, Sallan, Sanz

Osorio, & Llombart, 2012). There is a large number of research works based on LCL compensation (Huang, Boys, & Covic, 2013a; Keeling, Covic, & Boys, 2010; Raabe & Covic, 2013; Wu, Gilchrist, Sealy, & Bronson, 2012) that provides uninterrupted power but it reflects reactive power back onto the source (Amjad, Salam, Facta, & Mekhilef, 2013). Another compensation topology with high efficiency named LCC was used in the areas of EV charging (W. Li et al., 2015; Weihan et al., 2015; Zhu, Wang, Guo, Liao, & Li, 2016). Here, load independent voltage gain under coupling changes is very much difficult to obtain because of self coupling between the compensation inductor and main coil. At load independent voltage gain frequency, ZPA of the input impedance and high power transfer efficiency can be obtained in S-SP compensated resonant converter (Hou et al., 2013). The main limitation of this compensation technique is the higher order harmonics which are injected into the rectifier network. These higher order harmonics create the problems for filter design. Therefore, a novel compensation network for IPT based EV charging system is required which provides ZPA of the input impedance, misalignment tolerance and high efficiency at load independent voltage gain frequency.

1.3 Objectives of the study

Based on the design criteria of the selection of charging pad for the dynamic charging of EV, the following objectives are specified:

(a) To propose a new charging pad topology and compensation network for IPT based electric vehicle (EV) charging application.

(b) To design and implement the dynamic charging of electric vehicle system using proposed pad topology and compensation network.

(c) To analyze the performance of the proposed system with negligible power transfer fluctuation characteristics and load independent operation under the dynamic condition of the electric vehicle.

1.4 Thesis outline

This research work is divided into five chapters including this chapter. The first chapter gives a short description of the research background associated with the problem statement, objectives of the research and the research methodology.

Chapter 2 presents a review of the current literature in the area of commonly used IPT based EV charging methods, various types of charging pads and compensation topologies and the performance parameters of the EV charging system.

The performance of the proposed topology of charging pads associated with the new compensation network has been explained in chapter 3 with the aid of finite element analysis, mutual inductance and coupling coefficient, frequency domain analysis, and time domain analysis.

Chapter 4 provides the experimental results of the proposed charging pad and compensation network based dynamic charging of EV application with some discussions. Also, proposed charging pad and compensation network has been compared with the conventional IPT charging pads and the compensation networks.

Finally, chapter 5 concludes the whole research with some key points of the future works.

CHAPTER 2: LITERATURE REVIEW

2.1 Introduction

The detailed literature review of the IPT based EV charging system is highlighted in this chapter. This chapter mainly focuses on the developments of IPT pads as well as compensation networks suitable for the EV charging systems. BEVs (battery electric vehicles) are fully electric vehicles, meaning they are only powered by electricity and do not have a petrol engine, fuel tank or exhaust pipe. BEVs can be charged either in conductive or wireless.

2.2 Wireless charging for EV

In order to obtain high efficiency, maximum power transfer distance and better misalignment tolerance, different wireless charging methods have been established. Based on power transfer distance, wireless power transfer methods can be categorized into two types: near field and far field. Near field is non radioactive than far field technology. Because of this, IPT is a popular near field technology for electric vehicle charging, which provides high efficiency with less power transfer distance. Another near field technology is CPT (capacitive power transfer). But this method is not effective for EV charging as it has a small amount of power range with less power transfer distance. For far field technology, microwave radiation is used for power transfer. Although far field technology is capable to transfer high power over long distances, efficiency is too low for EV charging. From 1978-2016, there are a lot of works have been done for the EV charging system. Some wireless based EV charging projects are summarized in Table 2.1. Among them, most of the projects are based on dynamic charging of EV.

Table 2.1: IPT based EV charging projects

Institute/Corporation	Year of Installation	Location	Vehicle Type	Power	Air Gap	Efficiency
Lawrence Berkeley Laboratory	1978(Bolger, Kirsten, & Ng, 1978)	USA	_	20kW	25mm	-
The University of Auckland	1997(G.A. Covic)	New Zealand	5 Golf buses	20kW	50mm	90-91%
	2002-2003(G.A. Covic)	Italy	8-23 mini buses	60kW	30mm	_
	2005 (Chwei-Sen, Stielau, & Covic, 2005)	New Zealand	_	30kW	45mm	_
	2010("Qualcomm Halo, WEVC Trials,")	New Zealand	Private vehicles	3kW	180mm	85%
Oak Ridge National Laboratory (ORNL)(J.M. Miller; J. M. Miller, White, Onar, & Ryan, 2012)	2010	USA	_	4.2kW	254mm	92%(coil-to-coil)
	2012	USA	_	7.7kW	200mm	93%(coil-to-coil)
	2012	USA	GEM EV	2kW	75mm	91%(coil-to-coil)
Korea Advanced Institute of Science and Technology (KAIST)	2009 (Sungwoo et al., 2010)	Korea	Golf bus	3kW	10mm	80%
			Bus	6kW	170mm	72%
			SUV	17kW	170mm	71%
	2010(Jiseong et al., 2013)	Korea	Tram	62kW	130mm	74%
	2012(Jiseong et al., 2013)	Korea	Bus	100kW	200mm	75%
MIT WiTricity	2010(WiTricity, WiT-3300)	USA	Private vehicles	3.3kW	180mm	90%
Evatran	2010("Plugless Power, Plugless Power vehicle compatibility.,")	USA	Private vehicles	3.3kW	100mm	90%
New Energy and Industrial Technology Development Organization	2010(Nagatsuka, Ehara, Kaneko, Abe, & Yasuda, 2010)	Japan	_	1.5kW	70±20mm	95%
Power Electronic Systems Laboratory, ETH Zurich	2013(Bosshard et al., 2015)	Switzerland	_	5kW	52mm	96.5%
	2016(Bosshard & Kolar, 2016)	Switzerland	_	50kW	160mm	95.8%

Before 2012, most of the researchers focus on the magnetic coupling and air gap variation without focusing the frequency. Especially from 2011, researchers are trying to increase the air gap variation between the two pads.

After 2013, researchers use the high frequency because it has a very big role in the efficiency of wireless EV charging system. In 2016, a huge project of about 50kW power rating is proposed by some researchers of ETH Zurich in Switzerland for public transport. In this above project, all performance parameters of EV charging are optimized in an organized way.

2.3 IPT based EV charging system

It is predicted that future transportation systems will be dominated by electric vehicles. The decrease of fossil fuel reserves in various parts of the world as well as the adverse environmental effects of using fossil fuels are two main factors contributing to this prediction. Whole over the world, IPT method is very familiar due to its high power transfer efficiency in a variety of applications, especially in electric vehicles (Kalwar, Aamir, & Mekhilef, 2015). In recent years, IPT systems developments have attracted special interest for EV charging applications.

IPT based EV charging system uses a varying magnetic field in order to transfer power through an air gap to a load without any electrical connection. In the case of IPT charging, energy is transferred magnetically identical to the operational principle of conventional transformers. This type of EV charging provides galvanic isolation along with other merits such as longevity, elimination of hazardous problems caused by the excessive thermal heating. Although EV is a possible solution for depleting energy reserves and to overcome the environmental issues, the limited mileage and time needed to recharge, less misalignment toleration and overall cost involved are still limitations. These issues require special consideration for the successful implementation of an electrically driven vehicle system worldwide. The quest for the solutions to the aforesaid issues has led researchers to develop the most useful method of wireless charging of EVs. The block diagram of a

typical inductive EV charging system is shown in Figure 2.1. It includes several stages to charge an EV inductively. The utility AC power is first rectified to DC with power factor correction, and then a high frequency resonant inverter converts the DC power to AC power in order to drive the transmitter pad through a compensation network and produce a magnetic field. According to Faraday's law of electromagnetic induction, another AC with the same frequency is obtained due to the magnetic field induced in the receiver pad. By resonating with the receiver compensation network, the transferred power and efficiency are significantly improved. At last, the AC power is rectified by an AC/DC converter to charge the battery. Figure 2.1 depicts the following main parts of an IPT based EV charging system:

(a) Transmitting and receiving pads. Usually, the pads are built with ferrite and shielding structure.

(b) Compensation networks.

(c) Power electronics converters.

(d) Battery of the vehicle side.
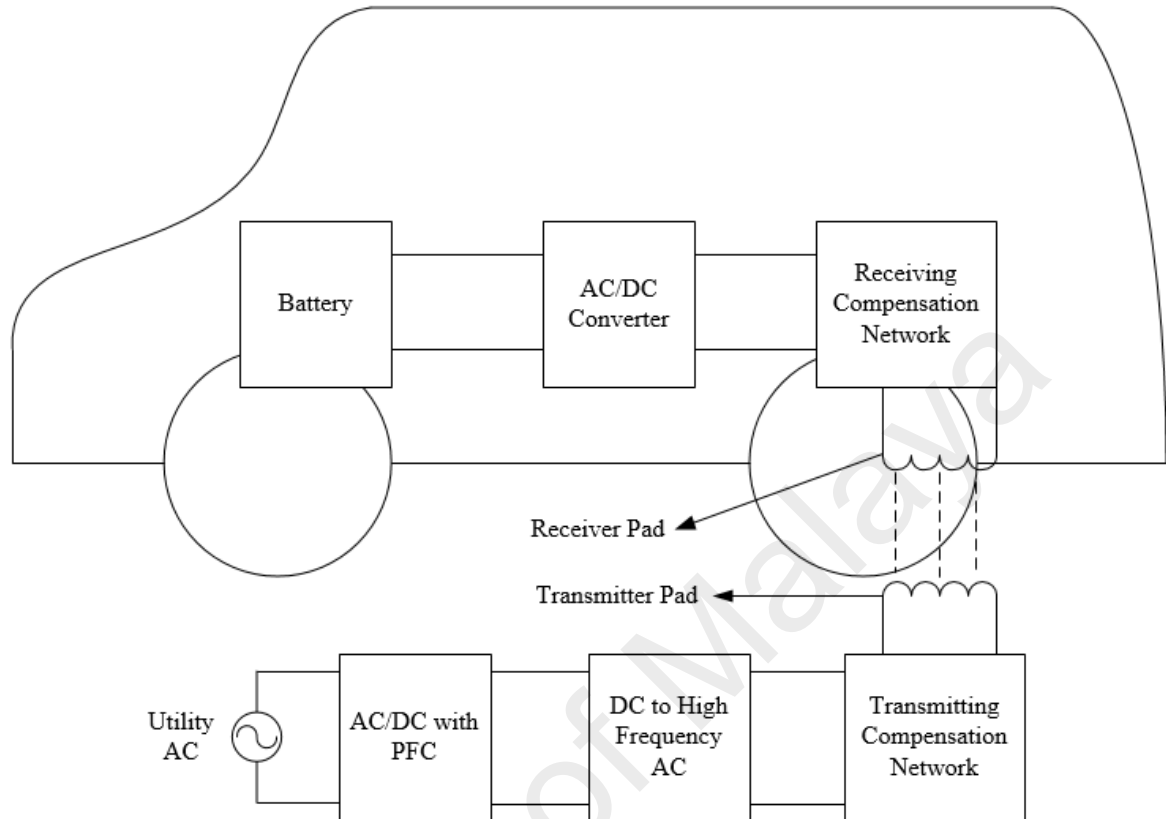
Figure 2.1: I PT based EV charging system.

2.4 Types of IPT based EV charging

In recent years, IPT systems developments have attracted special interest for EV charging applications. Electric vehicles as well as hybrid-electric vehicles can be inductively charged either in stationary mode or dynamic mode scheme.

2.4.1 Stationary charging

Depending on IPT systems, most of the researchers focus on the stationary charging. In the stationary charging mode, EV needs a specific place for charging. Electric vehicles are parked over the transmitter on the primary side and the receiver in the secondary side should be perfectly aligned with the transmitter.

Otherwise, large misalignment between the transmitter and receiver causes the significant drop in output power and efficiency (Deng et al., 2015). In addition, electromagnetic field radiation in the uncovered region has to be suppressed to minimize the harmful effects. It is noted that stationary charging system has higher market value and lower implementation cost compared to the dynamic charging system of EV. This charging system may be suitable for installation in homes, offices, parking areas, bus stops and hospitals.

Figure 2.2: Stationary charging of EV in Korea (WEVC, 2014).

2.4.2 Dynamic charging

On the other hand, dynamic charging EV system has been investigated; which can mitigate the weight, size of the battery and improve transportation efficiency (Gilchrist, Wu, & Sealy, 2012; Jan-Mou, Jones, Onar, & Starke, 2014; Jeong, Jang, & Kum, 2015). Based on vehicle position, EVs can be charged continuously while vehicles are in moving condition on the roadway. Dynamic charging of EV mainly categorized into two types, based on the design of transmitter: long-track (Jaegue et al., 2014; Pijl, Castilla, & Bauer, 2013; Prasanth & Bauer, 2014) and segmented-track(J. M. Miller et al., 2014).

Long-track based dynamic charging system can handle more vehicles at a time and this system is easier to control as whole track is supplied from a single source. It is commercially available in Korea, named as OLEV (Ko & Jang, 2013; W. Y. Lee et al., 2013). Because of the higher inductance of long-track, switching frequency should be limited. As a result, the efficiency of the long –track based system is low compared to the segmented-track based system. In the case of segmented-track, the transmitter is usually the same size of the transmitter in the stationary charging system (J. M. Miller, Jones, Jan-Mou, & Onar, 2015; Onar et al., 2013). Segmented-track based system gives higher efficiency and lower magnetic field emissions as transmitters are turned on and off according to the vehicle position. The major limitation of this system is its complexity as a huge number of compensation networks and power electronics converters are needed for this system. But, the need of a huge number of compensation networks and power electronic converters can be minimized by the different types of arrangement of transmitters (F. Lu, H. Zhang, H. Hofmann, & C. C. Mi, 2016b).
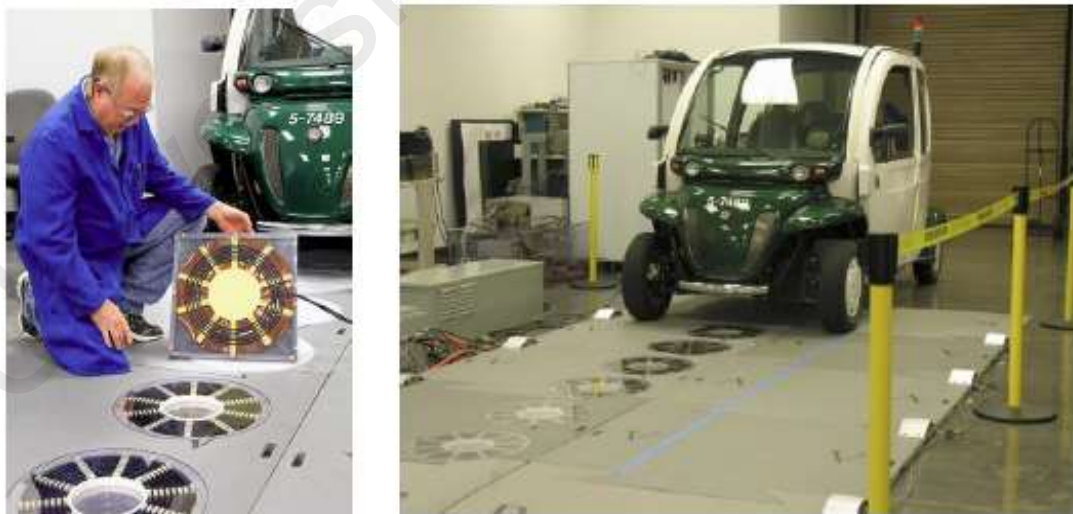
Figure 2.3: Dynamic charging test by ORNL (J. M. Miller et al., 2015).

2.4.3 Comparison of stationary and dynamic charging

Although most of the researchers focus on the stationary charging of EV, dynamic charging of EV is a promising technology for the future transportation system. A comparison between stationary and dynamic charging is represented in Table 2.2.

Table 2.2: Comparison between stationary and dynamic charging (Vilathgamuwa & Sampath, 2015)

Evaluation criteria	Stationary charging	Dynamic charging
Implementation cost	Low	High
Required power electronic converters	One	More than one
Market acceptance	High	Moderate
Misalignment tolerance	High	Not so high
Driving range	Limited	Unlimited
Battery in motion	Cannot be charged	Charged continuously
Number of vehicles handling	One	More than one
Transportation efficiency	Low	High

2.5 Equivalent circuit of the IPT based EV charging system

Even though IPT based system has various arrangements to compensate leakage or self inductance (Q. Chen et al., 2009; Xiaoyong et al., 2012), a SS compensated IPT based EV charging system with self-inductance compensation is selected for the equivalent circuit analysis because of its simplicity (Wei et al., 2014b). However, it minimizes the effect of

parameters that are associated with the optimization of efficiency. An IPT based network with SS compensation is depicted in Figure 2.4. L_T and L_R are the self-inductances of the transmitter and receiver side pads respectively and M is mutual inductance. C_T, C_R are the compensation capacitances of the transmitter and receiver side self inductances respectively. R_T and R_R are the internal parasitic resistances of the transmitter and receiver pads respectively and R_E is the ac equivalent load resistance of the rectifier and battery side. Figure 2.5 shows the T- equivalent circuit of the IPT based EV charging system of Figure 2.4.
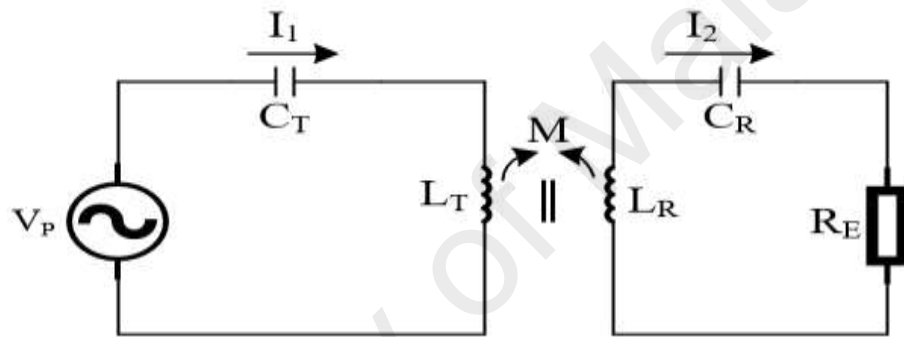
Figure 2.4: S-S compensated IPT based EV charging system.
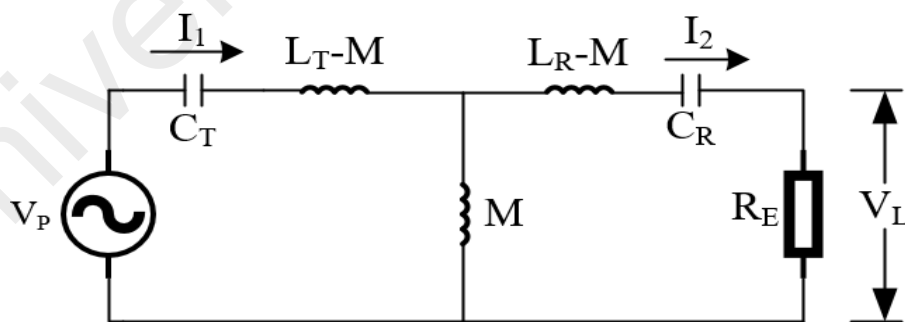
Figure 2.5: T-equivalent circuit of the IPT based EV charging system.

16

2.6 Performance parameters of IPT based EV charging

The main parameters that affect the efficiency and controllability of output power are: coupling factor, load independent operation and misalignment tolerance. In order to obtain high coupling coefficient and quality factor of the coils, load independent operation and better misalignment tolerance, most of the researchers have focused on the optimization of IPT-pad structures (Ahmed, Aamir, Uddin, & Mekhilef, 2015; Budhia et al., 2013; Budhia, Covic, Boys, et al., 2011). Another key factor that affects the efficiency and output power controllability of IPT system is the compensation network. Various types of compensation networks with the aid of control technique have been presented and explained in detail by many researchers (Budhia et al., 2013; Budhia, Covic, Boys, et al., 2011).

2.6.1 Coupling coefficient and quality factor of the coils

If there is no coupling between the transmitter and receiver, mutual inductance (M) between them is zero. Therefore, no coupling (k) exists. The traditional transformers having cores and no air gap termed as tightly coupled transformer. These transformers have $k \geq 0.5$. On the other hand, IPT transformers are referred to as loosely coupled transformers having $k \leq 0.5$. The value of M and thereby k depends on the physical dimensions and the number of turns of each pads, their relative position to one another and the magnetic properties of the core on which they are wound. There is also a probable reduction in the coupling coefficient due to the misalignment condition between the transmitting and receiver pads in both the stationary and dynamic charging of EVs. As efficiency is directly related to the coupling coefficient, it is greatly affected by the coupling coefficient in case of misalignment condition. The quality factor indicates that how much the coil is purely inductive. In order to make magnetic pad, a good quality factor based inductive coil is able to produce enough magnetic field for EV charging.

2.6.2 Load independent operation

To provide a smooth control of electric vehicles with IPT, load independent operation is desirable. Although load independent frequencies of IPT system are not always the resonant frequencies but it can give the better efficiency (Wei, Siu-Chung, Tse, & Qianhong, 2014a). Table 2.3 depicts a general characteristic of the load independent frequencies of IPT system. In case of S-S compensated IPT topology, a pair of constant voltage transfer (CVT) frequencies can be found subjected to the coupling coefficient k. On the other hand, only one CVT frequency exists for S-P compensated IPT topology which is always higher than the nominal frequency. However constant current transfer (CCT) frequencies have an opposite operation with the CVT frequencies. In case of S-S topology, nominal frequency acts as a CCT frequency whereas a pair of CCT frequency is used for S-P topology. It has the same location of the CVT frequencies of S-S topology.

Table 2.3: CVT/CCT frequency for S-S and S-P topologies

	S-S	S-P
ω_{CVT}	$\dfrac{\omega_0}{\sqrt{1 \pm k}}$	$\dfrac{\omega_0}{\sqrt{1 - k^2}}$
ω_{CCT}	ω_0	$\dfrac{\omega_0}{\sqrt{1 \pm k}}$

When the operating frequency is variable, S-S and S-P topologies can be operated between constant voltage and constant current mode. This is a desirable characteristic for EV charging because the battery is first charged first by constant current and then by a constant voltage. Therefore, under the load independent operation, there will be only three fixed frequencies under full range operation with no need to change the compensation capacitors. Load independent CVT characteristics of an S-S topology based IPT system is presented in

(Wei et al., 2014a). From Table 2.3, the load independent CVT frequencies are highly related to the coupling coefficient k. In the EV charging applications, the mutual inductance will change from zero to its maximum value and then back to zero when the vehicle is passing one of the primary pads (K. Lee, Pantic, & Lukic, 2014; J. M. Miller, Jones, Jan-Mou, & Onar, 2015; Wei, White, Abraham, & Mi, 2015). Also, coupling coefficient k is directly related to the mutual inductance. In such condition, the stable voltage transfer is hard to maintain. As a result, some researchers on load independent voltage transfer usually focus on the stationary conditions (Qu, Han, Wong, Tse, & Chen, 2015; Wei et al., 2014a). Variation of mutual inductance almost has a proportional influence on voltage transfer ratio. This effect gets severe when the load is heavy.

2.6.3 Misalignment tolerance

When receiver pad is not properly aligned with the transmitter pad is called misalignment which leads to the reduction of the efficiency associated with power transfer fluctuation. The misalignment between the charging pad which is mounted on the EV chassis and the charging pad which is buried under the road directly affects the power transfer and efficiency of the IPT based EV charging system (Villa et al., 2012; Wei et al., 2014b). Therefore, maximum misalignment tolerance of a charging pad is required in order to avoid the ineffectual power transfer due to the driver inaccuracy while parking the electric vehicle in the appropriate position (Budhia, Covic, & Boys, 2009). The IPT based EV charging system with precise alignment of receiver pad will minimize the leakage flux. Consequently, it reduces the intrusion of electromagnetic emission from the system. Misalignment can be categorized as lateral (horizontal) and longitudinal (vertical), in which horizontal misalignment can exist when coils are laterally misaligned and vertical misalignment can appear when the coils are unstable with respect to their length (Prasanth

& Bauer, 2013). Like charging pad, compensation networks also have a great contribution on the misalignment tolerance (Villa et al., 2012).It is possible to transfer the rated power by selecting the proper charging pad and compensation network.

2.7 Types of charging pad

Overall performance of the EV charging system is influenced by the design of the transmitter and receiver pads, misalignment and load condition etc. (Prasanth & Bauer, 2013; Stamati & Bauer, 2013; Wei, Siu-Chung, Tse, & Qianhong, 2014c). Based on those issues of performance parameters, transmitter pads are designed. Transmitter side pad placed under the road side is an important part of dynamic charging EV system developments. In general, transmitter pads are roughly categorized into two: long track (Elliott, Covic, Kacprzak, & Boys, 2006; Jaegue et al., 2014; Pijl, Castilla, & Bauer, 2013; Prasanth & Bauer, 2014) and segmented track (J. M. Miller et al., 2014; Onar et al., 2013; Sampath, Vilathgamuwa, & Arokiaswami, 2015).

Long track transmitter guided configuration is normally much longer than the length of EV. Therefore, it can handle more vehicles at a time (Covic, Boys, Kissin, & Lu, 2007). The structure of the long track guided based system is simple and easy to control, as it is supplied by the single source. This power processing transmitter system is composed of a high-frequency inverter and PFC (power factor correction) converter, partially built and tested in Korea, which is named as an online electric vehicle (OLEV) (Ko & Jang, 2013; W. Y. Lee et al., 2013). As the whole track transmitter is always in running condition, this system may cause the significant power loss and magnetic-field radiation effect with a lower magnetic coupling coefficient. To cancel out the magnetic-field radiation, this kind of transmitter can be warped into an "X" shape (S. Choi, Huh, Lee, Lee, & Rim, 2013) and an additional coil could be added to the transmitter assembly for field canceling purpose (S.

Y. Choi et al., 2014). In the case of lateral misalignment condition, the output power tolerance has been improved by the asymmetric design of the each of the transmitters and receiver pads (Huh, Lee, Lee, Cho, & Rim, 2011). In other cases, an extra quadrature coil can be added to the receiver pad to further increase of misalignment ability (Elliott, Raabe, Covic, & Boys, 2010; Raabe & Covic, 2013). The maximum efficiency of OLEV system is lowered from a practical point of view. Because, the inductance of the long-guided track transmitter becomes so large, the operating frequency of the high-frequency inverter is normally limited up to 20 kHz. As a result, the quality factor of the long track transmitter pad is actually lower than the segmented track transmitter pad which usually operates at 85 kHz.

In the case of segmented track transmitter pad setting, the size of the transmitter pad assembly is same as the transmitter itself in the stationary EV charging system which is typically within 1m (J. M. Miller et al., 2015). The segmented transmitter pads are arranged as an array to form a tracking lane for the EV. As each segmented transmitter pad with a certain structure has its own compensation network, it is more convenient to design and architect the effective length of the powered roadway. In addition to, these transmitter pads are turned in accordance with the receiver pad position. When the receiver pad passes over, transmitter pad can be turned off resulting in higher efficiency and lower magnetic leakage flux distribution (L. Chen, Nagendra, Boys, & Covic, 2015; K. Lee et al., 2014). The limitation of the segmented transmitter architecture is its complexity as it needs a huge number of compensation networks and power electronic converters. This configuration increases the cost than a long guided track transmitter. Therefore, several segmented transmitter coils can be connected in series or parallel to share the same power electronic converter in order to minimize the total cost. Another limitation is the power transfer

fluctuation, experienced by the receiver pad when it moves. Most of the transmitters are normally arranged far away from each other to minimize the self-coupling. Consequently, magnetic-field is weak and power of the receiver side drops when the receiver pad is in a position between the two transmitters (K. Lee et al., 2014). To reduce the power drops characteristics, transmitters can be placed so as to close each other. As a result, power received in the middle position can be increased due to an increase of magnetic field between the transmitters. It is noted that power transfer fluctuation phenomena still exists in (J. M. Miller et al., 2015; Onar et al., 2013). If the distance between the transmitters keeps decreasing, self-coupling between the transmitters has to be solved. The issues on self-coupling and power transfer fluctuation can be adjusted by the proper design of the transmitter and receiver pads as well as its arrangement.

In the case of stationary charging of electric vehicle, the transmitters are usually designed in a pad form whereas transmitters are basically in a track form for dynamic charging of electric vehicle. If each segmented track is short enough, the track becomes like a pad in the stationary charging. Also, the pads used in the stationary charging can be used for the dynamic charging of electric vehicles with different types of arrangements (Bertoluzzo, Buja, & Dashora, 2016; F. Lu, H. Zhang, H. Hofmann, & C. C. Mi, 2016b; Zhang et al., 2016). There are different types of charging pad used in charging of electric vehicles such as circular, flux pipe, DD, DDQ, QDQ, Bipolar.

2.7.1 Circular pad

Circular pad is a non polarized pad. Due to this property circular pads are not normally designed to couple with polarized pads. Therefore, if a vehicle is mounted with a circular pad as a receiver and parks over a polarized transmitter pad which is buried under the road there will be a loss of power and a significant leakage flux which is not desirable for EV

charging application (Covic et al., 2011).Fundamental flux path height of a circular pad is one-quarter of the pad diameter so that coupling is not good between two circular pads (Budhia, Covic, & Boys, 2010). To have a large air gap, the good coupling can be achieved by using the large diameter of the charging pad, which makes the whole system impractical and costly (Budhia, Covic, & Boys, 2011).Because of this, circular pad is very challenging for EV charging in case of large air gaps and high power. Circular pad as a transmitter generates the vertical field only. So that when another circular pad as a receiver perfectly aligned above the circular transmitter pad, a fair power transfer is possible. Due to the property of this type of field, circular pads do not show the good tolerance of misalignment as well as vertical separation. However, circular pads are not effective for dynamic charging of EV as they provide a null zone of power transfer when receiver pad is horizontally misaligned by 38% of the pad diameter of the transmitter pad (Budhia, Covic, & Boys, 2011).The basic layout of a circular pad is shown in Figure 2.6.
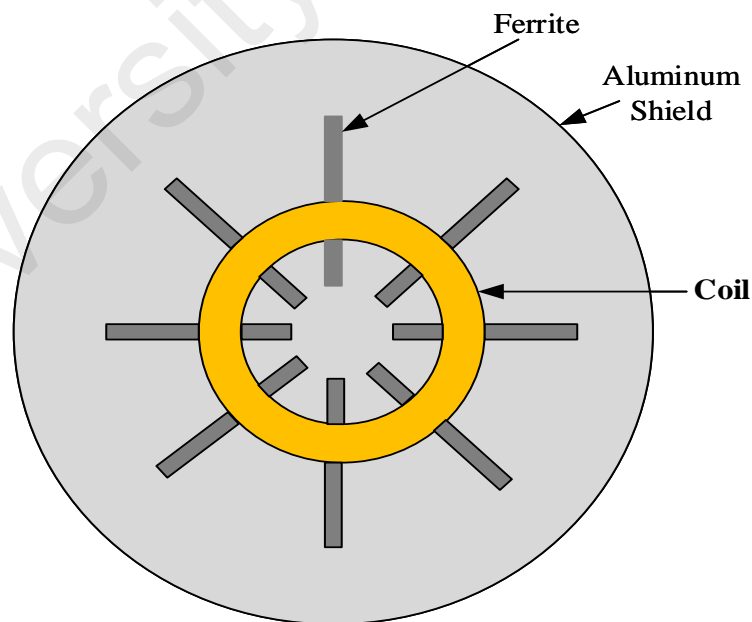
Figure 2.6: Circular pad.

2.7.2 Flux-pipe pad

To overcome the limitation of the flux path height of a circular pad topology, flux pipe pad topology is introduced in (Budhia et al., 2010). In this case, the pad is formed by a wounded coil along an H-shaped ferrite bar as shown in Figure 2.7.

This topology significantly minimizes its fundamental flux path height to about half of the pad length which helps to the reduction of the pad size with a better horizontal misalignment tolerance. Also, this flux pipe pad is responsible for producing the double sided flux path in which "non-useful flux" results in a particular loss in the aluminum shields which are set up behind the pad (Trong-Duy, Siqi, Weihan, & Mi, 2014).
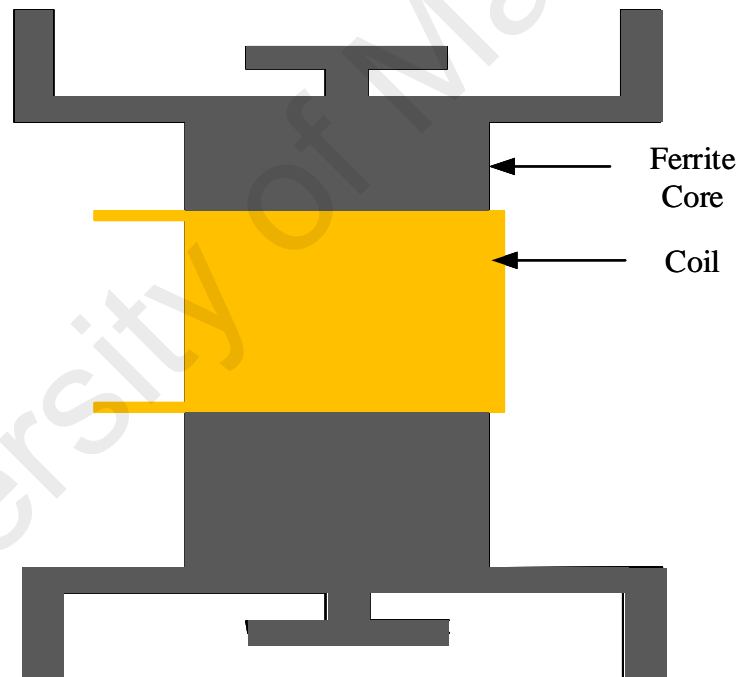
Figure 2.7: Flux-pipe pad.

2.7.3 DD pad

To overcome the limitation of the circular and flux pipe pad, a single sided flux path based polarized topology named DD pad is proposed in (Budhia et al., 2013).

It is formed using two "D" shaped coils with back to back connection to form a north and south pole shown in Figure 2.8. Consequently, this type of pad is referred to as DD pad. Since DD pad is polarized; it produces a horizontal field which enables remarkable improvements in coupling and misalignment tolerance. Like flux pipe pad, the flux path height of a DD pad is about half of the pad length. However, this flux path height can be controlled by adjusting the width of the overlapping part of the two "D" shaped coils. The charging zone of DD pad is about two times larger than the circular pad. If the driving direction is along the y-axis, DD pad gives a good solution for dynamic charging of EV. Because this pad provides a good misalignment tolerance in the y-direction. Similar to the circular pad, it also provides a null zone of power transfer in the horizontal misalignment of 34% of the pad length (Budhia et al., 2013).
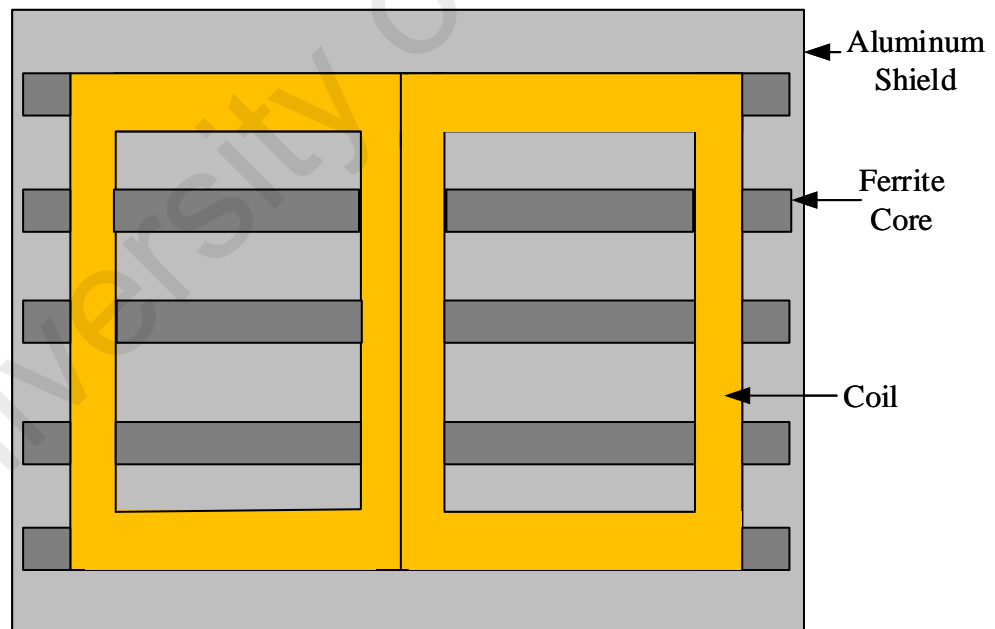
Figure 2.8: DD pad.

2.7.4 DDQ pad

To increase the horizontal misalignment tolerance, an additional quadrature (Q) coil is introduced to perform together with the DD pad which is called as DDQ pad (Budhia et al., 2013; Budhia, Covic, Boys, et al., 2011; Covic et al., 2011). Flux path height of a DDQ pad is about two times of circular pad with an extra single sided flux path. Although null zone of power transfer occurs at 77% of the pad length, it requires more copper than any other conventional pads (Zaheer, Kacprzak, & Covic, 2012). Figure 2.9 represents the basic layout of a typical DDQ pad.
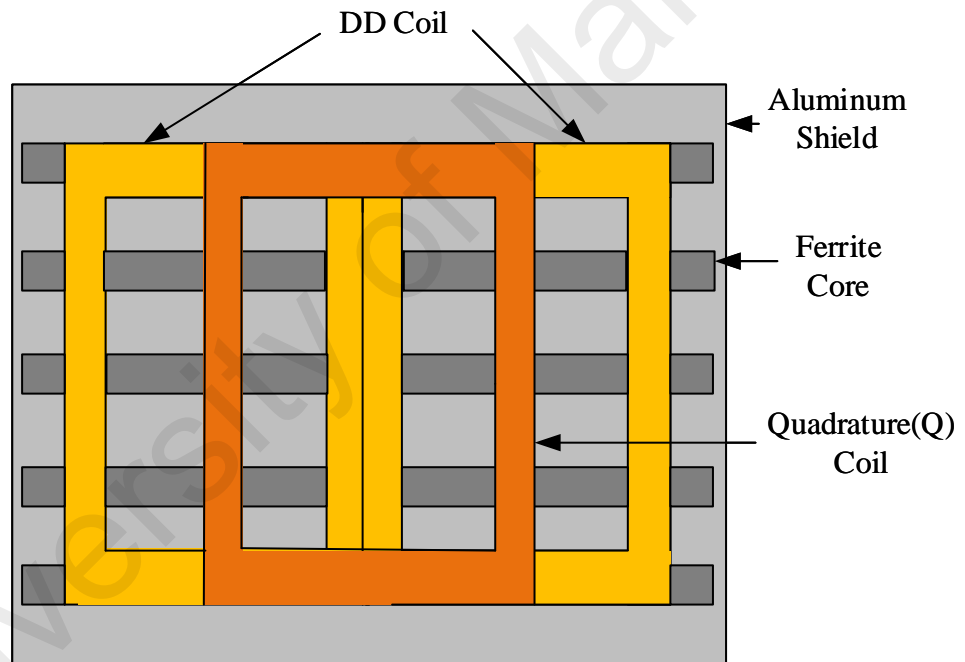
Figure 2.9: DDQ pad.

2.7.5 Bipolar pad

A moderate version of DD pad named bipolar pad is proposed by University of Auckland (Covic et al., 2011; Trong-Duy et al., 2014; Zaheer et al., 2012).By expanding the size of each pad and creating some overlap between the two D coils, this topology has a similar

performance of the DDQ pad with less amount of copper. The basic layout of the bipolar pad is shown in Figure 2.10.
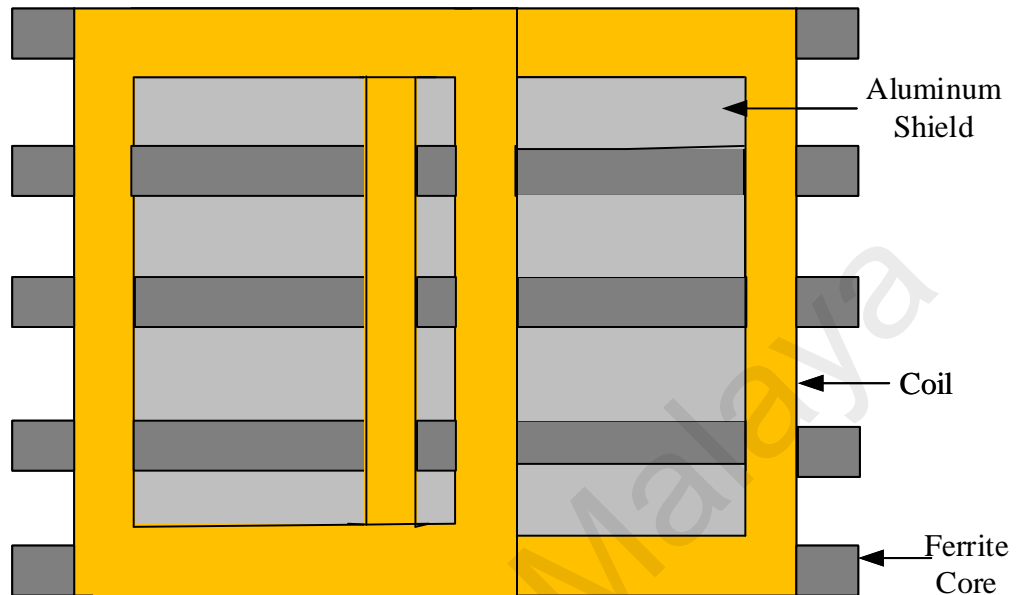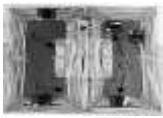
Figure 2.10: Bipolar pad.

2.8 Comparison of conventional IPT pads

Most commonly used pad topologies applicable for EV charging systems are circular, DD, DDQ and bipolar. Among all topologies, circular has very poor misalignment tolerance because of less flux path height. On the other hand, DDQ pad provides good misalignment tolerance like bipolar pad associated with the negligible effect of power transfer fluctuation when it is under misalignment condition. The detailed comparison of the different conventional pads is shown in Table 2.4.

Table 2.4: Comparison of different conventional pads

Pad topology	Evaluation criteria			
	Overview	Flux path height	Misalignment Tolerance	Null zones of power transfer with horizontal offset
Circular		1/4 of the pad diameter (Budhia et al., 2010)	Not so good	Occurs at about 38% of the pad diameter (Budhia, Covic, Boys, et al., 2011)
DD		½ of the pad length (Budhia, Covic, Boys, et al., 2011; Siqi & Mi, 2015)	Good tolerant in the y-direction	Creates at about 34% of the pad length (Budhia et al., 2013)
DDQ		2 times of circular with an extra single sided flux path (Budhia, Covic, Boys, et al., 2011)	DD coil provides good tolerant in y-direction and Q coil provides good tolerant in x-direction	Occurs at about 77% of the pad length (Zaheer et al., 2012)
Bipolar		2 times of circular	Good tolerant in both direction	Similar to DDQ (Zaheer et al., 2012)

2.9 Types of compensation network

Four conventional compensation techniques that are widely used named as S-S (series-series), S-P (series-parallel), P-S (parallel-series), and P-P (parallel-parallel).Some other compensation techniques used by the researchers are SP-S, LCL, LCC-LCC, S-SP. Transmitter and receiver compensation capacitances are selected based on the following criteria:

(a) Mainly receiver-capacitance is chosen so as to compensate the leakage inductance of the receiver side and the mutual inductance. Receiver compensation capacitance is very important because it causes the improvement of the power transfer to the load.

(b) On the other hand, transmitter-capacitance is selected in order to compensate the self inductance of the transmitter side and the inductance of the whole circuit. Transmitter compensation capacitance has a great contribution to get the unity power factor.

2.9.1 S-S compensation network

The efficiency of the S-S compensated converter is high when self inductances of the transmitter and receiver are tuned (Wei et al., 2014b). Comparison between self inductance compensation and leakage inductance compensation of S-S topology is presented in (Q. Chen et al., 2009; Xiaoyong et al., 2012). However, self-inductance tuned by the S-S compensation presents output voltage which is very sensitive to the output load changes (Wei et al., 2014b). In order to improve the sensitivity of the output voltage under wide load variation, SS compensated converter is designed to operate around the frequency of load independent voltage gain (Q. Chen et al., 2009; Xiaoyong et al., 2012). On the other hand, zero phase angle (ZPA) of the input impedance is not maintained at a frequency of load independent voltage gain. Therefore, efficiency may be lower because of circulating current. In (Wei et al., 2014b), a tradeoff between output voltage controllability and efficiency of the S-S topology is presented. Moreover, the problem still exists as tuning of compensating capacitors is not easy to obtain.
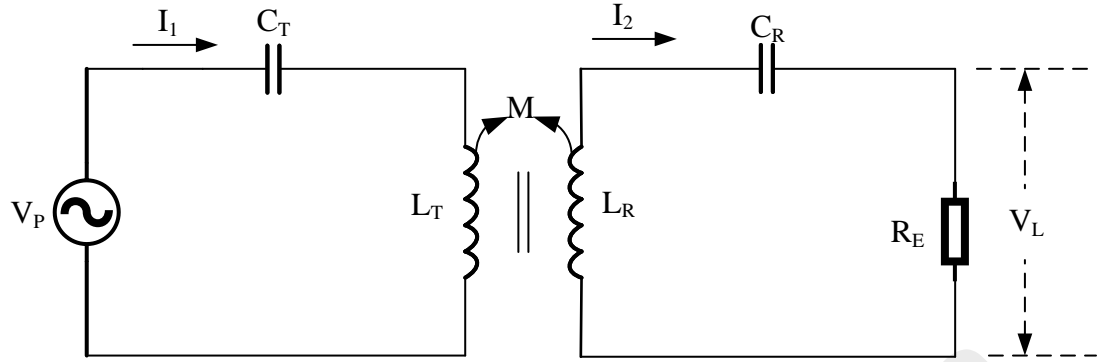
Figure 2.11: S-S compensated IPT system.

2.9.2 S-P compensation network

Since, S-P compensation provides ZPA of the input impedance at load independent voltage gain frequency (Wei et al., 2014a), which is suitable for high power applications (Hasanzadeh & Vaez-Zadeh, 2011). Furthermore, S-P compensation is not effective for a wide variation of coupling coefficient and misalignment as load independent voltage gain is inversely related to the coupling coefficient (Hou et al., 2013).
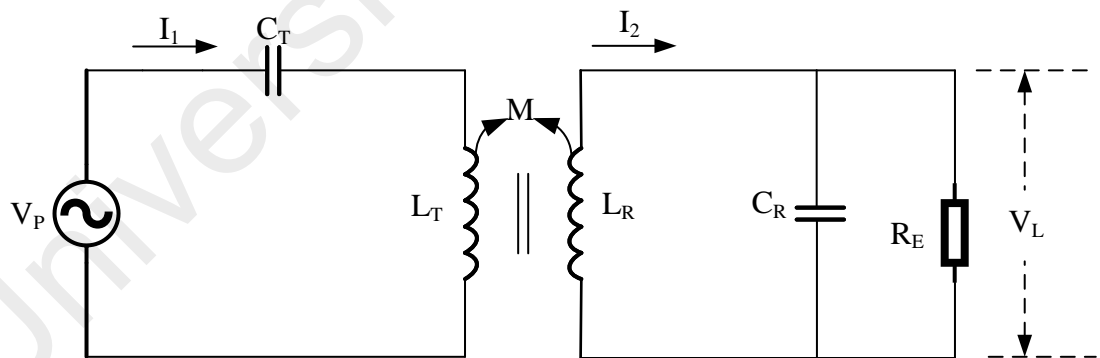
Figure 2.12: S-P compensated IPT system.

2.9.3 P-S and P-P compensation network

Among four compensation techniques, P-S and P-P compensated IPT systems are safe for the supply in the absence of pick-up coil. But these compensation techniques are not

suitable to transfer the rated power in case of misalignment condition, as resonant capacitor value strongly depends on the magnetic coupling coefficient and the output load (Chwei-Sen et al., 2004).

(a)

(b)
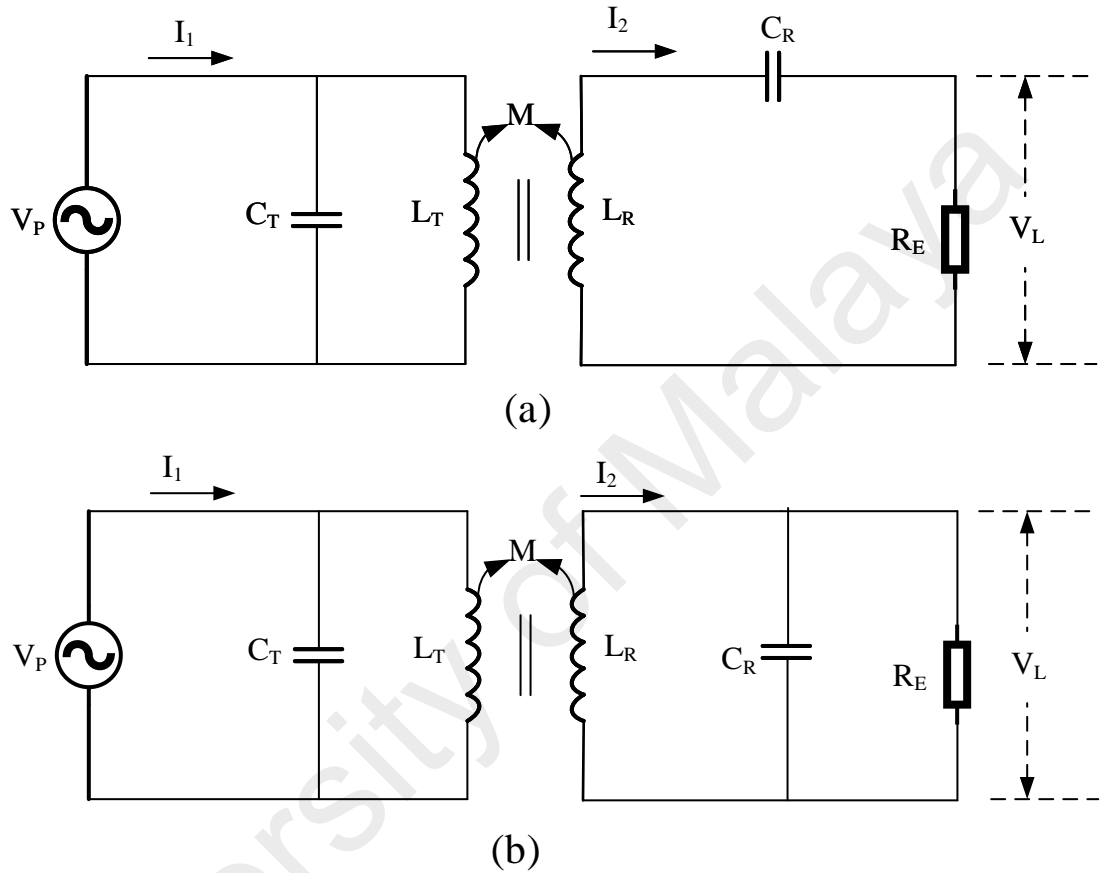
Figure 2.13: (a) P-S and (b) P-P compensated IPT system.

2.9.4 SP-S compensation network

To maintain a unique output power under the changes of coupling, SP-S compensation network was presented in (Villa et al., 2012). Basically, this network is the combination of the characteristics of S-S and P-S compensation networks.
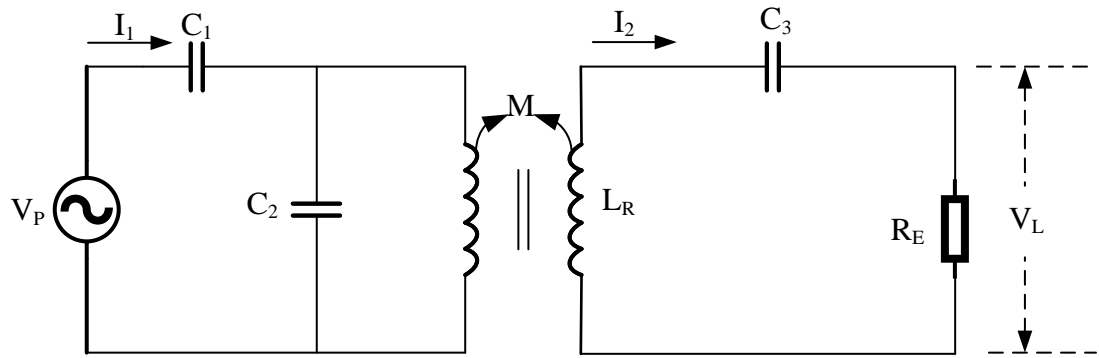
Figure 2.14: SP-S compensated IPT system (Villa et al., 2012).

2.9.5 LCL compensation network

There is a large number of research works based on LCL compensation (Huang, Boys, & Covic, 2013b; Keeling et al., 2010; Raabe & Covic, 2013; Wu et al., 2012).In (Huang et al., 2013b), a series-parallel LCL tuned unity pick up was presented, that provides uninterrupted power but it reflects reactive power back onto the source (Amjad et al., 2013).
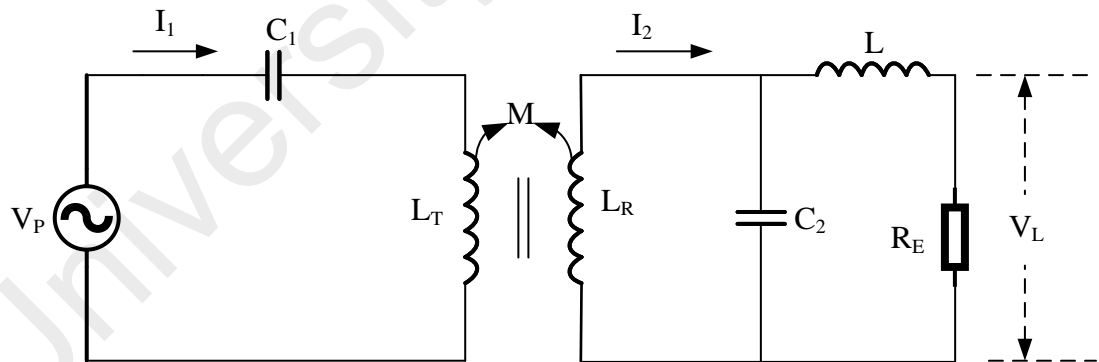
Figure 2.15: LCL compensated IPT system (Keeling et al., 2010).

2.9.6 LCC-LCC compensation network

Compensation topology with high efficiency named LCC was used in the areas of EV (electric vehicle) charging (F. Lu, H. Zhang, H. Hofmann, & C. Mi, 2016a; Zhu et al.,

2016). Here, load independent voltage gain under coupling changes is very much difficult to obtain because of self coupling between the compensation inductor and main coil. This kind of compensation network with appropriate tuning method secures that the resonant frequency is independent of coupling coefficient and load conditions (Li, Li, Deng, Nguyen, & Mi, 2015).
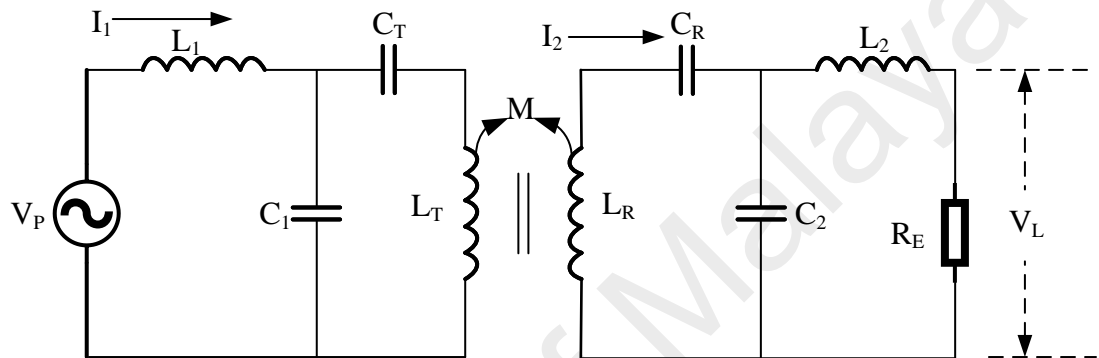
Figure 2.16: LCC-LCC compensated IPT system (Lu et al., 2016a).

2.9.7 S-SP compensation network

At load independent voltage gain frequency, ZPA of the input impedance and high power transfer efficiency can be obtained in S-SP compensated IPT system (Hou et al., 2013).The main limitation of this compensation technique is the higher order harmonics which are injected into the rectifier network. These higher order harmonics create the problems for filter design. S-SP compensation network gives the constant gain value, independent of load change and coupling coefficient.
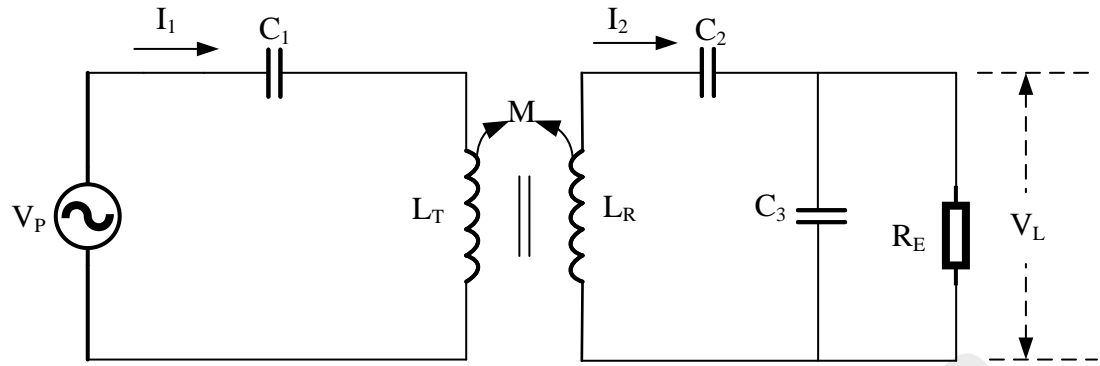
Figure 2.17: S-SP compensated IPT system (Jia, Qianhong, Siu-Chung, Tse, & Xinbo, 2015).

2.10 Comparison of different compensation networks

Tolerance of power factor to variable frequency is very higher in the case of S-S, P-S, S-SP and LCC-LCC compensation technique whereas tolerance of efficiency to variable frequency is higher only for S-P and P-P. Maximum efficiency is found for S-S and S-P compensation technique. On the other hand, load independent voltage gain is applicable for S-S, S-P, S-SP and SP-S whereas P-S, P-P and LCC-LCC compensation technique do not provide load independent voltage gain. The general comparison among different types of compensation networks is listed in Table 2.5.

Table 2.5: Comparison of different compensation networks

Compensation networks	Evaluation criteria			
	Maximum efficiency	Tolerance of efficiency to variable frequency	Tolerance of power factor to variable frequency	Load independent voltage gain
S-S (Wei et al., 2014b)	94.6%	Low	High	Directly related to coupling
S-P (Wei et al., 2014a)	94.6%	High	Low	Inversely related to coupling
P-S(Chwei-Sen et al., 2004)	94.2%	Low	High	Hard to obtain
P-P(Chwei-Sen et al., 2004)	94.3%	High	Low	Hard to obtain
S-SP (Jia et al., 2015)	93%	Low	High	Coupling independent
SP-S (Villa et al., 2012)	93%	Low	Low	Coupling dependent
LCC-LCC (S. Li et al., 2015)	93.5%	Low	High	Hard to obtain

2.11 Operating frequency selection

Operating frequency is related to the amount of power to be transferred. To transfer the high power, higher operating frequency should be selected. But the selection of high operating frequency is limited due to the switching speed of inverter. However, AC resistance increases with frequency due to skin effect losses. To ensure maximum efficiency, coupling coefficient and quality factor of the coil should be high. The coupling coefficient may be enhanced by the various shapes of the magnetic coil associated with ferrite core and aluminum shield. Generally, the inductance of a coil is determined by its architecture and that is not dependent on the operating frequency. Therefore, a highest quality factor of the coil can be achievable by selecting the optimum frequency. Keeping concern about EMF (Electromagnetic Field) exposure limit, SAE (Society of Automotive

Engineers) selected the operating frequency range of 80-90 kHz. In 1978, Lawrence Berkeley Laboratory used the frequency of 180Hz for an electric highway system and observed the problem of cost effectiveness because it needs huge conductor size for that low frequency (Bolger et al., 1978). After so many years, some researchers of University of Auckland increased the frequency to 20 kHz (Covic & Boys, 2013b) which reduces the weight of the power pads but efficiency is still not so high because of insufficient frequency. In 2010, a frequency of 30 kHz with efficiency less than 80% was used by Korea Advanced Institute of Science and Technology (KAIST). Finally, Bosshard and Kolar of ETH Zurich used the frequency of 85 kHz (SAE standard frequency) and got the efficiency of 95.8% in 2016 (Bosshard & Kolar, 2016).

2.12 Control methods

To control the transfer-power, different control methods are investigated by the researchers. Depending on the location of control action, control method can be classified as primary side control (Miller, White, Onar, & Ryan, 2012; Wei et al., 2012), secondary side control (Chwei-Sen, Stielau, & Covic, 2005; Hsu, Hu, & Swain, 2009) and dual side control(Wu, Gilchrist, Sealy, & Bronson, 2012).Usually, primary side and dual-side control are only suitable for transferring power from one transmitter pad to one receiver pad. However, secondary side control can be used in the system, where multiple receiver pads are powered from one transmitter pad or track. Primary side control can be investigated by changing the frequency, duty cycle and the phase between two legs. Secondary side control can be done by placing buck or boost converter, additional dc inductor, diode etc after the rectifier. Dual-side control is a combination of both primary and secondary side control. Using this control system, complication and cost may arise but the efficiency can be optimized.

2.13 Safety concerns of IPT based EV charging system

Although IPT based EV charging system has several advantages, it needs some safety considerations in response to electrical shock due to the high electrical power, high magnetic field exposure to the humans, and probable fire hazards. These considerations are due to the need of large power levels and electromagnetic field, operation in hazardous locations. Electromagnetic field (EMF) exposure is a major problem for IPT based EV charging system. EMF exposure needs to be strictly analyzed to be within tolerable levels by some international safety standards such as ICNIRP (International Commission on Non-Ionizing Radiation Protection) and ICES (International Committee on Electromagnetic Safety) for the normal condition as well as unusual conditions. IPT pads should be physically isolated to prevent any electrical shock of humans and animals to the conductors. Excessive heating due to the excessive current flow should be monitored to prevent any fire hazards.

2.14 Summary

A brief review of the performance parameters about the IPT based EV charging systems is explained in this chapter. This chapter mainly highlights the literature on the topology based classification of the charging pads associated with the different compensation networks, applicable for IPT based EV charging applications. Based on the analysis of the literature review, there is a need of charging pad associated with proper compensation network which will provide maximum power with minimum power transfer fluctuation under misalignment condition. In the next chapter, analysis of the proposed topology of the charging pad associated with the compensation network will be explained.

CHAPTER 3: RESEARCH METHODOLOGY

3.1 Introduction

Enhanced structure and optimization of IPT magnetic pad suitable for dynamic charging EV applications based on appropriate simulation, theoretical analysis, and experimental results are presented in this chapter. In this research, a large rectangular section of the transmitter pad is series connected with two zigzag shaped small rectangular sections. These small sections are back to back series connected and located inside the large rectangular section. An adjacent pair of proposed transmitter pads with back to back series connection, named as extended DD transmitter pad is used throughout this work. Also, a novel LC-LC^2 compensation network for IPT system is proposed in this research, which provides ZPA of the input impedance and high efficiency at load independent voltage gain frequency like S-SP compensated resonant converter.

3.2 Research methodology

To fulfill the above objectives of this research work, a detailed research methodology of this research topic is illustrated which is shown in the following figure. In order to develop the proposed EV charging system, mathematical modeling and theoretical analysis are performed to find out the design specifications. Each part of the proposed system is examined using simulation software MATLAB/Simulink and COMSOL. After implementing the hardware set-up, experimental results are analyzed with the simulation results based on the optimum selection parameters of the system.
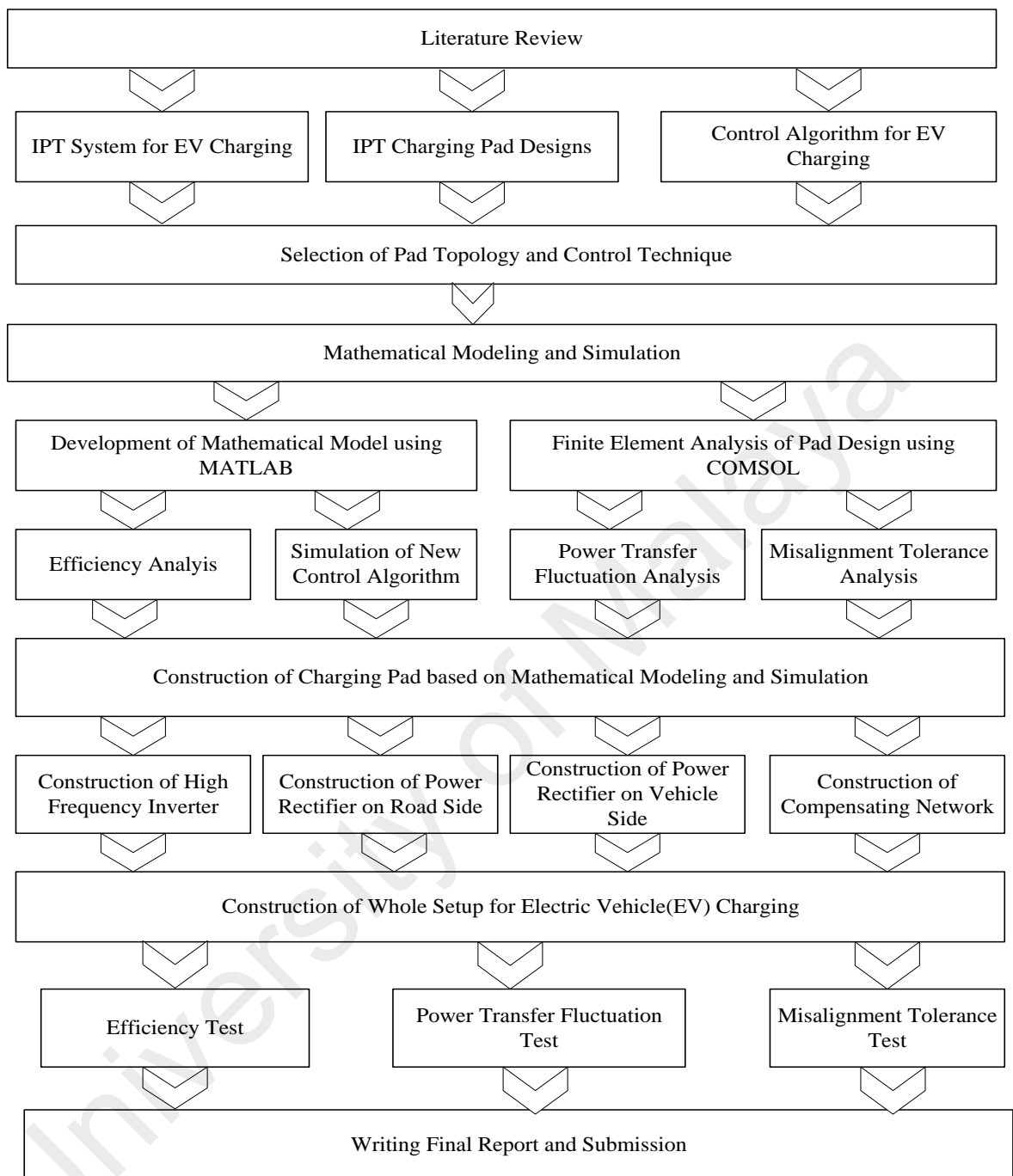
Figure 3.1 : Detailed flow chart of the research methodology.

3.3 Design criteria for IPT based EV charging

Generally, maximum power transfer for IPT system occurs in the resonant frequency (f)

condition. However, to obtain the resonant condition, some parameters are responsible.

Those are transmitter and receiver inductances (L_T and L_R) with their respective

compensation capacitances (C_T and C_R) respectively. To get the maximum power transfer efficiency under a resonant condition, the following condition has to be maintained:

$$f = \frac{1}{2\pi\sqrt{L_T C_T}} = \frac{1}{2\pi\sqrt{L_R C_R}} \tag{3-1}$$

However, design process of IPT based EV system also depends on coupling coefficient, the quality factor of the coils, load condition and the amount of power transfer. Depending on those parameters resonant frequency, inductances, and capacitances are chosen. Usually, the air gap of IPT systems is set at less than the radius of the transmitter or receiver coils to maintain a high efficiency. The distance of IPT in the case of energy transfer can be extended by applying a high quality factor based IPT coils with the aid of high operating frequency. Furthermore, a high operating frequency could cause large power losses and question for good power regulation. Consequently, an IPT system operating from 10 kHz – 200 kHz should be satisfactory for high power applications (kW level) like electric vehicle charging and is a superior trade-off between power transfer capability, efficiency, and robustness of the system.

3.4 Proposed magnetic pad structure

Under the following assumptions, magnetic pads are designed:

(a) Receiver pad is identical to one part of the extended DD transmitter pad.

(b)   Mutual inductances under perpendicular segments are negligible.

(c) Transient conditions for all switching states are not changed significantly from one transmitter pad to another.

The design procedure of the magnetic pad is explained with the help of flow chart, shown in Figure 3.2. The design procedure of the magnetic pad is performed with the help of geometry and frequency evaluation. Geometry evaluation is observed with the help of

mutual inductance and surface magnetic field optimization techniques using FEA. On the other hand, frequency evaluation is carried out by the load independent voltage gain and efficiency optimization. Each of the transmitting and receiving pads has three rectangular sections shown in Figure 3.4. The adjacent pair of transmitter pads with back to back series connection named as extended DD transmitter, driven by a single source, depicts a bipolar characteristic. Inside each of the sections of extended DD transmitter, two small rectangular sections having zigzag shape are located with back to back series connection.

It is noted that large rectangular section is also series connected with the smaller sections. Because of this zigzag shape, the uniform magnetic flux distribution is obtained. Since the identical current direction reinforces the magnetic fields of the neighboring transmitter pads; this brings about a near stable mutual inductance under misalignment condition of the receiver coil. As extended DD transmitter represents the bipolar characteristics, this helps to eliminate the self-coupling between the transmitters (Covic et al., 2011).
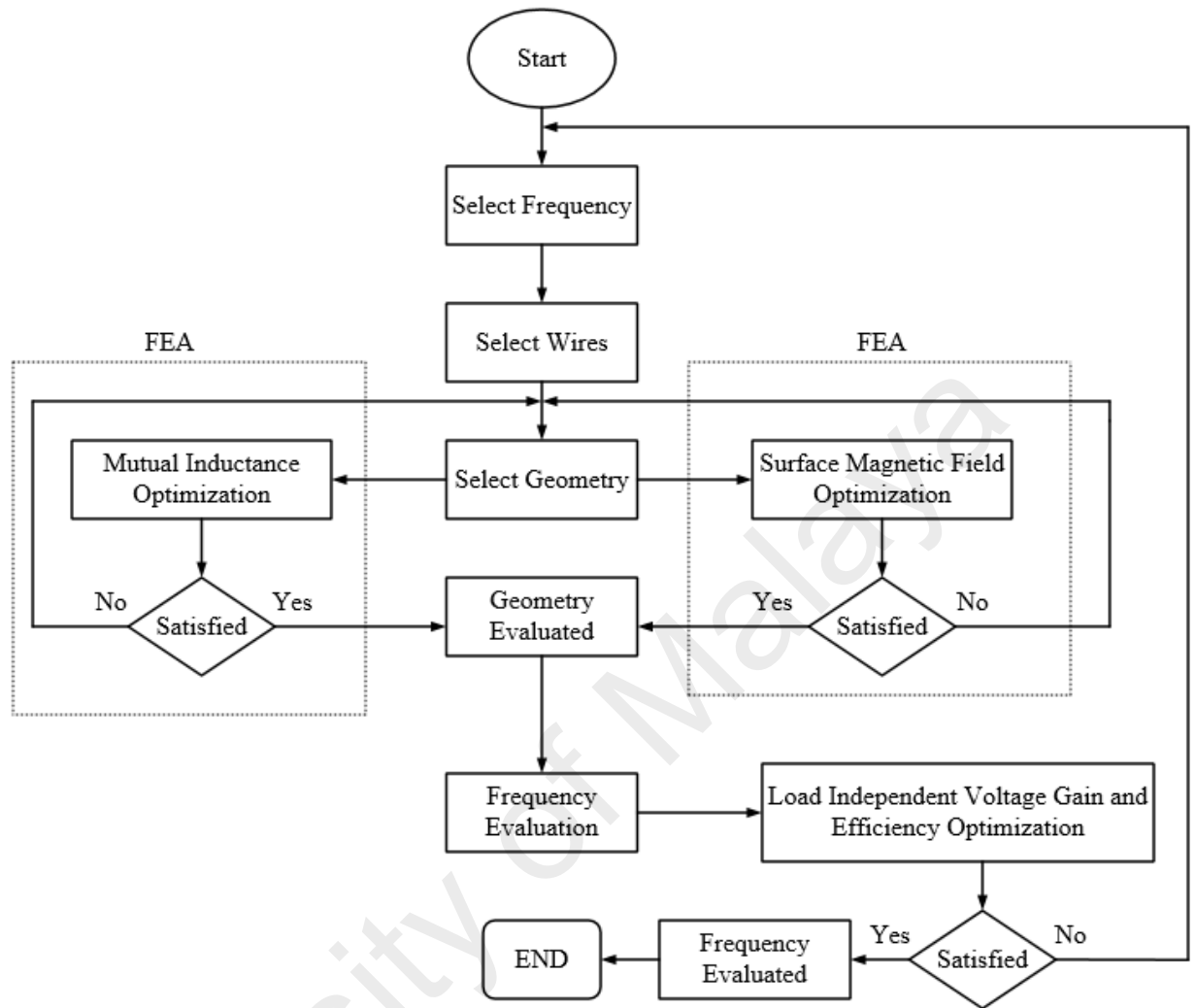
Figure 3.2: Design procedure of the proposed magnetic pad.

In this research, Litz wire is used to build the coils. Coil thickness is decided by the diameter of the Litz wire. The diameter of the Litz wire is selected by the current of the coil and number of turns is chosen by the required output power. Litz wire contains 180 strands of AWG (American Wire Gauge) 38 and the total diameter is 1.85mm with 0.35mm thick insulation of modified polyurethane for each turn. Ferrite plates are used with both the transmitter and receiver to enhance the magnetic coupling. The thickness of the ferrite plate is selected as 4mm. Both transmitter and receiver pads have the 'I' shape ferrite plate leaned on their external faces so that most of the flux lines are confined within the volume

between those pads. The relative permeability (μ_r) and the magnetic loss tangent (tanϴ) of the ferrite plate are chosen as 2300 and 0.008 respectively. Furthermore, aluminum shields are used behind the ferrite plate of each pad, to reduce the unwanted leakage magnetic field. The aluminum alloy used in this shield is 99.5% pure aluminum with conductivity σ of 33MS/m. As a result, its skin depth, δ at f=80 kHz is calculated as $\delta = \sqrt{\dfrac{1}{\pi f \mu_0 \sigma}}$ =0.3mm. The thickness of the aluminum shield is selected as 1.2mm, which is approximately 4δ. The distance between ferrite plate and aluminum shield is set to 20mm to reduce the eddy current loss in an aluminum shield. The vertical distance between the transmitter and receiver, h is kept to140 mm to minimize the inductance variations of them due to their relative position. In the actual case, the coil is constructed with a rounded corner as it has the minimum bending radius. But for simulation, the square corner is used to remove the complexity of the proposed model. The summarize parameters associated with Litz wire, ferrite core and aluminum shield are listed in Table 3.1.

Table 3.1: Evaluation parameters associated with IPT pad

Evaluation parameters	Litz wire	Ferrite core	Aluminum shield
Dimension	Diameter: 1.85 mm (For single turn)	Total length of each ferrite strip=5 x I43=215 mm	400 x 400 mm
Amount	Each turn contains 180 strands of AWG 38	Each ferrite strip contains five "I" shaped plate cores.	One for each pad.
Thickness	Thickness of insulation: 0.35 mm	4 mm	1.2 mm
Others		$\mu_r = 2300$	σ=33 MS/
		$\tan\Theta$=0.008	$\delta=\sqrt{\frac{1}{\pi f \mu_0 \sigma}}$ =0.3mm
			99.5% pure

The length of each pad is determined by the length of the ferrite strip, a number of turns of

the coil and the distance between ferrite strip and the inner side of each width of the coil.

On the other hand, width is primarily determined by the number of turns of the coil, number of ferrite strips and the spacing between two strips. Ferrite strip in each coil is made up of 5×I43 plate cores resulting in a total length of 215mm. Depending on the number of turns of the coil and thick insulation of modified polyurethane for each turn, the distance between ferrite strip and the inner side of each width of the coil is selected as 45.5 mm. The distance between two strips is selected as 67.2 mm. Each iterative simulation of FEA is done by the four number of rows of ferrite strip having five 'I' shaped plate cores for each row.

3.5 Analysis of the proposed system

3.5.1 Finite element analysis of proposed pad

Mutual inductance is a measure of the total flow of magnetic flux from one current carrying path that passes through another closed path. So that,

$$N_{(path2)}\emptyset_{(path1-path2)} = M_{(path1-path2)}I_{(path1)} \tag{3-2}$$

where $M_{(path1-path2)}$ is the mutual inductance between path1 and path2, $I_{(path1)}$ is current of path1, $N_{(path2)}$ is the number of turns of path2 and $\emptyset_{(path1-path2)}$ is magnetic flux generated by path1 that links with path2.

Equation (3-2) is represented as,

$$N_{(path2)}\emptyset_{(path1-path2)} = \iint_{(path2)} \mathbf{B}_{(path1)} \cdot \mathbf{n}dS_{(path2)} \tag{3-3}$$

where $\mathbf{B}_{(path1)}$ is magnetic flux density generated by $I_{(path1)}$, $S_{(path2)}$ is the surface of path2 and $\mathbf{n}$ is normal vector to the $S_{(path2)}$.

Using (3-2) and (3-3), mutual inductance is as follows:

$$M_{(path1-path2)} = \frac{\iint_{(path2)} \mathbf{B}_{(path1)} \cdot \mathbf{n}dS_{(path2)}}{I_{(path1)}} \tag{3-4}$$

As magnetic surface flux density creates coupling between the two paths, so mutual inductance is directly related to the magnetic surface flux density (SFD). Therefore,

$$\text{Coupling coefficient, k} = \frac{M_{(path1-path2)}}{\sqrt{L_{(path1)}L_{(path2)}}} \qquad (3\text{-}5)$$

where L_{path1} and L_{path2} are the inductances of path1 and path2 respectively. According to (3-4) and (3-5), it is clear that SFD has a great effect on the coupling coefficient. Negligible variation of coupling is so much desirable for dynamic charging EV applications. This is possible if SFD is uniform over the whole charging area. So that, before the transmitter is made, mutual inductance can be conversely used to evaluate the uniformity of magnetic SFD. Magnetic SFD for different types of conventional pads, with a frequency of 80 kHz (SAE standard frequency) is shown in Figure 3.3 using an FEA simulation tool of COMSOL.
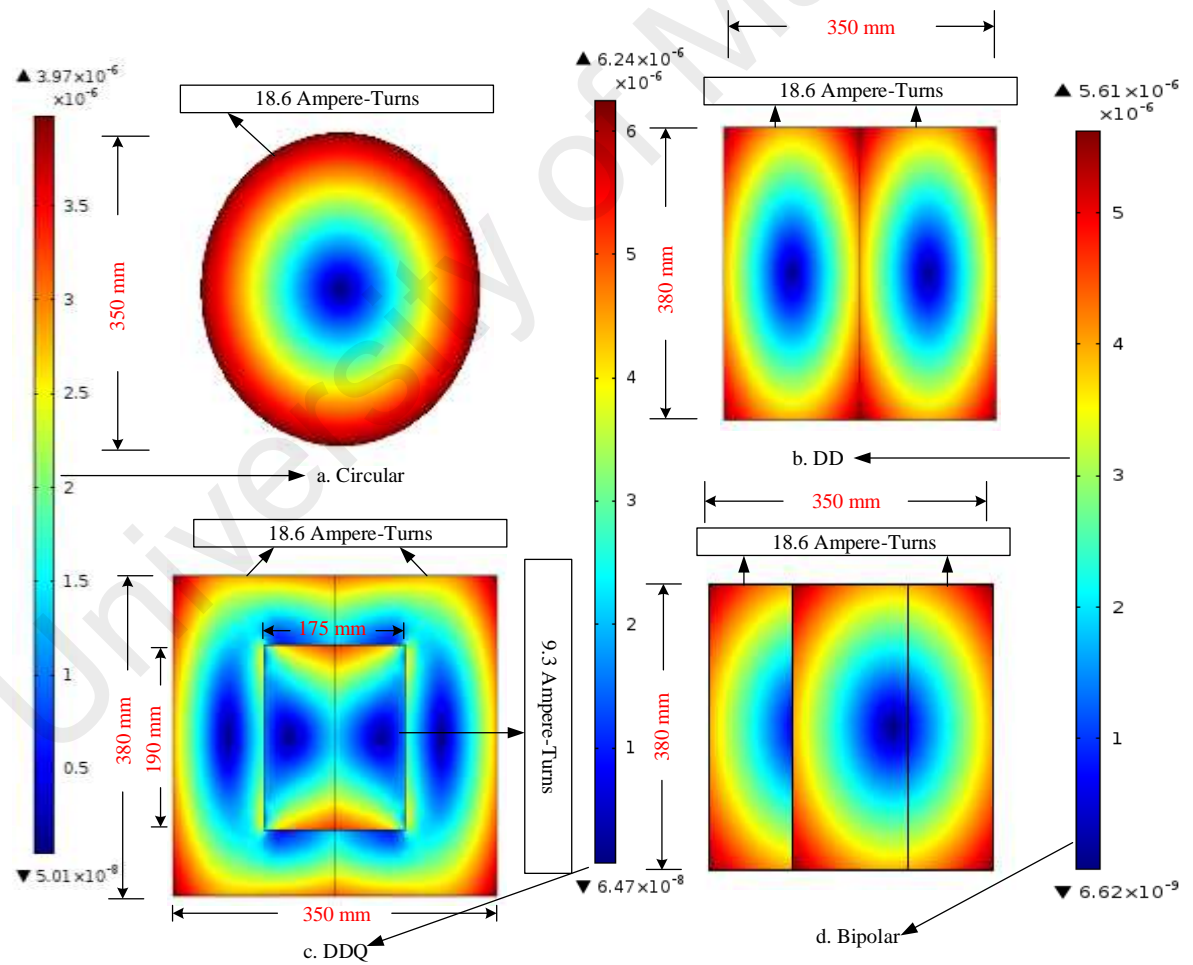
Figure 3.3: Magnetic surface flux density of different conventional shape pads.

Design values about the optimum dimension of the proposed pad are shown in Figure 3.4. The dimension of the larger section is 350mm x 380mm. Others are 100mm x 130mm. Here, number of turns is selected as 10 and 5 for the large and small rectangle respectively.
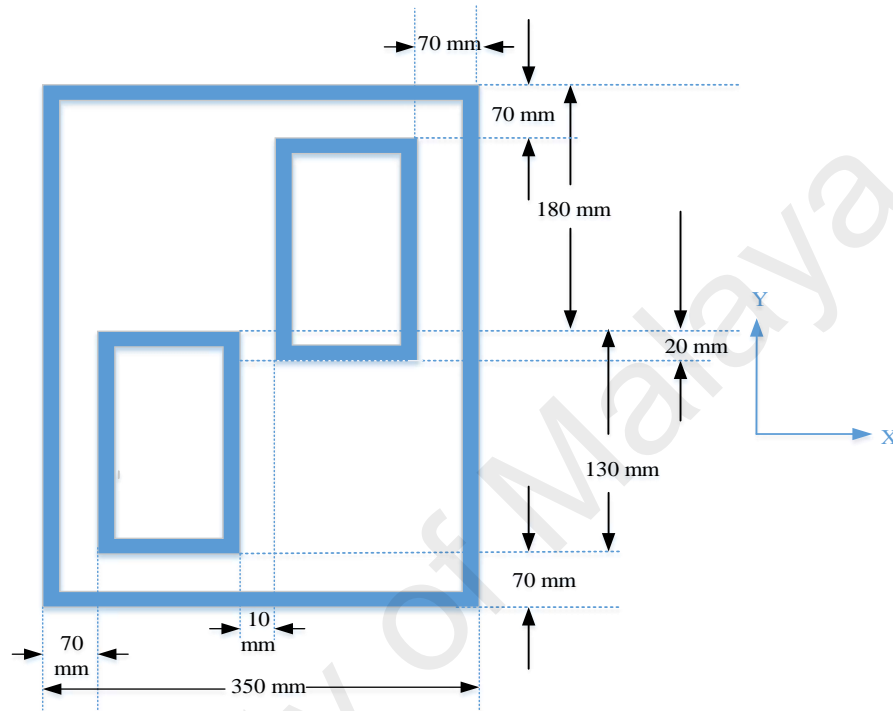
Figure 3.4: The optimum dimension of the proposed pad.

Considering the effect of back to back connection of small rectangular sections, the magnetic SFD distribution for the proposed transmitter pad with same frequency like for Figure 3.3 is shown in Figure 3.5.
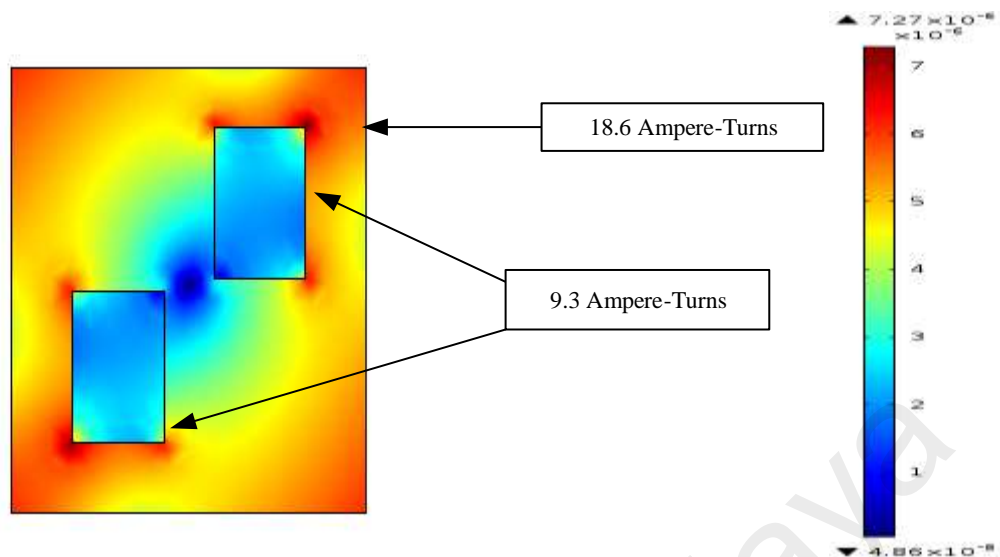
Figure 3.5: Magnetic surface flux density (T) of proposed pad.

From Figure 3.3 and Figure 3.5, it is clear that magnetic SFD of the proposed pad is almost uniformly distributed than any other conventional pad. In addition, magnetic SFD of the proposed pad is higher than any other conventional pads. That means mutual inductance, as well as coupling between the transmitter and receiver, can be kept uniform for the proposed geometry. Due to this property, power transfer fluctuation can be solved for different misalignment conditions, which is verified by the experimental results of chapter 4. Ferrite core which is used in each coil directs the main flux upwards. As a result, single sided flux path is produced (i.e. no flux goes downwards behind the transmitter pad or upwards above the receiver pad). Using hypothesis (a), magnetic flux density plot between transmitter and receiver pads is shown in Figure 3.6. Flux path height is observed as 140mm which is $\frac{1}{2.5}$ times of the transmitter pad length.

(a) Magnetic flux density distribution   (b) Proposed pad
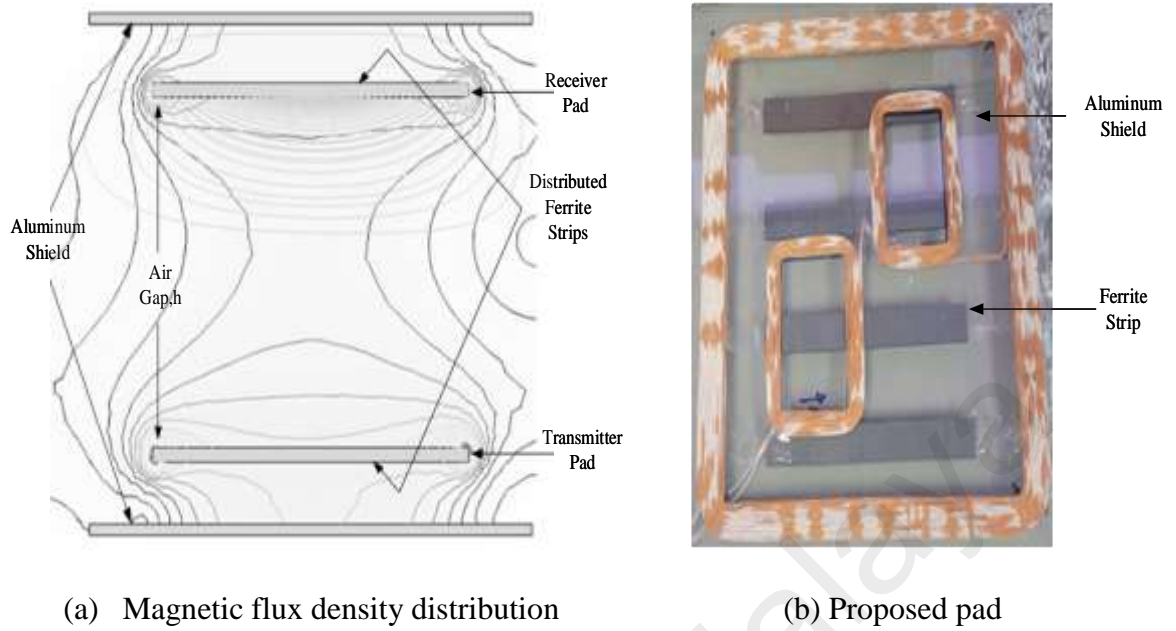
Figure 3.6: Magnetic flux density distribution with proposed pad.

In the case of extended DD transmitter pad, mutual inductance for different misalignment positions of receiver pad with respect to the transmitter pad position is simulated by FEA. In this finite-element analysis, a number of turns for large (N_{large}) and small (N_{small}) rectangular sections of each pad is considered.
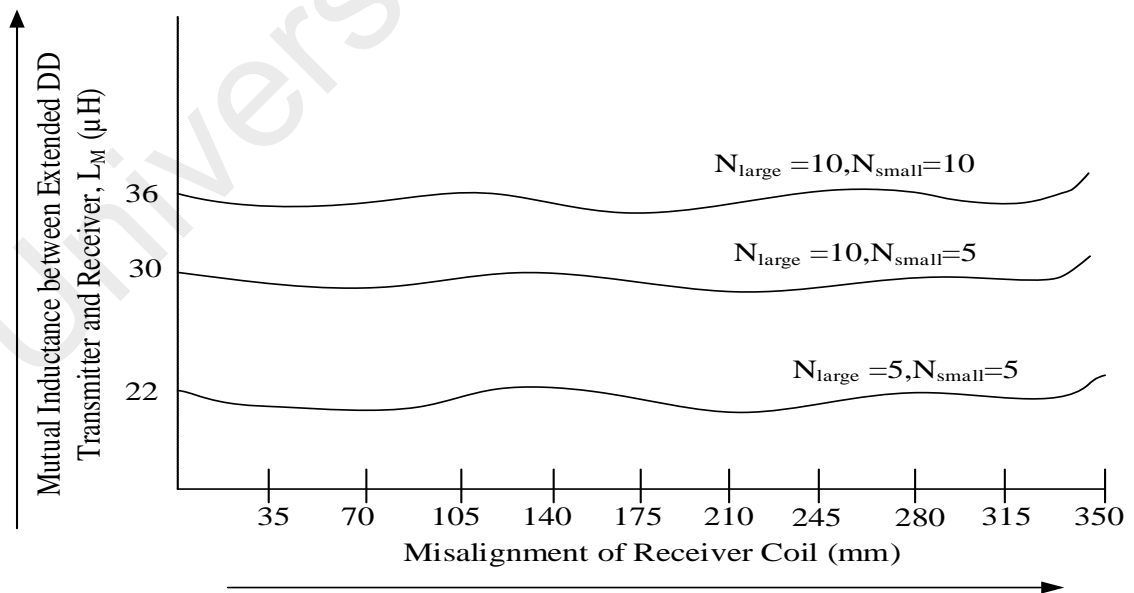
Figure 3.7: Observation of mutual inductance for different horizontal (x-direction) misalignment positions of receiver pad.

From Figure 3.7, it is clear that maximum mutual inductance (L_M) is about 36μH when number of turns for large as well as small rectangular sections is 10. Considering cost effect of Litz wire, the number of turns is selected as 10 for large section whereas 5 for small sections. In this case, mutual inductance is about 30μH for different misalignment positions.

Considering vertical air gap distance of 140mm, between extended DD transmitter and receiver, uncompensated load power is simulated using frequency of 80 kHz shown in Figure 3.8.
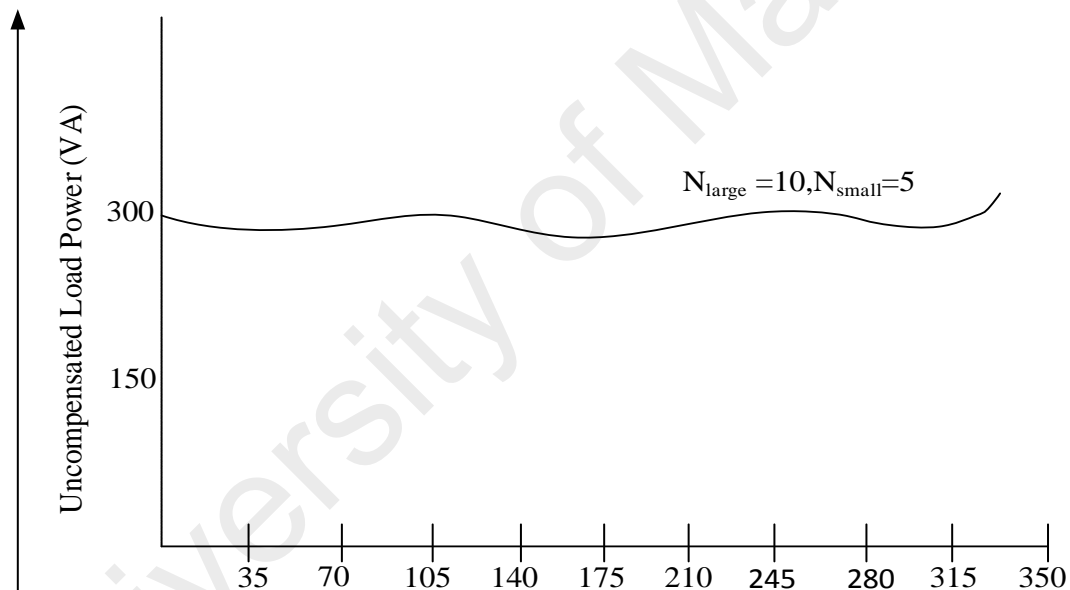
Figure 3.8: Uncompensated load power for different horizontal (x-direction) misalignment positions of receiver pad.

3.5.2 Mutual inductance and coupling coefficient

In case of extended DD transmitter, the overall IPT system for EV charging is shown in Figure 3.9. In this system, LC-LC^2 compensation technique is used in order to obtain the load independent constant voltage gain under different misalignment conditions. This is a desirable characteristic for high efficiency and output voltage controllability.

50
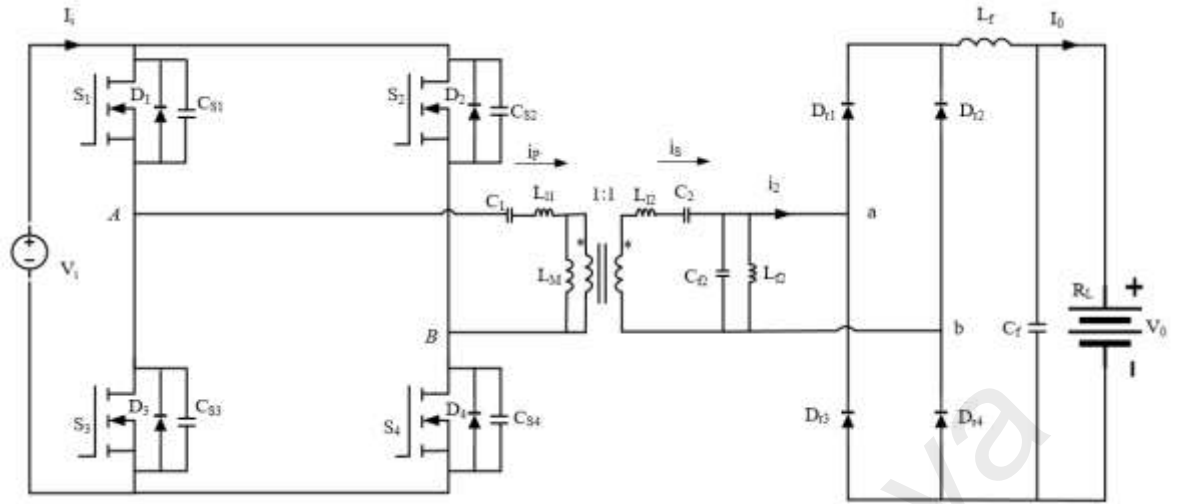
Figure 3.9: Overall inductive power transfer system for electric vehicle charging.

Here, L_{l1} is the leakage inductance of the extended DD transmitter pad as stated before and leakage inductance of the receiver pad is L_{l2}; C_1, C_2 and C_{f2} are the compensation capacitance for L_{l1}, L_{l2} and L_{Mf} respectively. L_M is the mutual inductance between extended DD transmitter and receiver; V_i is the input dc supply for high frequency inverter and V_0 is the voltage across the battery which resistance is R_L. L_f and C_f are used for filtering purpose in order to get pure dc after the high frequency rectifier. In this case, we choose the T-model for proposed IPT transformer with turn ratio 1: n.

$$L_{Mf} = n^2 L_M \parallel L_{f2} = \frac{n^2 L_M L_{f2}}{n^2 L_M + L_{f2}} \tag{3-6}$$

In dynamic charging EV system, a huge waste of energy and prospective dangers have been occurred due to the conventional centralized power system. In addition to reduction of mutual inductance between transfer pads results in a reduction of transfer efficiency. Therefore, a promoted design for both transmitter and receiver pad is developed to get the negligible fluctuation of mutual inductance. To calculate the mutual inductance easily, Figure 3.4 is shifted by 90^0 as depicted in Figure 3.10 (mirror image).
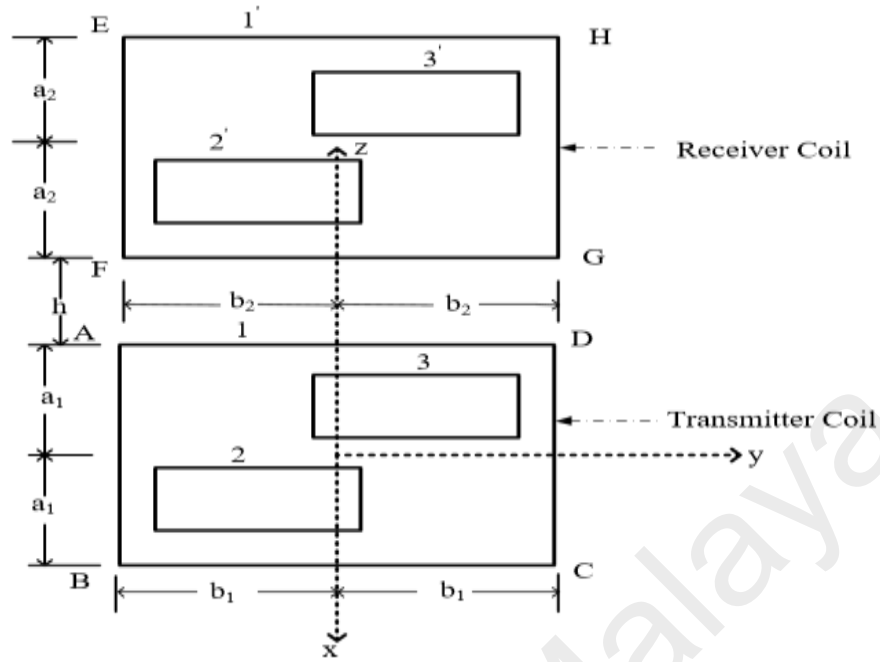
Figure 3.10: Schematic overview of proposed transmitter and receiver pads.

Figure 3.10 shows the structure of two pads (transmitter and receiver), whose geometric centers are on the same vertical axis. Segments, ABCD and EFGH represent the transmitter and receiver pads respectively. Here, the center of transmitter pad is set as the ordinate origin (0, 0, 0), while the coordinate of receiver pad center is (0, s, h) (Zhong et al., 2015). Several segments are associated with both coils and mutual inductances are calculated based on this. Here, $AB=CD=2a_1$, $BC=AD=2b_1$, $EF=GH=2a_2$, $EH=FG=2b_2$. Large rectangular section of transmitter coil is represented as 1 whereas, 1′ for large rectangular section of receiver coil. On the other hand, (2, 3) and (2′, 3′) are for smaller sections of transmitter and receiver coils respectively.

Considering unit vectors for each section of transmitter and receiver pad,

$$d\mathbf{b_1} = dx_1\mathbf{x} \quad + \quad dy_1\mathbf{y} \tag{3-7}$$

$\quad$ (-a_1 to a_1) $\quad\quad$ (-b_1 to b_1)

$$d\mathbf{b_2} = dx_2\mathbf{x} \quad + \quad dy_2\mathbf{y} \tag{3-8}$$

$\quad$ (-a_2 to a_2) $\quad\quad$ (-b_2 to b_2)

52

Define,

$$\mathbf{r_1} = x_1\mathbf{x} + b_1\mathbf{y} \tag{3-9}$$

$$\mathbf{r_2} = x_2\mathbf{x} + b_2\mathbf{y} + h\mathbf{z} \tag{3-10}$$

where, $r = |\mathbf{r_1} - \mathbf{r_2}| = \sqrt{(x_1 - x_2)^2 + (b_1 - b_2)^2 + h^2}$ \hfill (3 -11)

Considering, pad-currents of the transmitter and receiver are I_1 and I_2 respectively. Therefore, the magnetic flux generated by N_{AB} turns of AB segment that links with segment EF is derived as,

$$\emptyset_{AB,\,EF} = \oint_{EF} \mathbf{A}_{AB} \cdot d\mathbf{b_2} = \oint_{EF} \left(\frac{\mu_0 N_{AB} I_1}{4\pi} \oint_{AB} \frac{d\mathbf{b_1}}{r} \right) \cdot d\mathbf{b_2} \tag{3-12}$$

where, $\mathbf{A}_{AB} = \frac{\mu_0 N_{AB} I_1}{4\pi} \oint_{AB} \frac{d\mathbf{b_1}}{r}$ = magnetic vector potential of segment AB \hfill (3-13)

Using (3-12),

$$\emptyset_{AB,\,EF} = \frac{\mu_0 I_1 N_{AB}}{4\pi} \int_{-a_1}^{+a_1} \int_{-a_2}^{+a_2} \frac{dx_1\mathbf{x}.dx_2\mathbf{x}}{r} = \frac{\mu_0 I_1 N_{AB}}{4\pi} \int_{-a_1}^{a_1} \int_{-a_2}^{a_2} \frac{dx_1 dx_2}{\sqrt{(x_1-x_2)^2+(b_1-b_2)^2+h^2}} \tag{3-14}$$

Also, the magnetic flux generated by N_{EF} turns of EF segment that links with segment AB is expressed as,

$$\emptyset_{EF,\,AB} = \oint_{AB} \mathbf{A}_{EF} \cdot d\mathbf{b_1} = \oint_{AB} \left(\frac{\mu_0 N_{EF} I_2}{4\pi} \oint_{EF} \frac{d\mathbf{b_2}}{r} \right) \cdot d\mathbf{b_1} \tag{3-15}$$

where, $\mathbf{A}_{EF} = \frac{\mu_0 N_{EF} I_2}{4\pi} \oint_{EF} \frac{d\mathbf{b_2}}{r}$ = magnetic vector potential of segment EF \hfill (3-16)

From (3-15),

$$\emptyset_{EF,\,AB} = \frac{\mu_0 I_2 N_{EF}}{4\pi} \int_{-a_1}^{+a_1} \int_{-a_2}^{+a_2} \frac{dx_1\mathbf{x}.dx_2\mathbf{x}}{r} = \frac{\mu_0 I_2 N_{EF}}{4\pi} \int_{-a_1}^{a_1} \int_{-a_2}^{a_2} \frac{dx_1 dx_2}{\sqrt{(x_1-x_2)^2+(b_1-b_2)^2+h^2}} \tag{3-17}$$

Using (3-14) and (3-17), mutual inductance between AB & EF is represented as,

$$M_{AB,\,EF} = \frac{N_{EF}\emptyset_{AB,EF}}{I_1} = \frac{N_{AB}\emptyset_{EF,AB}}{I_2} = \frac{\mu_0 N_{AB} N_{EF}}{4\pi} \int_{-a_1}^{a_1} \int_{-a_2}^{a_2} \frac{dx_1 dx_2}{\sqrt{(x_1-x_2)^2+(b_1-b_2)^2+h^2}} \tag{3-18}$$

Using hypothesis (b), mutual inductance between two larger rectangular sections (1 and 1') is calculated as,

53

$$M_{11'} = M_{AB,EF} + M_{AB,GH} + M_{CD,EF} + M_{CD,GH} + M_{BC,FG} + M_{BC,EH} + M_{AD,FG} + M_{AD,EH} \quad (3\text{-}19)$$

(Greenhouse, 1974)

Considering, $N_1 = N_{1'} = 10 = N_{large}$ and $N_2 = N_{2'} = N_3 = N_{3'} = 5 = N_{small}$; above equation is

modified as, $M_{11'} = \sum_{i=1}^{N_1} \sum_{j=1}^{N_{1'}} M_{ij}$ \quad (3-20)

Similarly, other mutual inductances are derived as,

$$M_{22'} = \sum_{i=1}^{N_2} \sum_{j=1}^{N_{2'}} M_{ij} \quad (3\text{-}21)$$

$$M_{33'} = \sum_{i=1}^{N_3} \sum_{j=1}^{N_{3'}} M_{ij} \quad (3\text{-}22)$$

$$M_{12'} = \sum_{i=1}^{N_1} \sum_{j=1}^{N_{2'}} M_{ij} \quad (3\text{-}23)$$

$$M_{13'} = \sum_{i=1}^{N_1} \sum_{j=1}^{N_{3'}} M_{ij} \quad (3\text{-}24)$$

$$M_{21'} = \sum_{i=1}^{N_2} \sum_{j=1}^{N_{1'}} M_{ij} \quad (3\text{-}25)$$

$$M_{23'} = \sum_{i=1}^{N_2} \sum_{j=1}^{N_{3'}} M_{ij} \quad (3\text{-}26)$$

$$M_{31'} = \sum_{i=1}^{N_3} \sum_{j=1}^{N_{1'}} M_{ij} \quad (3\text{-}27)$$

$$M_{32'} = \sum_{i=1}^{N_3} \sum_{j=1}^{N_{2'}} M_{ij} \quad (3\text{-}28)$$

By the aid of above equations, mutual inductance (L_{M1}) between transmitter (ABCD) and

receiver (EFGH) coil can be calculated (Cheng & Shu, 2014). In case of extended DD

transmitter, mutual inductance (L_M) is given as,

$$L_M = L_{M1} + L_{M2} \quad (3\text{-}29)$$

where, L_{M2} is the mutual inductance, between another part of extended DD transmitter and

the receiver coil. So that, effective coupling coefficient,

$$k = \frac{L_{M1} + L_{M2}}{\sqrt{L_T L_R}} = \frac{L_M}{\sqrt{L_T L_R}} \quad (3\text{-}30)$$

Here, L_T is the inductance of the extended DD transmitter pad as stated before; the inductance of the receiver pad is L_R.

As discussed earlier in section, L_M is almost constant in every horizontal misalignment position of the receiver coil which is desirable for dynamic charging of EV applications. In view of this fact, negligible coupling changes can be achievable in each horizontal misalignment position. This is experimentally observed in the chapter 4.

3.5.3 Frequency domain analysis

According to Figure 3.8, frequency domain analysis of the whole setup is explained. Here, a novel LC-LC^2 compensation scheme is used for dynamic charging EV applications, which provides the load independent voltage transfer characteristics of the receiver coil at certain frequencies. In this case, current is controlled by choosing the optimum load of R_L. When equivalent inductance L_{MF} and all leakage inductances of the proposed compensation based IPT system are compensated at once,

$$\omega_r = \frac{1}{\sqrt{L_{l1}C_1}} = \frac{1}{\sqrt{L_{l2}C_2}} = \frac{1}{\sqrt{L_{Mf}C_{f2}}} \tag{3-31}$$

where ω_r is the resonant frequency.

Using Kirchhoff's voltage law, fundamental components of V_{LM}, V_{AB} and V_{ab} can be represented as,

$$V_{L_M} = V_{AB} \frac{j\omega L_M \| \frac{Z_2 + (-j\frac{1}{\omega C_{f2}}) \| (j\omega L_{f2}) \| R_E}{n^2}}{j\omega L_M \| \frac{Z_2 + (-j\frac{1}{\omega C_{f2}}) \| R_E \| (j\omega L_{f2})}{n^2} + Z_1} \tag{3-32}$$

$$V_{ab} = nV_{L_M} \frac{(-j\frac{1}{\omega C_{f2}}) \| R_E \| (j\omega L_{f2})}{Z_2 + (-j\frac{1}{\omega C_{f2}}) \| R_E \| (j\omega L_{f2})} \tag{3-33}$$

where $R_E = \left(\frac{\pi^2}{8}\right) R_L$ = equivalent ac load resistance looking into the high frequency rectifier, $Z_1 = j(\omega L_{l1} - \frac{1}{\omega C_1})$ and $Z_2 = j(\omega L_{l2} - \frac{1}{\omega C_2})$.

By the aid of Fourier analysis, V_{AB} can be depicted as,

$$V_{AB} = \frac{4V_i}{\pi} \tag{3-34}$$

Because of L_{f2}, most of the higher order harmonics those tend to be injected to the rectifier can be eliminated. In later, experimental results of LC-LC^2 compensated resonant converter will compare the efficiency with the results of S-SP compensated resonant converter. Consequently, V_{ab} can be considered as a sine wave. Therefore, voltage across the battery can be simplified as,

$$V_0 = \frac{1}{\pi} \int_0^\pi V_{ab}(\sin \omega t)\, d\omega t = \frac{2}{\pi} V_{ab} \tag{3-35}$$

From (3-32), (3-33), (3-34) and (3-35), voltage gain of the LC-LC^2 compensated IPT system can be written as,

$$G_V(\omega) = \frac{V_0}{V_i} = \left| \frac{\frac{2V_{ab}}{\pi}}{\frac{\pi V_{AB}}{4}} \right| = \frac{8}{\pi^2} \left| \frac{V_{ab}}{V_{AB}} \right| = \frac{8}{\pi^2} \left| \frac{V_{ab}}{V_{L_M}} \cdot \frac{V_{L_M}}{V_{AB}} \right| =$$

$$\frac{8}{\pi^2} \left| \frac{n}{1 + \frac{C_{f2}[(Z_2 + n^2 Z_1)j\omega L_M + Z_1 Z_2]}{L_M} - (n^2 L_M + L_{f2})(Z_3 + j\frac{1}{\omega C_{f2}})(\frac{Z_1}{\omega^2 L_M L_{f2}^2} - j\frac{Z_1 Z_2}{\omega^3 L_M^2 L_{f2}^2 n^2} + \frac{Z_2}{\omega^2 L_M L_{f2}^2 n^2} + \frac{Z_1}{\omega^2 L_M^2 L_{f2} n^2}) + \frac{\delta}{j\omega^3 L_M R_E C_1 C_2}} \right| \tag{3-36}$$

where $Z_3 = j(\omega L_{Mf} - \frac{1}{\omega C_{f2}})$ and

$$L_T = L_{l1} + L_M \tag{3-37}$$

$$L_R = L_{l2} + n^2 L_M \tag{3-38}$$

$$\delta = \omega^4 C_1 C_2 (n^2 L_M{}^2 - L_T L_R) + \omega^2 (L_T C_1 + L_R C_2) - 1 \tag{3-39}$$

Equation (3-39) can be expressed as,

$$\delta = \omega^2 C_1 C_2 [Z_1 Z_2 + j\omega L_M (Z_2 + n^2 Z_1)] \tag{3-40}$$

From (3-36), it is clear that voltage gain is independent of load when $\delta=0$.

Using $\delta=0$, we get two load independent voltage gain frequencies

$$\omega_L = \sqrt{\frac{\omega_T{}^2 + \omega_R{}^2 - \sqrt{(\omega_T{}^2 + \omega_R{}^2)^2 - 4(1-k^2)\omega_T{}^2\omega_R{}^2}}{2(1-k^2)}} \tag{3-41}$$

$$\omega_H = \sqrt{\frac{\omega_T{}^2 + \omega_R{}^2 + \sqrt{(\omega_T{}^2 + \omega_R{}^2)^2 - 4(1-k^2)\omega_T{}^2\omega_R{}^2}}{2(1-k^2)}} \tag{3-42}$$

where $\omega_T = \frac{1}{\sqrt{L_T C_1}}$ and $\omega_R = \frac{1}{\sqrt{L_R C_2}}$

Voltage gain at the above frequencies can be obtained as,

$$G_V(\omega_L) =$$

$$\frac{8}{\pi^2} \frac{n}{\left| 1 + \frac{C_{f2}[(Z_2 + n^2 Z_1)j\omega_L L_M + Z_1 Z_2]}{L_M} - (n^2 L_M + L_{f2})\left(Z_3 + j\frac{1}{\omega_L C_{f2}}\right)\left(\frac{Z_1}{\omega_L{}^2 L_M L_{f2}{}^2} - j\frac{Z_1 Z_2}{\omega_L{}^3 L_M{}^2 L_{f2}{}^2 n^2} + \frac{Z_2}{\omega_L{}^2 L_M L_{f2}{}^2 n^2} + \frac{Z_1}{\omega_L{}^2 L_M{}^2 L_{f2} n^2}\right) \right|} \tag{3-43}$$

$$G_V(\omega_H) =$$

$$\frac{8}{\pi^2} \frac{n}{\left| 1 + \frac{C_{f2}[(Z_2 + n^2 Z_1)j\omega_H L_M + Z_1 Z_2]}{L_M} - (n^2 L_M + L_{f2})\left(Z_3 + j\frac{1}{\omega_H C_{f2}}\right)\left(\frac{Z_1}{\omega_H{}^2 L_M L_{f2}{}^2} - j\frac{Z_1 Z_2}{\omega_H{}^3 L_M{}^2 L_{f2}{}^2 n^2} + \frac{Z_2}{\omega_H{}^2 L_M L_{f2}{}^2 n^2} + \frac{Z_1}{\omega_H{}^2 L_M{}^2 L_{f2} n^2}\right) \right|} \tag{3-44}$$

Considering that, load independent voltage gain frequency is ω_r. To get a constant voltage gain at ω_r, the following equation should be fulfilled:

$$\frac{C_{f2}[(Z_2 + n^2 Z_1)j\omega_r L_M + Z_1 Z_2]}{L_M} - (n^2 L_M + L_{f2})\left(Z_3 + j\frac{1}{\omega_r C_{f2}}\right)\left(\frac{Z_1}{\omega_r{}^2 L_M L_{f2}{}^2} - j\frac{Z_1 Z_2}{\omega_r{}^3 L_M{}^2 L_{f2}{}^2 n^2} + \right.$$

$$\left. \frac{Z_2}{\omega_r{}^2 L_M L_{f2}{}^2 n^2} + \frac{Z_1}{\omega_r{}^2 L_M{}^2 L_{f2} n^2}\right) = 0 \tag{3-45}$$

By putting $Z_1 = j\left(\omega L_{l1} - \frac{1}{\omega C_1}\right)$, $Z_2 = j\left(\omega L_{l2} - \frac{1}{\omega C_2}\right)$, $Z_3 = j\left(\omega L_{Mf} - \frac{1}{\omega C_{f2}}\right)$ and $\delta=0$ into

(3-45), gives

$$\frac{C_{f2}[(Z_2 + n^2 Z_1)j\omega_r L_M + Z_1 Z_2]}{L_M} - (n^2 L_M + L_{f2})\left(Z_3 + j\frac{1}{\omega_r C_{f2}}\right)\left(\frac{Z_1}{\omega_r{}^2 L_M L_{f2}{}^2} - j\frac{Z_1 Z_2}{\omega_r{}^3 L_M{}^2 L_{f2}{}^2 n^2} + \right.$$

$$\left. \frac{Z_2}{\omega_r{}^2 L_M L_{f2}{}^2 n^2} + \frac{Z_1}{\omega_r{}^2 L_M{}^2 L_{f2} n^2}\right) = \frac{\delta}{\omega_r{}^2 C_1 C_2} - \frac{L_M}{C_{f2}}\left(\frac{jZ_1 n^2}{\omega_r L_{f2}} + \frac{Z_1 Z_2}{\omega_r{}^2 L_M L_{f2}} + j\frac{Z_2}{\omega_r L_{f2}} + j\frac{Z_1}{\omega_r L_M}\right) = 0$$

$$\tag{3-46}$$

Therefore, $Z_1 = Z_2 = 0$. Substituting $Z_1 = Z_2 = 0$ into (3-40), we get

$$\delta = \omega_r{}^2 C_1 C_2 [Z_1 Z_2 + j\omega_r L_M (Z_2 + n^2 Z_1)] = 0 \tag{3-47}$$

So that, load independent constant voltage gain with no effect of coupling coefficient is obtained when, $Z_1 = Z_2 = 0$.

The input impedance of the proposed IPT system is calculated as,

$$Z_i(\omega)$$

$$= Z_1 + \frac{j\omega L_M [j\omega L_{f2}(j\omega C_{f2} Z_2 R_E + Z_2 + R_E) + Z_2 R_E]}{j\omega n^2 L_M [j\omega L_{f2}(j\omega C_{f2} R_E + 1) + R_E] + j\omega L_{f2}(j\omega C_{f2} Z_2 R_E + Z_2 + R_E) + Z_2 R_E} \tag{3-48}$$

Substituting $Z_1 = Z_2 = 0$ into (3-48), yields

$$Z_i(\omega_r) = \frac{j\omega_r L_M L_{f2} R_E}{j\omega_r n^2 L_M L_{f2} + (L_{f2} R_E + n^2 L_M R_E - \omega_r{}^2 n^2 L_{f2} C_{f2} L_M R_E)} \tag{3-49}$$

In order to obtain ZPA of Z_i at ω_f, the following imaginary part should be equal to zero. The imaginary part of the input impedance of (3-49) can be obtained as,

$$\text{Im}[Z_i(\omega_r)] = \frac{-\omega_r{}^2 L_M L_{f2} C_{f2} R_E{}^2 (n^2 L_M + L_{f2}) Z_3}{(\omega_r n^2 L_M L_{f2})^2 + (L_{f2} R_E + n^2 L_M R_E - \omega_r{}^2 n^2 L_{f2} C_{f2} L_M R_E)^2} \tag{3-50}$$

Under the full compensation, (3-41) and (3-42) yields,

$$\omega_L = \frac{1}{\sqrt{L_T C_1 + n^2 L_M C_2}} \tag{3-51}$$

$$\omega_H = \frac{1}{\sqrt{L_{l1} C_1}} \tag{3-52}$$

Equation (3-52) follows the equation (3-31). Therefore, constant voltage gain and ZPA of input impedance both can be obtained, under the full compensation ($Z_1 = Z_2 = Z_3 = 0$) condition. This is a recommended characteristic to obtain high efficiency and well controllability of output voltage. From (3-36), the required constant voltage gain can be calculated as,

$$G_V(\omega_r) = \frac{8n}{\pi^2} \tag{3-53}$$

58

3.5.4 Time domain analysis

To explain the time domain analysis, the following assumptions are made:

(a) All semiconductor switches and diodes are ideal.

(b) Receiver current i_s is almost sinusoidal since proposed converter operates near the resonant frequency.

Figure 3.12–Figure 3.15 depicts the equivalent circuits during different intervals of operation of the proposed system for the operating waveforms shown in Figure 3.11.
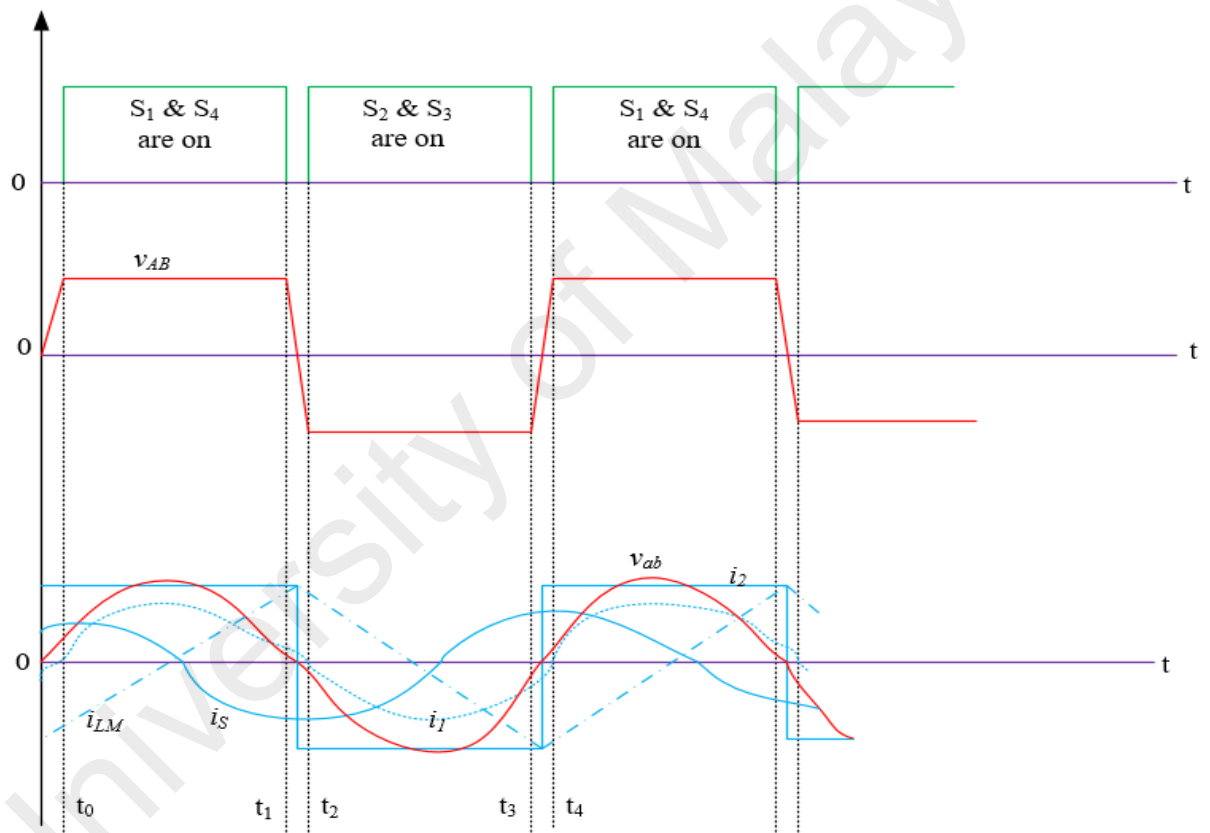

Figure 3.11: Operating waveforms of the proposed LC-LC^2 compensated IPT system.
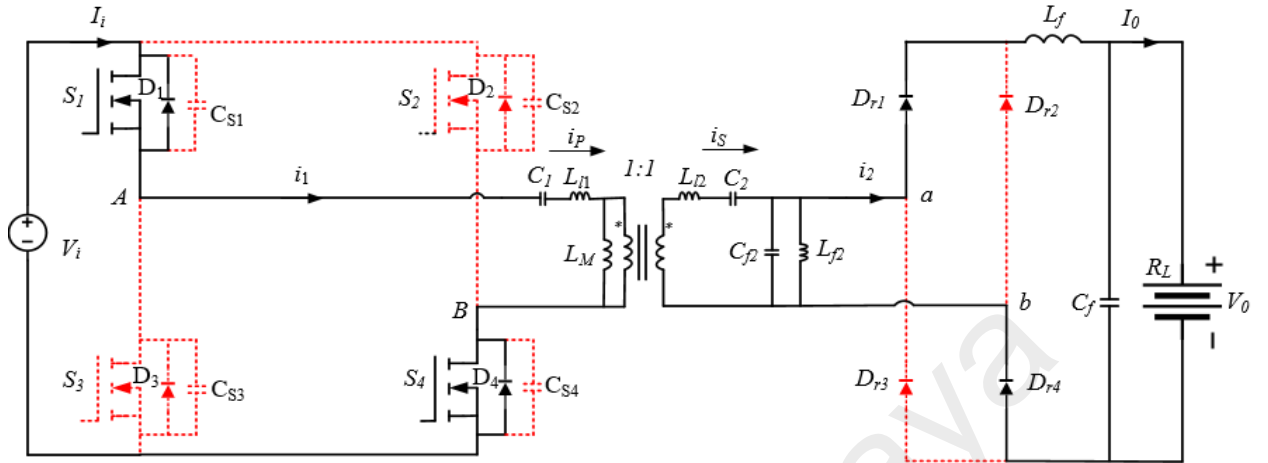
Mode 1 [t_0-t_1]:

Figure 3.12: Equivalent circuit for switching mode 1 [t_0-t_1].

Consider that at time instant t_0, diagonal switch pair (S_1 and S_4) of the proposed converter

is in conduction and another diagonal switch pair (S_2 and S_3) is in off mode.

At that time V_{AB} is positively equal to V_i. Firstly, transmitter current i_P flows through the

body diodes of S_1 and S_4, after that S_1 and S_4 start to conduct with the changing of current

direction. Consequently, ZVS is obtained.

Throughout this period, current flowing into L_M can be expressed as,

$$i_{L_M}(t) = \frac{V_i}{L_M}\left(t - \frac{T_S}{4}\right)$$

3-53

where T_S is the time period.

Also, receiver current, i_S can be obtained as,

$$i_S(t) = \frac{4n}{\pi}V_i \times \left\{j\left(\omega C_{f2} - \frac{1}{\omega L_{f2}}\right) + \frac{1}{R_E}\right\}\sin\left(\omega t + \tan^{-1}\left(\omega C_{f2} - \frac{1}{\omega L_{f2}}\right)R_E\right)$$

3-54

Therefore, transmitter current, i_P can be calculated as,

$$i_P(t) = i_{L_M}(t) + ni_S(t) = \frac{V_i}{L_M}\left(t - \frac{T_S}{4}\right) + n\frac{4n}{\pi}V_i \times \left\{j\left(\omega C_{f2} - \frac{1}{\omega L_{f2}}\right) + \frac{1}{R_E}\right\}\sin\left(\omega t + \right.$$

$$\tan^{-1}\left(\omega C_{f2} - \frac{1}{\omega L_{f2}}\right)R_E\right)$$

3-55

Mode 2 [t_1-t_2]:
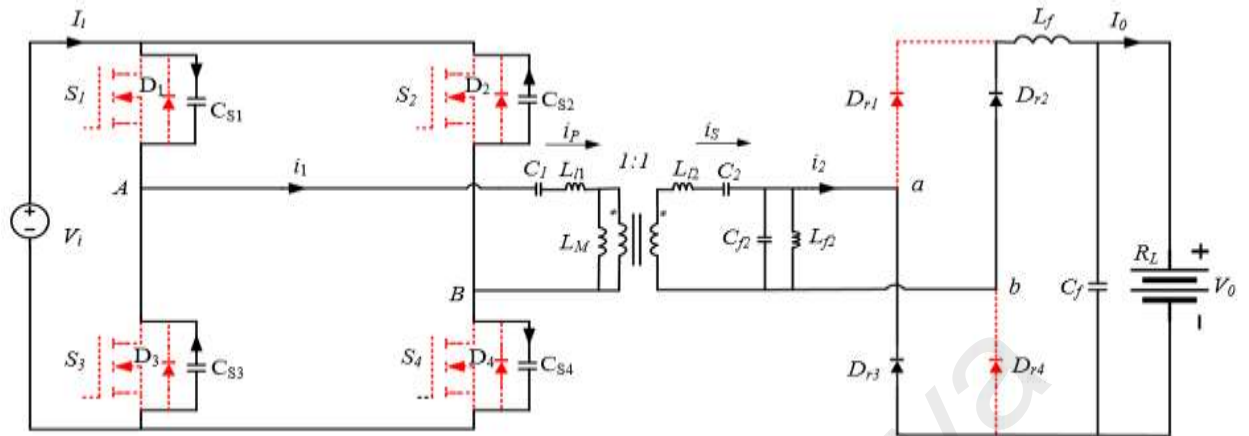
Figure 3.13: Equivalent circuit for switching mode 2 [t_1-t_2].

Diagonal switch pair (S_1 and S_4) is in off mode at t_1. So that i_P charges the C_{S1} and C_{S4} and discharges C_{S2} and C_{S3}. Next, S_1 and S_4 are turned off at ZVS as C_{S1} and C_{S4} limit the rising voltage rate across the switches. In this case, the direction of i_P can be considered as unchanged because of the short time interval of this mode. At time instant t_2, the voltage across the switches S_2 and S_3 are fully discharged whereas complete charging of S_1 and S_4 occurs from 0 to V_i. Then, to maintain the continuity of i_P, D_2 and D_3 start to conduct. So V_{AB} becomes to -V_i.

Mode 3[t_2-t_3]:
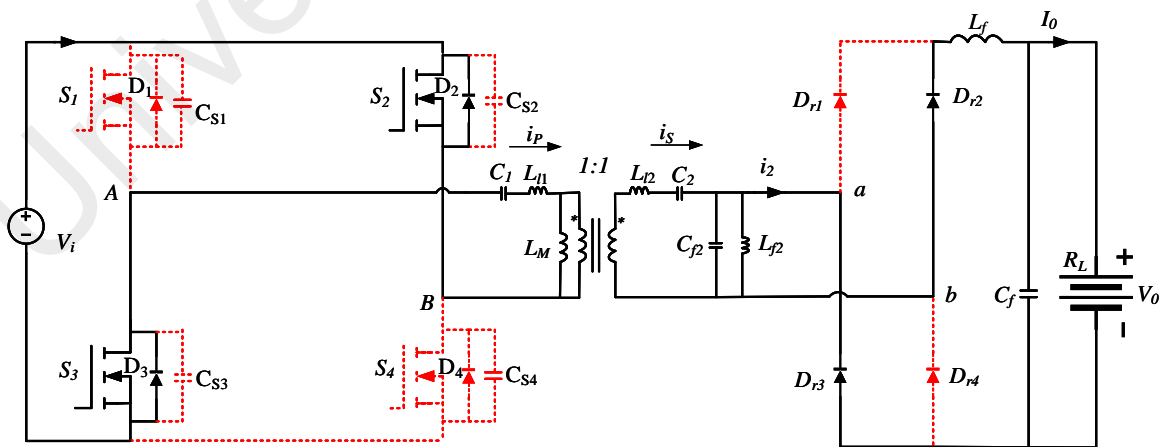
Figure 3.14: Equivalent circuit for switching mode 3 [t_2-t_3].

After the conduction of D_2 and D_3, diagonal switch pair (S_2 and S_3) of the proposed converter is in conduction with ZVS. Here, V_{AB} equals to $-V_i$. During this period, this mode is similar to the mode 1. In the beginning, body diodes of S_2 and S_3 conduct, after that S_2 and S_3 start to conduct with the changing of current direction. Throughout this period, current flowing into L_M can be expressed as,

$$i_{L_M}(t) = \frac{V_i}{L_M}\left(-t + \frac{3T_S}{4}\right)$$

3-56

Using (3-54), transmitter current, i_p can be expressed as,

$$i_P(t) = \frac{V_i}{L_M}\left(-t + \frac{3T_S}{4}\right) + n\frac{4n}{\pi}V_i \times \left\{j\left(\omega C_{f2} - \frac{1}{\omega L_{f2}}\right) + \frac{1}{R_E}\right\}\sin\left(\omega t + \tan^{-1}\left(\omega C_{f2} - \frac{1}{\omega L_{f2}}\right)R_E\right)$$

3-57

Mode 4[t_3-t_4]:
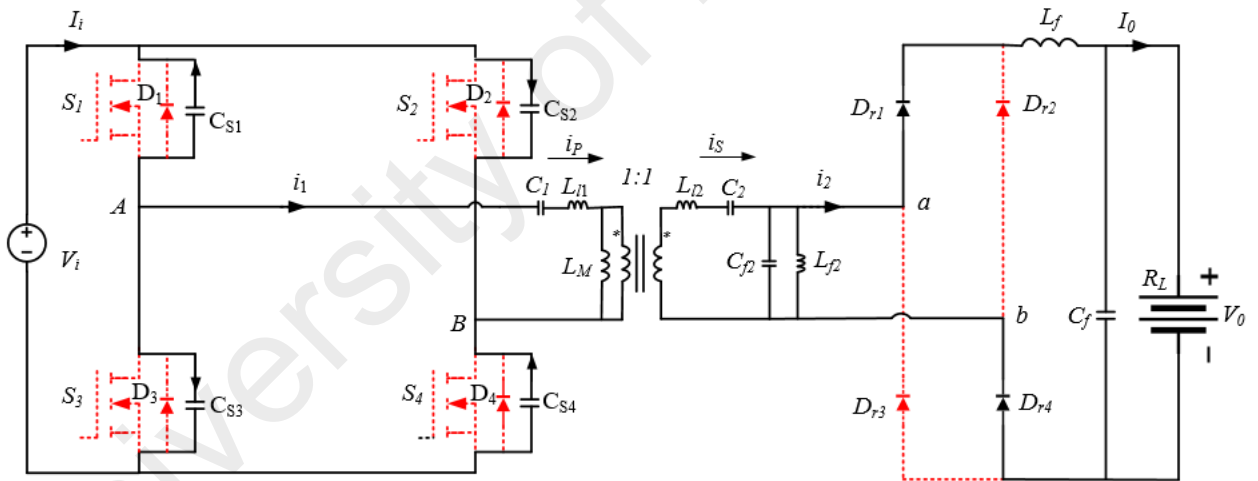
Figure 3.15: Equivalent circuit for switching mode 4 [t_3-t_4].

This mode is similar to mode 2. Diagonal switch pair (S_2 and S_3) is in off mode with ZVS at t_3. At time instant t_4, the voltage across the switches S_1 and S_4 are fully discharged whereas complete charging of S_2 and S_3 occurs from 0 to V_i. Then, to maintain the continuity of i_P, D_1 and D_4 start to conduct. Therefore, ZVS turn on condition occurs for S_1 and S_4. So V_{AB} becomes to $+V_i$.

3.6 Control strategy

Specific frequency control is used in the proposed resonant converter since it is simple and reliable. A specific frequency control needs more analytical operating conditions such as limited tolerance for the positioning of the coupled pads and the size of the air gap between the pads, since the power transfer and efficiency can be considerably minimized by misalignments (Yabiao Gao, Farley, & Tse, 2015; Y. Gao, Ginart, Farley, & Tse, 2016). However, this type of control is uncomplicated in the case of both software programming and hardware implementation. Figure 3.16 represents the control block diagram of the specific frequency control. Based on ZVS condition, selection of the specific frequency is observed.
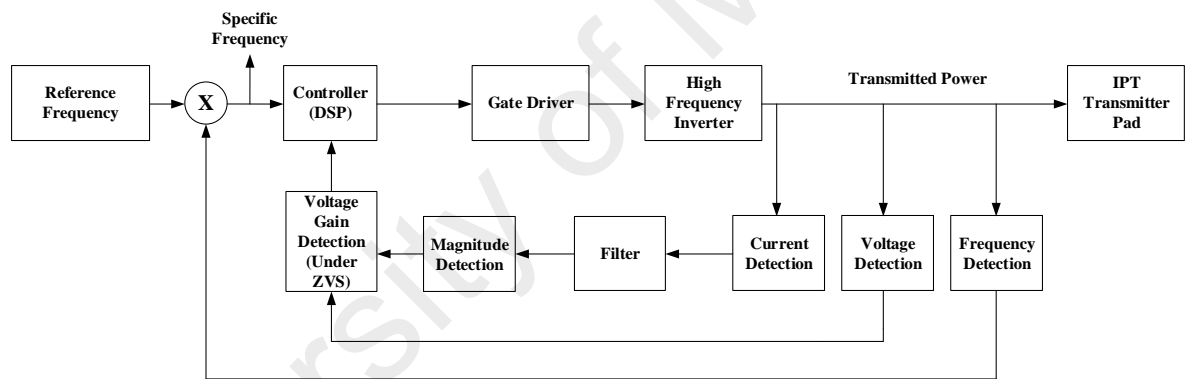
Figure 3.16: Control block diagram of specific frequency control.

In this control technique, only primary sided control technique is used in the transmitter side IPT pad for the reliable and simple operation. Here, Controller (DSP) controls the transmitted power by the specific frequency which is found from a comparison of the reference frequency and the frequency coming from the inverter. Voltage gain detection block gets the output voltage and current from the inverter output and provides the digital signal to the DSP that operates the gate driver to turn on the inverter. For this specific frequency control, voltage gain detection block helps the controller to provide the load independent operation.

3.7 Summary

In this chapter, the proposed extended DD pad with LC-LC^2 compensation has been presented. The design procedure of the proposed magnetic pad structure is illustrated step by step in an organized way. The proposed magnetic pad with LC-LC^2 compensation based EV charging system has been analyzed in according to the finite element analysis, mutual inductance analysis, frequency and time domain analysis and specific frequency control strategy. Proposed dynamic EV charging system is validated in the following chapter by the experimental results.

CHAPTER 4: RESULTS AND DISCUSSIONS

4.1 Introduction

In this chapter, experimental results of the whole system are presented with the aid of design specifications. Coupling between the transmitter and receiver pad is observed on the basis of different receiver pad positions compared to the transmitter pad position. Load power under different receiver pad positions is also experimentally evaluated in this chapter. Load independent voltage gain and zero phase angle (ZPA) of the input impedance are also verified by the laboratory results associated with the theoretical results obtained from the chapter 3. Comparison between LC-LC^2 and S-SP compensated IPT based EV charging system depicts that, LC-LC^2 compensated system has better tolerance of air gap variation than S-SP compensated system. A well defined comparison between the proposed magnetic pad and other conventional pads is presented also. Finally, to overcome the power transfer fluctuation condition, a method is proposed.

4.2 Experimental setup

In this proposed system, H-bridge inverter is used as a high frequency inverter which provides the power supply to the proposed transmitter pads. Transmitter pads are compensated by the simple series compensation whereas receiver pad is compensated by the modified SP compensation. Both compensation together named as LC-LC^2. Transmitted power is controlled by the DSP controller using specific frequency control technique. After getting the power from the receiver pad, this power is rectified by the bridge rectifier and then filtered in order to charge the battery. The block diagram of the overall EV charging system is shown in Figure 4.1.
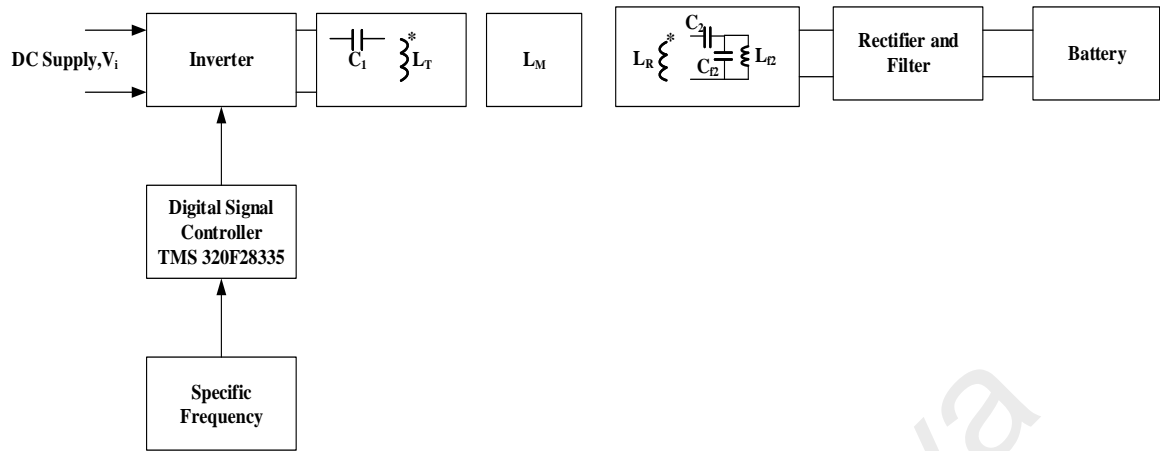
Figure 4.1: Block diagram of the whole EV charging system.

The design specifications of dynamic charging EV systems are found by considering the fundamental component of V_{AB}, which are shown in Table 4.1.

Table 4.1: Design specifications of the proposed system

Design Specifications	Value
Resonant frequency	f=80 kHz
Parameters of IPT transformer	n=1,L_{l1}=165.9μH, L_{l2}=82.05μH,L_M=30.1μH,k=0.203
Compensating inductor	L_{f2}=20μH
Resonant capacitors	C_1=23.86nF,C_2=48.24nF,C_{f2}=329.27nF
Load resistance	R_L=33Ω - 200Ω
Load power	P_L= 500W
Air gap	h=140 mm

A 500 W laboratory prototype for the proposed dynamic charging system of electric vehicles is shown in Figure 4.2. Extended DD transmitter and receiver pads have been built and experimental results have been recorded with the help of proposed compensation technique. The achieved experimental results are explained in the following sections.
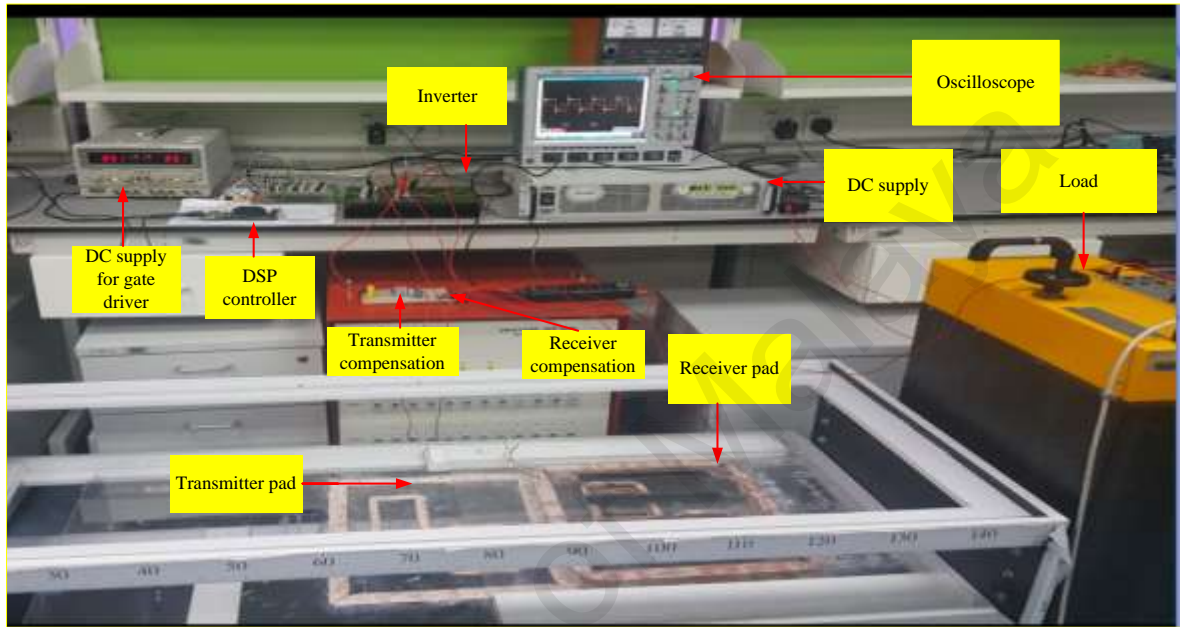
Figure 4.2: Experimental laboratory setup of the dynamic charging system of electric vehicles.

4.3 Measured coupling coefficient, voltage gain, and efficiency

To get the load independent unique voltage gain, it is needed to design a system with almost negligible mutual inductance changes under the large range of misalignment. Coupling coefficient as well as mutual inductance is directly related to the surface flux density. As the proposed pad provides uniform surface flux density, coupling coefficient is less affected by the misalignment condition of the receiver pad. Measured coupling coefficient in according to the changes of receiver pad position is shown in Figure 4.3. Here, the coupling coefficient is measured between extended DD transmitter and receiver pad. It is noted that variation of coupling is within ±7% which is very negligible.
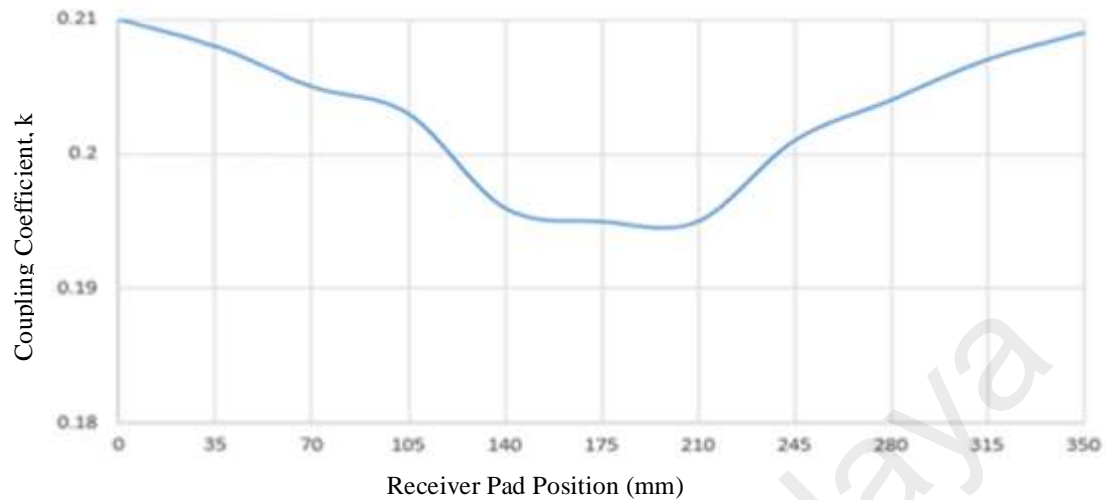
Figure 4.3: Measured coupling coefficient with different receiver pad positions (x-direction).

According to the simulation result of mutual inductance value of Figure 3.7, coupling coefficient k was found 0.3 in case of $N_{large}=10$ and $N_{small}=5$. On the other hand, the highest value of coupling coefficient is 0.21 in case of experimental result shown in Figure 4.3. Figure 4.4 depicts measured phase angle of the input impedance with the specifications listed in Table 4.1. From the Figure 4.4, it is clear that load independent ZPA of the input impedance is obtained when the proposed IPT transformer is fully compensated. Because of load independent voltage gain and negligible variation of coupling coefficient, efficiency should be high.
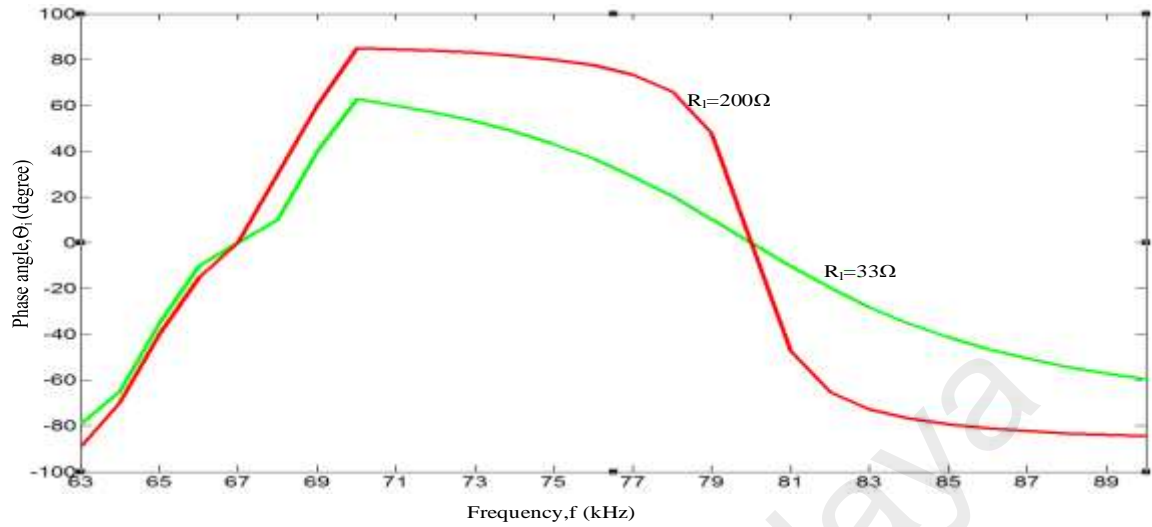
Figure 4.4: Measured input phase angle of the 500W LC-LC² compensated IPT system for EV charging.
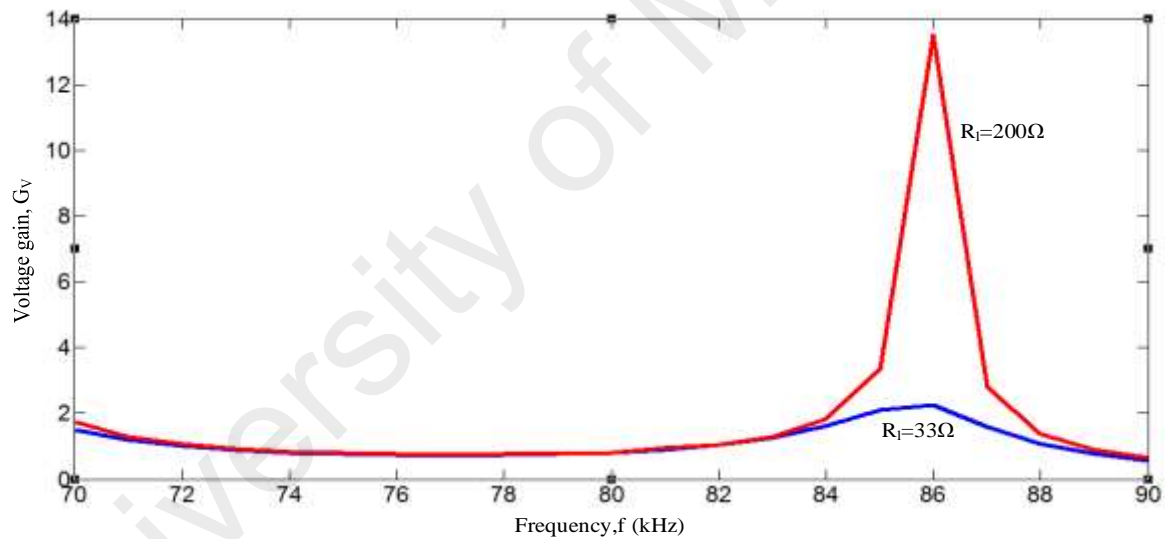
Figure 4.5: Measured voltage gain of the 500W LC-LC² compensated IPT system for EV charging.

The measured voltage gain corresponding to the frequency is shown in Figure 4.5. Comparing Figure 4.4 and Figure 4.5; we can say that load independent voltage gain and ZPA of the input impedance, both can be obtained at the frequency of ω_H. The

experimental load regulation curve of the proposed magnetic pad based LC-LC^2 compensated IPT system is shown in Figure 4.6.
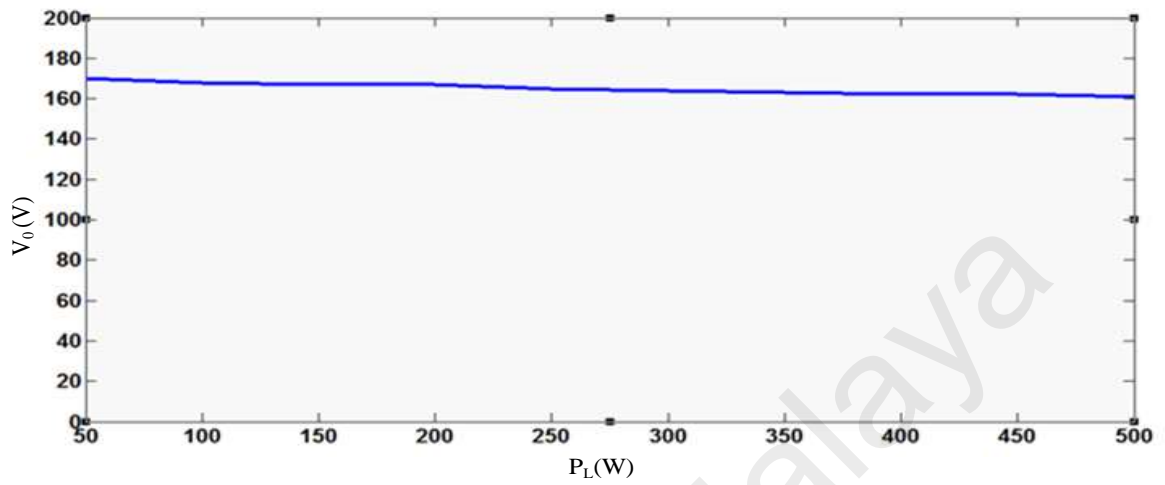
Figure 4.6: Measured load regulation of the 500W LC-LC^2 compensated IPT system for the proposed magnetic pad.

The experimental efficiency from dc supply to the battery is measured for given mutual inductance as well as another mutual inductance with a different air gap (180mm).
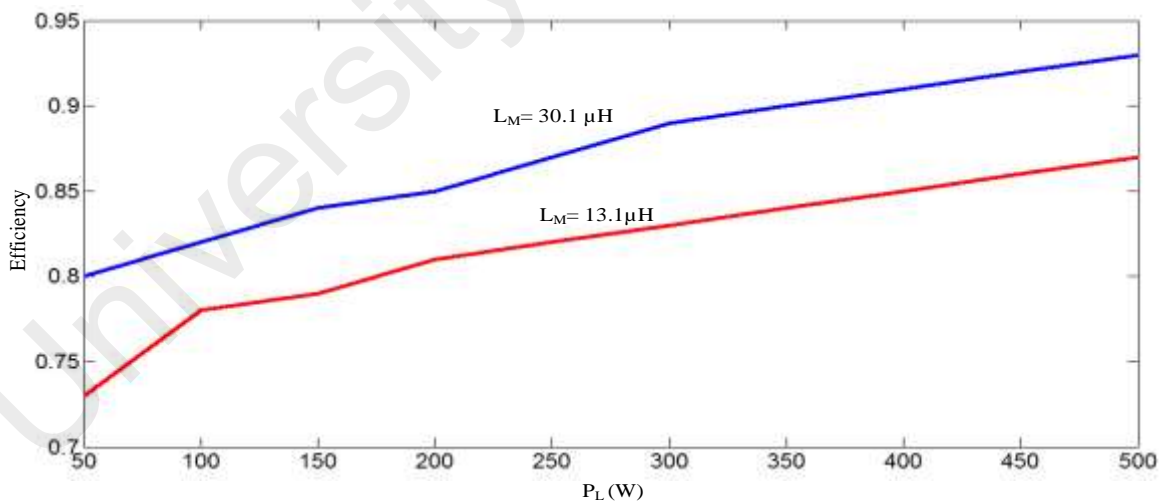
Figure 4.7: Efficiency of the 500W LC-LC^2 compensated IPT system for proposed magnetic pad.

To compare the coupling tolerance of the proposed converter with S-SP compensated converter, the specifications for 500W S-SP compensated converter are: V_{in}=211V,

V_0=171V, P_0=500W, C_1=47.71nF, C_2=48.24nF, C_{f2}=156.75nF, an air gap of 140 mm, R_L=33Ω - 200Ω. In the case of S-SP compensated converter, C_{f2} compensates the mutual inductance, L_M. On the other hand, equivalent inductance $L_{Mf} = n^2L_M \parallel L_{f2}$ is compensated by C_{f2} in the case of the proposed converter.
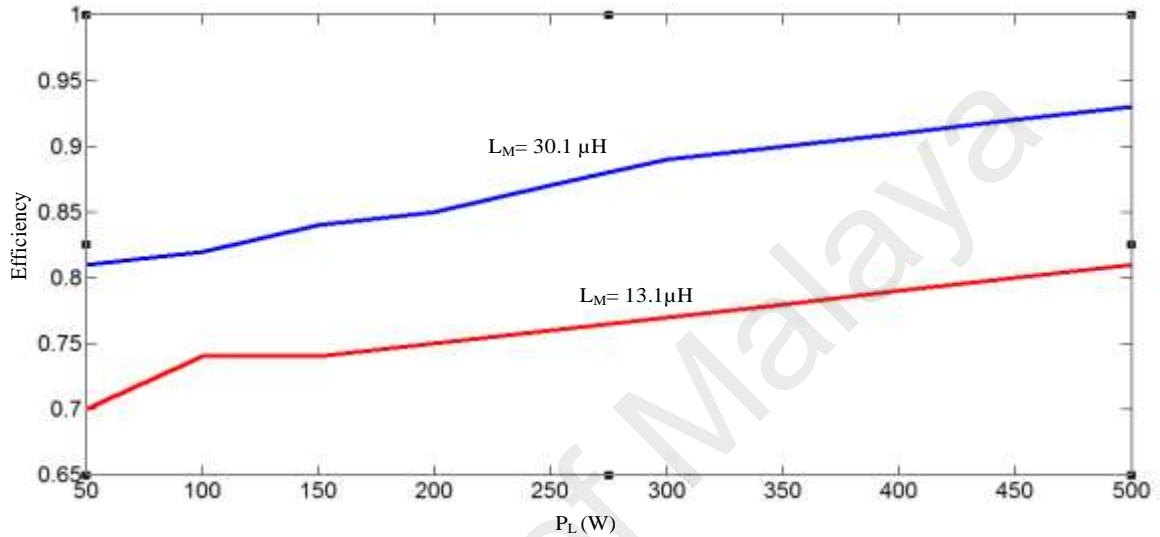
Figure 4.8: Efficiency of the 500W S-SP compensated IPT system.

Comparing Figure 4.7 and Figure 4.8, when the mutual inductance is about 13.1µH, efficiency is much affected in case of S-SP resonant converter. Because efficiency of the S-SP compensated resonant converter directly related to the mutual inductance whereas efficiency of the LC-LC^2 compensated resonant converter related to the equivalent inductance, $L_{Mf} = n^2L_M \parallel L_{f2}$. Therefore, LC-LC^2 compensated resonant converter provides better efficiency than S-SP compensated resonant converter in case of variant air gap condition by which mutual inductance changes. Figure 4.9 shows the typical laboratory results of the proposed compensated IPT system. At the defined air gap, the current i_l is in phase with the high frequency inverter output voltage V_{AB}.

71
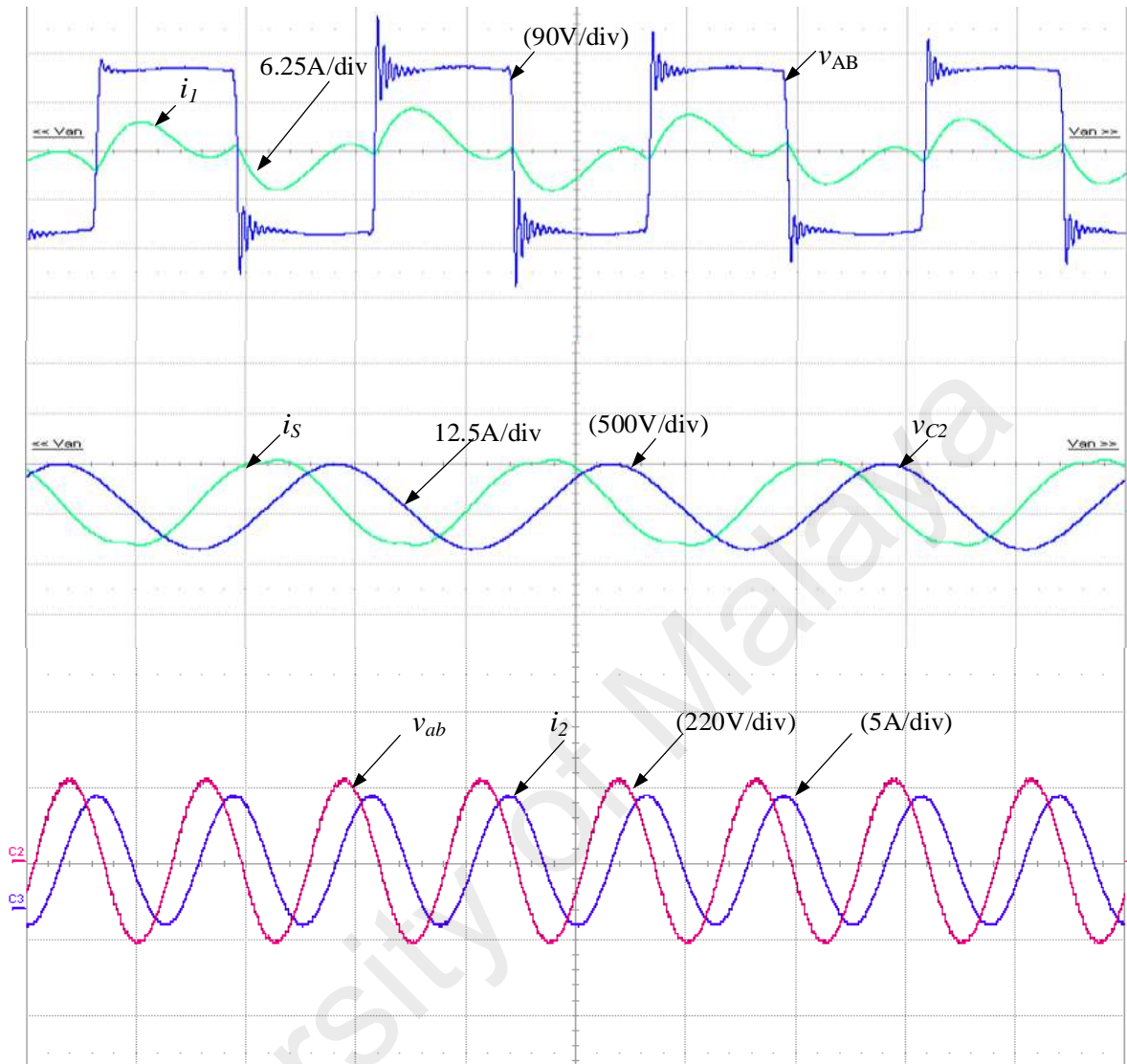
Figure 4.9: Laboratory results of the proposed LC-LC² compensated IPT system under full load condition.

4.4 Power transfer fluctuation

The long transmitter has the considerable fluctuation of power transfer because of a lower coupling coefficient when the receiver pad moves along the transmitter. In the case of segmented transmitter pads, if each pad is spaced by a little distance (J. M. Miller et al., 2015) and separately powered on, fluctuation also exists.

Besides, high coupling coefficient and high efficiency are obtained. In this case, zero power transfer occurs at certain positions of the receiver pad. Therefore, this method is unsuitable for dynamic charging.

If all transmitter pads are apart from each other with zero distances and also supplied by separately, still considerable fluctuation of power transfer exists. On the other hand, if the pads are connected to parallel and common power supply is applied, similar performance is observed (Kibok, Pantic, & Lukic, 2014). In this case, the null zone of power transfer is eliminated though it is less effective for the dynamic charging system.

In the case of dynamic charging, a method is proposed. In this method, when the receiver pad is perfectly aligned on any proposed transmitter pad, at a time adjacent pad is back to back series connected with previous one and supplied by the source. When receiver pad fully crosses the first transmitter pad, then first transmitter pad is turned off and third transmitter pad is again back to back series connected with the second one and supplied by the power supply as previous. This sequence is continued with consecutive all primary transmitter pads buried under the road. It is noted that, when the receiver pad is fully aligned with the first transmitter pad, power transfer rate is almost 93% of the power supply until third transmitter pad is turned on. In addition to the proposed method of dynamic charging, power transfer fluctuation is within ±6% for different horizontal misalignment positions of receiver pad shown in Figure 4.10.
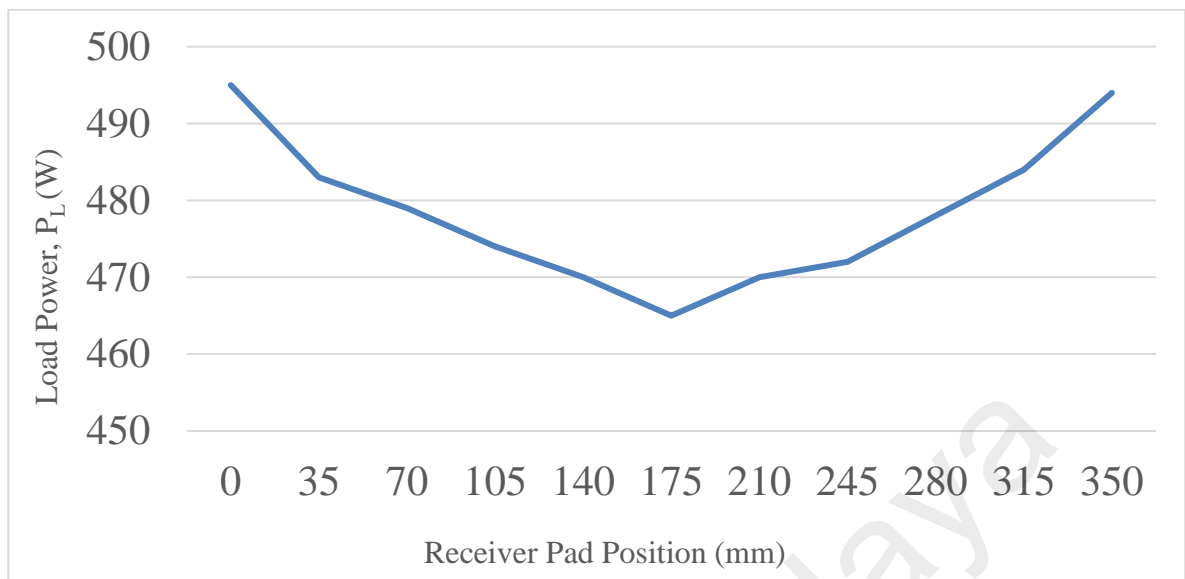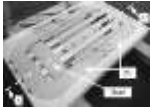
Figure 4.10: Measured load power under variable receiver pad positions (x-direction).

From the Figure 4.10, it is observed that this method provides a negligible power transfer fluctuation with no null-zone situation of power. To conclude, this method is helpful to acquire almost constant power transfer for dynamic charging of EV applications.

4.5 Comparison of different geometry with proposed pad

Although DD pad has more flux path height compared to the circular pad, both pads have strong null zone situation of power transfer in response to the horizontal misalignment. In the case of null zone situation of power transfer, DDQ and bipolar pads are far away from circular and DD pads. On the other hand, proposed pad has no null zone situation of power transfer associated with the moderate flux path height regarding the horizontal misalignment condition. The key points of the proposed pad compared to the conventional geometry of the pads are explained using Table 4.2.

Table 4.2: Comparison of different geometry with proposed pad

Pad topology	Evaluation criteria			
	Overview	Flux path height	Polarization	Null zones of power transfer with horizontal offset
Circular		1/4 of the pad diameter (Budhia et al., 2010)	Not polarized	Occurs at about 38% of the pad diameter (Budhia, Covic, Boys, et al., 2011)
DD		½ of the pad length (Budhia, Covic, Boys, et al., 2011; Siqi & Mi, 2015)	Polarized	Creates at about 34% of the pad length (Budhia et al., 2013)
DDQ		2 times of circular with an extra single sided flux path (Budhia, Covic, Boys, et al., 2011)	Polarized	Occurs at about 77% of the pad length (Zaheer et al., 2012)
Bipolar		2 times of circular	Polarized	Similar to DDQ (Zaheer et al., 2012)
Proposed		1/2.5 of the pad length	Smaller sections are polarized	Not happens for extended DD transmitter

In case of proposed pad, no null zone of power transfer occurred under the misalignment condition of the vehicle position. This is the main contribution that we found in the above comparison table.

4.6 Comparison of LC-LC^2 compensation with S-SP compensation

The general comparison between S-SP compensation and other conventional compensation networks is already described in Table 2.3. LC-LC^2 compensation technique has less

efficiency variation than any other compensation technique in response to the variation of mutual inductance. That means, efficiency variation is not so much in case of air gap variation of receiver pad. LC-LC^2 is better than the S-SP compensation technique as it has two "LC" combination in the receiver side which acts as a filter for harmonic injection. Because of this, higher order harmonics are not injected to the rectifier side. Comparison between S-SP compensation and LC-LC^2 compensation is shown in Table 4.3.

Table 4.3: Comparison of LC-LC^2 compensation with S-SP compensation

Compensation networks	Evaluation criteria			
	Maximum efficiency	Air gap	Efficiency variation	Higher order harmonics
S-SP (Jia et al., 2015)	93%	200 mm	Affected by the mutual inductance changes	Injected to the rectifier side
LC-LC^2	93%	140 mm	Less affected by the mutual inductance changes	Not injected to the rectifier side

4.7 Summary

This chapter depicts the experimental results about the coupling capability, load independent operation, load regulation, efficiency and tolerance of power transfer fluctuation of the proposed experimental setup of the dynamic charging system of the electric vehicle. This chapter also provides a summarize concept about the proposed magnetic pad in comparison to the other conventional pads.

CHAPTER 5: CONCLUSION

5.1 Conclusion

In this research, a new set of pad design with a special arrangement procedure has been proposed for maintaining almost uniform coupling factor as well as negligible power transfer fluctuation. This arrangement of the pad is effective, especially for dynamic charging of EV. With the help of FEA, the design of the pad has been explained. One of the contributions of this work is uniform magnetic flux distribution produced by the zigzag shape of small rectangular sections located inside the large rectangular section. Regardless of the misalignment condition of the receiver pad, negligible power transfer fluctuation with a slight variation of coupling has been justified for extended DD transmitter by the aid of load independent voltage transfer ratio and power transfer fluctuation analysis. This is the major contribution of this research. Almost uniform power transfer efficiency of 93% has been achieved at a load independent constant voltage transfer ratio (CVTR) frequency of 80 kHz under the horizontal misalignment condition of the receiver pad, with 140mm vertical air gap distance between the transmitter and receiver. The proposed LC-LC^2 compensated resonant converter provides the ZPA of the input impedance and load independent voltage gain characteristics at a common resonant frequency. Using a common resonant frequency, experimental results of the proposed LC-LC^2 compensated resonant converter are obtained. In IPT based EV charging application, efficiency is directly related to the air gap variation. Efficiency-comparison between LC-LC^2 and S-SP compensated resonant converter depicts that efficiency of the LC-LC^2 compensated resonant converter is less sensitive to the air gap variation than the S-SP compensated resonant converter. Due to the less sensitivity of the air gap variation, proposed compensation technique is very much effective in the IPT based dynamic EV charging application.

In the next, a simple process to select the suitable switching position of the extended DD transmitters has been recommended based upon the receiver pad position for sequential operation of all transmitter pads buried under the road.

5.2 Future works

To replace the conventional vehicles with the electric vehicles, the future research can be concentrated on the following points:

(a) Control technologies of the power transfer from the transmitting pads should be controlled in an effective way with respect to the position of the transmitter pads. If it is not effectively controlled, it will create the substantial amount of power loss.

(b) Since the parasitic elements of charging pads have the great effect on the efficiency, designing of the EV charger is very challenging. Therefore, effects of the parasitic elements can be more analyzed in the future research.

(c) In order to maintain the safety issues and to increase the power level of an EV charger, needs the improvement of shielding arrangement. Because poor shielding arrangement creates the stray field effects.

(d) A comparative study between IPT and CPT for EV charging applications.

References

Ahmed, K., Aamir, M., Uddin, M. K., & Mekhilef, S. (2015). A new coil design for enhancement in misalignment tolerance of Wireless Charging System.Paper presented at the IEEE Student Conference on Research and Development (SCOReD),Malaysia.

Aldhaher, S., Luk, P. C. K., & Whidborne, J. F. (2014). Electronic Tuning of Misaligned Coils in Wireless Power Transfer Systems.IEEE Transactions on Power Electronics, 29(11), 5975-5982.

Amjad, M., Salam, Z., Facta, M., & Mekhilef, S. (2013). Analysis and Implementation of Transformerless LCL Resonant Power Supply for Ozone Generation. IEEE Transactions   on Power Electronics,28(2),650-660.

Bertoluzzo, M., Buja, G., & Dashora, H. K. (2016). Lumped Track Layout Design for Dynamic Wireless Charging of Electric Vehicles. IEEE Transactions on Industrial Electronics, 63(10),6631-6640.

Bolger, J. G., Kirsten, F. A., & Ng, L. S. (1978). Inductive power coupling for an electric highway system. Paper presented at the 28th IEEE Vehicular Technology Conference,California,USA.

Bosshard, R., & Kolar, J. W. (2016). Multi-Objective Optimization of 50 kW/85 kHz IPT System for Public Transport. IEEE Journal of Emerging and Selected Topics in Power Electronics, 4(4), 1370-1382.

Bosshard, R., Kolar, J. W., Muhlethaler, J., Stevanovic, I., Wunsch, B., & Canales, F. (2015). Modeling and η-α-Pareto Optimization of Inductive Power Transfer Coils for Electric Vehicles. IEEE Journal of Emerging and Selected Topics in Power Electronics, , 3(1), 50-64.

Boys, J. T., Elliott, G. A. J., & Covic, G. A. (2007). An Appropriate Magnetic Coupling Co-Efficient for the Design and Comparison of ICPT Pickups. IEEE Transactions on Power Electronics, 22(1), 333-335.

Budhia, M., Boys, J. T., Covic, G. A., & Chang-Yu, H. (2013). Development of a Single-Sided Flux Magnetic Coupler for Electric Vehicle IPT Charging Systems. IEEE Transactions on Industrial Electronics, 60(1), 318-328.

Budhia, M., Covic, G., & Boys, J. (2010). A new IPT magnetic coupler for electric vehicle charging systems. Paper presented at the IECON 2010 - 36th Annual Conference on IEEE Industrial Electronics Society.

Budhia, M., Covic, G. A., & Boys, J. T. (2009). Design and optimisation of magnetic structures for lumped Inductive Power Transfer systems. Paper presented at the IEEE Energy Conversion Congress and Exposition.

Budhia, M., Covic, G. A., & Boys, J. T. (2011). Design and Optimization of Circular Magnetic Structures for Lumped Inductive Power Transfer Systems. IEEE Transactions on Power Electronics, 26(11), 3096-3108.

Budhia, M., Covic, G. A., Boys, J. T., & Chang-Yu, H. (2011). Development and evaluation of single sided flux couplers for contactless electric vehicle charging. Paper presented at the IEEE Energy Conversion Congress and Exposition (ECCE).

Chau, K. T., Wong, Y. S., & Chan, C. C. (1999). An overview of energy sources for electric vehicles. Energy Conversion and Management, 40(10), 1021-1039.

Chen, L., Nagendra, G. R., Boys, J. T., & Covic, G. A. (2015). Double-Coupled Systems for IPT Roadway Applications. IEEE Journal of Emerging and Selected Topics in Power Electronics, 3(1), 37-49.

Chen, Q., Wong, S. C., Tse, C. K., & Ruan, X. (2009). Analysis, Design, and Control of a Transcutaneous Power Regulator for Artificial Hearts. IEEE Transactions on Biomedical Circuits and Systems, 3(1), 23-31.

Cheng, Y., & Shu, Y. (2014). A New Analytical Calculation of the Mutual Inductance of the Coaxial Spiral Rectangular Coils. IEEE Transactions on Magnetics, 50(4), 1-6.

Choi, S., Huh, J., Lee, W. Y., Lee, S. W., & Rim, C. T. (2013). New Cross-Segmented Power Supply Rails for Roadway-Powered Electric Vehicles. IEEE Transactions on Power Electronics, 28(12), 5832-5841.

Choi, S. Y., Gu, B. W., Lee, S. W., Lee, W. Y., Huh, J., & Rim, C. T. (2014). Generalized Active EMF Cancel Methods for Wireless Electric Vehicles. IEEE Transactions on Power Electronics, 29(11), 5770-5783.

Chwei-Sen, W., Covic, G. A., & Stielau, O. H. (2004). Power transfer capability and bifurcation phenomena of loosely coupled inductive power transfer systems. IEEE Transactions on Industrial Electronics, 51(1), 148-157.

Chwei-Sen, W., Stielau, O. H., & Covic, G. A. (2005). Design considerations for a contactless electric vehicle battery charger. IEEE Transactions on Industrial Electronics, 52(5), 1308-1314.

Covic, G. A., & Boys, J. T. (2013). Modern Trends in Inductive Power Transfer for Transportation Applications. IEEE Journal of Emerging and Selected Topics in Power Electronics, 1(1), 28-41.

Covic, G. A., Boys, J. T., Kissin, M. L. G., & Lu, H. G. (2007). A Three-Phase Inductive Power Transfer System for Roadway-Powered Vehicles. IEEE Transactions on Industrial Electronics, 54(6), 3370-3378.

Covic, G. A., Kissin, M. L. G., Kacprzak, D., Clausen, N., & Hao, H. (2011). A bipolar primary pad topology for EV stationary charging and highway power by inductive coupling. Paper presented at the IEEE Energy Conversion Congress and Exposition.

Deng, J., Fei, L., Li, W., Ruiqing, M., & Mi, C. (2015, 15-19 March 2015). ZVS double-side LCC compensated resonant inverter with magnetic integration for electric vehicle wireless charger. Paper presented at the IEEE Applied Power Electronics Conference and Exposition (APEC).

EIA. (2012). The Damage Done in Transportation .Retrieved from :http://news.thomasnet.com/imt/2012/04/30/the-damage-done-in-transportation-which-energy-source-will-lead-to-the-greenest-highways.

Elliott, G. A. J., Covic, G. A., Kacprzak, D., & Boys, J. T. (2006). A New Concept: Asymmetrical Pick-Ups for Inductively Coupled Power Transfer Monorail Systems. IEEE Transactions on Magnetics, 42(10), 3389-3391.

Elliott, G. A. J., Raabe, S., Covic, G. A., & Boys, J. T. (2010). Multiphase Pickups for Large Lateral Tolerance Contactless Power-Transfer Systems. IEEE Transactions on Industrial Electronics, 57(5), 1590-1598.

G.A. Covic , J. B.(2010). Inductive power transfer (IPT) powering our future. Paper presented at the Power Electron. Research Group, Univ. Auckland, New Zealand, Tech. Rep.

Gao, Y., Farley, K., & Tse, Z. (2015). A Uniform Voltage Gain Control for Alignment Robustness in Wireless EV Charging. Energies, 8(8), 8355. Retrieved from http://www.mdpi.com/1996-1073/8/8/8355

Gao, Y., Ginart, A., Farley, K. B., & Tse, Z. T. H. (2016). Misalignment effect on efficiency of wireless power transfer for electric vehicles. Paper presented at the IEEE Applied Power Electronics Conference and Exposition (APEC).

Gilchrist, A., Wu, H., & Sealy, K. (2012). Novel system for wireless in-motion EV charging and disabled vehicle removal. Paper presented at the IEEE International Electric Vehicle Conference (IEVC).

Greenhouse, H. (1974). Design of Planar Rectangular Microelectronic Inductors. IEEE Transactions on Parts, Hybrids, and Packaging, 10(2), 101-109.

Hasanzadeh, S., & Vaez-Zadeh, S. (2011). Enhancement of overall coupling coefficient and efficiency of contactless energy transmission systems. Paper presented at the 2nd Power Electronics, Drive Systems and Technologies Conference.

Hou, J., Chen, Q., Yan, K., Ren, X., Wong, S. C., & Tse, C. K. (2013). Analysis and control of S/SP compensation contactless resonant converter with constant voltage gain. Paper presented at the IEEE Energy Conversion Congress and Exposition.

Hsu, J. U. W., Hu, A. P., & Swain, A. (2009). A Wireless Power Pickup Based on Directional Tuning Control of Magnetic Amplifier. IEEE Transactions on Industrial Electronics, 56(7), 2771-2781.

Huang, C. Y., Boys, J. T., & Covic, G. A. (2013a). LCL Pickup Circulating Current Controller for Inductive Power Transfer Systems. IEEE Transactions on Power Electronics, 28(4), 2081-2093.

Huang, C. Y., Boys, J. T., & Covic, G. A. (2013b). LCL Pickup Circulating Current Controller for Inductive Power Transfer Systems. IEEE Transactions on Power Electronics, 28(4), 2081-2093.

Huh, J., Lee, S. W., Lee, W. Y., Cho, G. H., & Rim, C. T. (2011). Narrow-Width Inductive Power Transfer System for Online Electrical Vehicles. IEEE Transactions on Power Electronics, 26(12), 3666-3679.

Jaegue, S., Seungyong, S., Yangsu, K., Seungyoung, A., Seokhwan, L., Guho, J., . . . Dong-Ho, C. (2014). Design and Implementation of Shaped Magnetic-Resonance-Based Wireless Power Transfer System for Roadway-Powered Moving Electric Vehicles. IEEE Transactions on Industrial Electronics, 61(3), 1179-1192.

Jan-Mou, L., Jones, P. T., Onar, O., & Starke, M. (2014). Coupling electric vehicles and power grid through charging-in-motion and connected vehicle technology. Paper presented at the IEEE International Electric Vehicle Conference (IEVC).

Jeong, S., Jang, Y. J., & Kum, D. (2015). Economic Analysis of the Dynamic Charging Electric Vehicle. IEEE Transactions on Power Electronics, 30(11), 6368-6377.

Jia, H., Qianhong, C., Siu-Chung, W., Tse, C. K., & Xinbo, R. (2015). Analysis and Control of Series/Series-Parallel Compensated Resonant Converter for Contactless Power Transfer. IEEE Journal of Emerging and Selected Topics in Power Electronics, 3(1), 124-136.

Jiseong, K., Jonghoon, K., Sunkyu, K., Hongseok, K., In-Soo, S., Nam Pyo, S., . . . Seungyoung, A. (2013). Coil Design and Shielding Methods for a Magnetic Resonant Wireless Power Transfer System. Proceedings of the IEEE, 101(6), 1332-1342.

Kalwar, K. A., Aamir, M., & Mekhilef, S. (2015). Inductively coupled power transfer (ICPT) for electric vehicle charging – A review. Renewable and Sustainable Energy Reviews, 47, 462-475.

Keeling, N. A., Covic, G. A., & Boys, J. T. (2010). A Unity-Power-Factor IPT Pickup for High-Power Applications. IEEE Transactions on Industrial Electronics, 57(2), 744-751.

Kibok, L., Pantic, Z., & Lukic, S. M. (2014). Reflexive Field Containment in Dynamic Inductive Power Transfer Systems. IEEE Transactions on Power Electronics, 29(9), 4592-4602.

Kim, H., Song, C., Kim, D. H., Jung, D. H., Kim, I. M., Kim, Y. I., . . . Kim, J. (2016). Coil Design and Measurements of Automotive Magnetic Resonant Wireless Charging System for High-Efficiency and Low Magnetic Field Leakage. IEEE Transactions on Microwave Theory and Techniques, 64(2), 383-400.

Ko, Y. D., & Jang, Y. J. (2013). The Optimal System Design of the Online Electric Vehicle Utilizing Wireless Power Transmission Technology. IEEE Transactions on Intelligent Transportation Systems, 14(3), 1255-1265.

Kurschner, D., Rathge, C., & Jumar, U. (2013). Design Methodology for High Efficient Inductive Power Transfer Systems With High Coil Positioning Flexibility. IEEE Transactions on Industrial Electronics, 60(1), 372-381.

Lee, K., Pantic, Z., & Lukic, S. M. (2014). Reflexive Field Containment in Dynamic Inductive Power Transfer Systems. IEEE Transactions on Power Electronics, 29(9), 4592-4602.

Lee, W. Y., Huh, J., Choi, S. Y., Thai, X. V., Kim, J. H., Al-Ammar, E. A., . . . Rim, C. T. (2013). Finite-Width Magnetic Mirror Models of Mono and Dual Coils for Wireless Electric Vehicles.IEEE Transactions on Power Electronics,28(3), 1413-1428.

Li, S., Li, W., Deng, J., Nguyen, T. D., & Mi, C. C. (2015). A Double-Sided LCC Compensation Network and Its Tuning Method for Wireless Power Transfer. IEEE Transactions on Vehicular Technology, 64(6), 2261-2273.

Li, W., Zhao, H., Li, S., Deng, J., Kan, T., & Mi, C. C. (2015). Integrated LCC Compensation Topology for Wireless Charger in Electric and Plug-in Electric Vehicles. IEEE Transactions on Industrial Electronics, 62(7), 4215-4225.

Lu, F., Zhang, H., Hofmann, H., & Mi, C. C. (2016b). A Dynamic Charging System With Reduced Output Power Pulsation for Electric Vehicles. IEEE Transactions on Industrial Electronics, 63(10), 6580-6590.

Madawala, U. K., & Thrimawithana, D. J. (2011). A Bidirectional Inductive Power Interface for Electric Vehicles in V2G Systems. IEEE Transactions on Industrial Electronics, 58(10), 4789-4796.

Miller, J. M.(2012). Wireless Plug-in Electric Vehicle (PEV) Charging. Oak Ridge National Laboratory,Tech. Rep.

Miller, J. M., Jones, P. T., Jan-Mou, L., & Onar, O. C. (2015). ORNL Experience and Challenges Facing Dynamic Wireless Power Charging of EV's. IEEE Circuits and Systems Magazine, 15(2), 40-53.

Miller, J. M., Onar, O. C., White, C., Campbell, S., Coomer, C., Seiber, L., . . . Steyerl, A. (2014). Demonstrating Dynamic Wireless Charging of an Electric Vehicle: The Benefit of Electrochemical Capacitor Smoothing. IEEE Power Electronics Magazine, 1(1), 12-24.

Miller, J. M., White, C. P., Onar, O. C., & Ryan, P. M. (2012). Grid side regulation of wireless power charging of plug-in electric vehicles. Paper presented at the IEEE Energy Conversion Congress and Exposition (ECCE).

Nagatsuka, Y., Ehara, N., Kaneko, Y., Abe, S., & Yasuda, T. (2010). Compact contactless power transfer system for electric vehicles. Paper presented at the International Power Electronics Conference (IPEC).

Onar, O. C., Miller, J. M., Campbell, S. L., Coomer, C., White, C. P., & Seiber, L. E. (2013). A novel wireless power transfer for in-motion EV/PHEV charging. Paper presented at the Twenty-Eighth Annual IEEE Applied Power Electronics Conference and Exposition (APEC).

Pijl, F. F. A. v. d., Castilla, M., & Bauer, P. (2013). Adaptive Sliding-Mode Control for a Multiple-User Inductive Power Transfer System Without Need for Communication. IEEE Transactions on Industrial Electronics, 60(1), 271-279.

Plugless Power, Plugless Power vehicle compatibility. Retrieved from: www. pluglesspower.com/go-plugless/wireless-ev-charging/supported-evs/.

Prasanth, V., & Bauer, P. (2013). Study of misalignment for On Road Charging. Paper presented at the IEEE Transportation Electrification Conference and Expo (ITEC).

Prasanth, V., & Bauer, P. (2014). Distributed IPT Systems for Dynamic Powering: Misalignment Analysis. IEEE Transactions on Industrial Electronics, 61(11), 6013-6021.

Qu, X., Han, H., Wong, S. C., Tse, C. K., & Chen, W. (2015). Hybrid IPT Topologies With Constant Current or Constant Voltage Output for Battery Charging Applications. IEEE Transactions on Power Electronics, 30(11), 6329-6337.

Qualcomm Halo, WEVC Trials.Retrieved from: http://www.qualcommhalo.com index.php/ wevc-trials.html.

Raabe, S., & Covic, G. A. (2013). Practical Design Considerations for Contactless Power Transfer Quadrature Pick-Ups. IEEE Transactions on Industrial Electronics, 60(1), 400-409.

Sampath, J. P. K., Vilathgamuwa, D. M., & Arokiaswami, A. (2015). Efficiency Enhancement for Dynamic Wireless Power Transfer System with Segmented Transmitter Array. IEEE Transactions on Transportation Electrification, 2(1), 76-85.

Siqi, L., & Mi, C. C. (2015). Wireless Power Transfer for Electric Vehicle Applications. IEEE Journal of Emerging and Selected Topics in Power Electronics, 3(1), 4-17.

Stamati, T. E., & Bauer, P. (2013). On-road charging of electric vehicles. Paper presented at the IEEE Transportation Electrification Conference and Expo (ITEC).

Su, W., Eichi, H., Zeng, W., & Chow, M. Y. (2012). A Survey on the Electrification of Transportation in a Smart Grid Environment. IEEE Transactions on Industrial Informatics, 8(1), 1-10.

Sungwoo, L., Jin, H., Changbyung, P., Nam-Sup, C., Gyu-Hyeoung, C., & Chun-Taek, R. (2010). On-Line Electric Vehicle using inductive power transfer system. Paper presented at the IEEE Energy Conversion Congress and Exposition (ECCE).

Tesla, N. (1914). Apparatus for transmitting electrical energy: Google Patents.

Tie, S. F., & Tan, C. W. (2013). A review of energy sources and energy management system in electric vehicles. Renewable and Sustainable Energy Reviews, 20, 82-102.

Trong-Duy, N., Siqi, L., Weihan, L., & Mi, C. C. (2014). Feasibility study on bipolar pads for efficient wireless power chargers. Paper presented at the Twenty-Ninth Annual IEEE Applied Power Electronics Conference and Exposition (APEC).

Vilathgamuwa, D. M., & Sampath, J. P. K. (2015). Wireless Power Transfer (WPT) for Electric Vehicles (EVs)—Present and Future Trends. In S. Rajakaruna, F. Shahnia, & A. Ghosh (Eds.), Plug In Electric Vehicles in Smart Grids: Integration Techniques (pp. 33-60). Singapore: Springer Singapore.

Villa, J. L., Sallan, J., Sanz Osorio, J. F., & Llombart, A. (2012). High-Misalignment Tolerant Compensation Topology For ICPT Systems. IEEE Transactions on Industrial Electronics, 59(2), 945-951.

Wei, Q., Guo, W., Sun, X., Wang, G., Zhao, X., Li, F., & Li, Y. (2012). A New Type of IPT System with Large Lateral Tolerance and its Circuit Analysis. Paper presented at the International Conference on Connected Vehicles and Expo (ICCVE).

Wei, Z., Siu-Chung, W., Tse, C. K., & Qianhong, C. (2014a). Analysis and Comparison of Secondary Series- and Parallel-Compensated Inductive Power Transfer Systems Operating for Optimal Efficiency and Load-Independent Voltage-Transfer Ratio. IEEE Transactions on Power Electronics, 29(6), 2979-2990.

Wei, Z., Siu-Chung, W., Tse, C. K., & Qianhong, C. (2014b). Design for Efficiency Optimization and Voltage Controllability of Series-Series Compensated Inductive Power Transfer Systems. IEEE Transactions on Power Electronics, 29(1), 191-200.

Wei, Z., Siu-Chung, W., Tse, C. K., & Qianhong, C. (2014c). An Optimized Track Length in Roadway Inductive Power Transfer Systems.IEEE Journal of Emerging and Selected Topics in Power Electronics, 2(3), 598-608.

Wei, Z., White, J. C., Abraham, A. M., & Mi, C. C. (2015). Loosely Coupled Transformer Structure and Interoperability Study for EV Wireless Charging Systems. IEEE Transactions on Power Electronics, 30(11), 6356-6367.

Weihan, L., Han, Z., Siqi, L., Junjun, D., Tianze, K., & Mi, C. C. (2015). Integrated LCC Compensation Topology for Wireless Charger in Electric and Plug-in Electric Vehicles. IEEE Transactions on Industrial Electronics, 62(7), 4215-4225.

WEVC. (2014). Green Power ,Korea :3.3kW WEVC installed on HMC EV Soul. IEEE Sensors Journal, 17(5), 1549-1561.

WiTricity, WiT-3300. Paper presented at the http://www.witricity.com/pages/ev-charging-system.html.

Wu, H. H., Gilchrist, A., Sealy, K. D., & Bronson, D. (2012). A High Efficiency 5 kW Inductive Charger for EVs Using Dual Side Control. IEEE Transactions on Industrial Informatics, 8(3), 585-595.

Xiaoyong, R., Qianhong, C., Lingling, C., Xinbo, R., Siu-Chung, W., & Tse, C. K. (2012). Characterization and control of self-oscillating contactless resonant converter with fixed voltage gain. Paper presented at the Proceedings of The 7th International Power Electronics and Motion Control Conference.

Zaheer, A., Kacprzak, D., & Covic, G. A. (2012). A bipolar receiver pad in a lumped IPT system for electric vehicle charging applications. Paper presented at the IEEE Energy Conversion Congress and Exposition (ECCE).

Zhang, H., Lu, F., Hofmann, H., Liu, W., & Mi, C. (2016). A 4-Plate Compact Capacitive Coupler Design and LCL-Compensated Topology for Capacitive Power Transfer in Electric Vehicle Charging Applications. IEEE Transactions on Power Electronics, 31(12), 8541-8551.

Zhang, X., Yuan, Z., Yang, Q., Li, Y., Zhu, J., & Li, Y. (2016). Coil Design and Efficiency Analysis for Dynamic Wireless Charging System for Electric Vehicles. IEEE Transactions on Magnetics, 52(7).

Zhong, C., Wuwei, J., Xueliang, H., Linlin, T., Chen, C., & Wei, W. (2015). A Promoted Design for Primary Coil in Roadway-Powered System. IEEE Transactions on Magnetics, 51(11), 1-4.

Zhu, Q., Guo, Y., Wang, L., Liao, C., & Li, F. (2015). Improving the Misalignment Tolerance of Wireless Charging System by Optimizing the Compensate Capacitor. IEEE Transactions on Industrial Electronics, 62(8), 4832-4836.

Zhu, Q., Wang, L., Guo, Y., Liao, C., & Li, F. (2016). Applying LCC Compensation Network to Dynamic Wireless EV Charging System. IEEE Transactions on Industrial Electronics, 63(10), 6557-6567.

LIST OF PUBLICATIONS AND PAPERS PRESENTED

Journals

1. **Md Morshed Alam**, Saad Mekhilef, Mehdi Seyedmahmoudian, Ben Horan (**2017**). Dynamic Charging of Electric Vehicle with Negligible Power Transfer Fluctuation. **Published in "Energies**" (MDPI). ISSN: 1996-1073.10(5), 701 (ISI-cited publication, I.F.: 2.262, **Q2**).

2. **Md Morshed Alam**, Saad Mekhilef. Analysis of LC-LC^2 Compensated Inductive Power Transfer for High Efficiency and Load Independent Voltage Gain. **Under review in IET Power Electronics.** ISSN: 1755-4543 (ISI-cited publication, I.F.:3.547, **Q1).**

3. **Md Morshed Alam**, Saad Mekhilef. A Critical Review of Coil Geometry and Compensation Network for Inductive Power Transfer (IPT) based Electric Vehicle (EV) Charging. **Ready for submission in Renewable and Sustainable Energy Reviews**. ISSN: 1364-0321 (ISI-cited publication, I.F.:8.050, **Q1**).

Conferences

1. **Md Morshed Alam**, Saad Mekhilef. Load Independent Voltage Gain of a S-LCC Compensation based IPT System for Electric Vehicle Applications. Accepted for presentation at 12th IEEE International Conference on Power Electronics and Drive Systems (PEDS) held in Honolulu, Hawaii, USA.